

AN EXPERIMENTAL INVESTIGATION OF THE EFFECT
OF A TRANSVERSE HYPERSONIC FLOW VELOCITY
UPON A LOW-DENSITY D. C. ELECTRICAL DISCHARGE IN AIR

Thesis by
Gary L. Marlotte

In Partial Fulfillment of the Requirements
For the Degree of
Doctor of Philosophy

California Institute of Technology
Pasadena, California

1962

ACKNOWLEDGMENTS

The author wishes to express his sincere appreciation to Dr. Anthony Demetriades and Professor Lester Lees for their encouragement and guidance throughout the course of this investigation. He also wishes to thank the staff of the Hypersonic Wind Tunnel for their assistance and advice during testing; the members of the Machine Shop for constructing the test equipment; Mrs. Truis van Harreveld for her able assistance in carrying out the desk computations; Mrs. Betty Wood for preparing the figures; and Mrs. Roberta Duffy for her typing of the manuscript.

The author acknowledges with gratitude the receipt of a fellowship from the Douglas Aircraft Corporation for the year 1959-1960.

This study is part of a general hypersonics investigation being conducted at GALCIT under the sponsorship and with the financial support of the U. S. Army Research Office and the Advanced Research Projects Agency, Contract No. DA-04-495-ORD-3231.

ABSTRACT

The low-density D. C. electrical discharge in a uniform gas stationary with respect to the electrodes has been studied extensively. However, when the gas moves at a hypersonic speed transverse to the electrodes, several completely new effects are introduced. Experiments were carried out with air in the GALCIT 5-inch by 5-inch hypersonic wind tunnel with a nominal Mach number of 5.8. D. C. breakdown voltages and steady-state sub-normal glow voltages were measured across a channel formed by two sharp-edged insulating flat plates in which flat-plate "Rogowski" electrodes were embedded. Segmented electrodes were then used in the normal glow regime to measure current distributions at each electrode for various electrode segment combinations, total currents, and densities.

Some important results of the present study are the following. For the characteristic dimensions and speeds involved, the explicit dependence of electrical breakdown upon the velocity of the stream is small compared to the effect of boundary layer density defects. A theoretical treatment of breakdown is given and qualitative agreement with experiments is obtained. In the normal glow regime using segmented electrodes, an unmistakable explicit flow velocity effect was observed, with the discharge current paths being displaced downstream compared to static bell-jar tests at equivalent densities.

TABLE OF CONTENTS

| PART | | PAGE |
|------|---|------|
| | ACKNOWLEDGMENTS | |
| | ABSTRACT | |
| | TABLE OF CONTENTS | |
| | LIST OF FIGURES | |
| | LIST OF SYMBOLS | |
| I. | INTRODUCTION | 1 |
| II. | BREAKDOWN VOLTAGES | 7 |
| | II. 1. Approach and Objectives | 7 |
| | II. 2. Description of Experiments | 8 |
| | II. 2. 1. Wind Tunnel Description | 8 |
| | II. 2. 2. Electrode Geometry | 9 |
| | II. 2. 3. Flow Geometry | 10 |
| | II. 2. 4. Test Equipment | 11 |
| | II. 2. 5. Test Procedure | 11 |
| | II. 2. 6. Experimental Results | 12 |
| | II. 3. Theoretical Considerations | 14 |
| | II. 3. 1. Velocity Effects | 14 |
| | II. 3. 2. Density Gradient Effects | 17 |
| | II. 4. Comparison of Theory with Experiment | 21 |
| III. | SUB-NORMAL GLOW CURRENTS | 23 |
| | III. 1. Approach and Objectives | 23 |
| | III. 2. Description of Experiments | 26 |
| | III. 2. 1. Electrode and Flow Geometry | 26 |
| | III. 2. 2. Stability Considerations | 27 |

| PART | PAGE |
|--|------|
| III. 2. 3. Test Equipment | 28 |
| III. 2. 4. Test Procedure | 28 |
| III. 3. Results and Discussion | 29 |
| IV. NORMAL GLOW CURRENTS | 33 |
| IV. 1. Approach and Objectives | 33 |
| IV. 2. Description of Experiments | 37 |
| IV. 2. 1. Electrode and Flow Geometry | 37 |
| IV. 2. 2. Test Equipment | 38 |
| IV. 2. 3. Static Tests | 38 |
| IV. 2. 4. Results and Discussion of Static Tests | 39 |
| IV. 2. 5. Dynamic Tests | 41 |
| IV. 3. Results and Discussion | 42 |
| V. SUGGESTIONS FOR FURTHER STUDY | 47 |
| V. 1. Analysis | 47 |
| V. 2. Suggested Experiments | 48 |
| VI. CONCLUSIONS | 51 |
| REFERENCES | 53 |
| APPENDIX A. Derivation of α . | 55 |
| APPENDIX B. Integration of the Breakdown Equation. | 57 |
| APPENDIX C. Calculation of Sub-Normal Glow Current Level. | 59 |
| FIGURES | 62 |

LIST OF FIGURES

| NUMBER | | PAGE |
|--------|--|------|
| 1 | Electrode Geometry | 62 |
| 2 | Typical Total Pressure Traverse on Electrode and on Flat Insert | 63 |
| 3 | Density and Neutral-Neutral Mean Free Path as Functions of Tunnel Pressure | 64 |
| 4 | Density Profile between Electrodes | 65 |
| 5 | Fraction of Electrode Separation Disturbed by Density Gradients as a Function of the Product of Free-Stream Density and Electrode Separation | 66 |
| 6 | Pressure at Room Temperature as a Function of Free-Stream Density | 67 |
| 7 | Diagram of Power Supply and Recording Circuit | 68 |
| 8 | Experimental Breakdown Voltages | 69 |
| 9 | Effect of the Ratio of Electrode Streamwise Length to Separation upon Breakdown | 70 |
| 10 | Breakdown Voltage as a Function of the Ratio of Electrode Streamwise Length to Separation | 71 |
| 11 | Fraction of Electrode Separation Disturbed by Density Gradients as a Function of the Product of Free-Stream Density and Electrode Separation with Breakdown Voltage as a Parameter | 72 |
| 12 | Theoretical Breakdown Voltages | 73 |
| 13 | Typical Voltage-Current Characteristic of a Discharge | 74 |
| 14 | Experimental Arrangement for Measuring Glow Currents | 75 |
| 15 | Voltage-Current Characteristics of Large Electrodes | 76 |
| 16 | Voltage as a Function of Density with Current as a Parameter | 77 |
| 17 | Cathode Currents Measured with Cathode Held at Various Fixed Potentials Relative to the Wind Tunnel | 78 |

| NUMBER | | PAGE |
|--------|--|------|
| 18 | Voltage-Current Characteristics of Small Electrodes | 79 |
| 19 | Comparison of Static Voltage-Current Characteristics between Large and Small Electrodes | 80 |
| 20 | Segmented Electrode Details | 81 |
| 21 | Measuring Circuit | 82 |
| 22 | Static Test Apparatus | 83 |
| 23 | Static Voltage-Total Current Characteristics of Segmented Electrodes | 84 |
| 24 | Current Distributions at Anode and Cathode. $P = 2 \text{ mm Hg.}$ | 85 |
| 25 | Current Distribution at Each Electrode with No. 1 Opposite Electrode Segment Operating. $P = 2 \text{ mm Hg.}$ | 86 |
| 26 | Current Distributions at Anode and Cathode. $P = 4 \text{ mm Hg.}$ | 87 |
| 27 | Current Distribution at Each Electrode with No. 1 Opposite Electrode Segment Operating. $P = 4 \text{ mm Hg.}$ | 88 |
| 28 | Dynamic Test Apparatus | 89 |
| 29 | Dynamic Electrode Installation | 90 |
| 30 | Schlieren Flow Pictures | 91 |
| 31 | Dynamic Voltage-Total Current Characteristics of Segmented Electrodes | 92 |
| 32 | Current Distributions at Anode and Cathode. $P_o = 0 \text{ psig.}$ | 93 |
| 33 | Current Distribution at Each Electrode with No. 1 Opposite Electrode Segment Operating. $P_o = 0 \text{ psig.}$ | 94 |
| 33B | Current Distribution at the Anode with No. 2 Cathode Segment Operating. $P_o = 0 \text{ psig.}$ | 95 |

| NUMBER | | PAGE |
|--------|--|------|
| 34 | Current Distributions at Anode and Cathode. $P_o = 20$ psig. | 96 |
| 35 | Current Distribution at Each Electrode with No. 1 Opposite Electrode Segment Operating. $P_o = 20$ psig. | 97 |
| 35B | Current Distribution at the Anode with No. 2 Cathode Segment Operating. $P_o = 20$ psig. | 98 |
| 36 | Current Distributions at Anode and Cathode. $P_o = 40$ psig. | 99 |
| 37 | Current Distribution at Each Electrode with No. 1 Opposite Electrode Segment Operating. $P_o = 40$ psig. | 100 |
| 37B | Current Distribution at the Anode with No. 2 Cath- ode Segment Operating. $P_o = 40$ psig. | 101 |
| 38 | Current Distributions at Anode and Cathode. $P_o = 60$ psig. | 102 |
| 39 | Current Distribution at Each Electrode with No. 1 Opposite Electrode Segment Operating. $P_o = 60$ psig. | 103 |
| 39B | Current Distribution at the Anode with No. 2 Cath- ode Segment Operating. $P_o = 60$ psig. | 104 |
| 40 | Appearance of Different Electrode Segment Com- binations. $P_o = 0$ psig; $I = 1 \mu A$. | 105 |

LIST OF SYMBOLS

| | |
|-----------|--|
| a | speed of sound |
| A | constant for a gas (m^2/Kg) |
| B | constant for a gas (Vm^2/Kg) |
| \bar{c} | average thermal velocity of gas molecule |
| c_p | specific heat at constant pressure |
| d | separation of electrodes |
| e | basic unit of charge |
| E | electric field strength |
| F | force of stream acting on a discharge particle |
| I | current |
| J | current density |
| k | mobility (m^2/Vs) |
| l | ionization length |
| m | mass of particle under discussion |
| M | Mach number |
| M | parameter = $(\lambda - \frac{\eta(1-\lambda)}{(1-\eta)})$ |
| n | number of electrons at distance y |
| N | parameter = $(1-\lambda)/(1-\eta)$ |
| P | pressure |
| F^* | tunnel pressure in mm Hg converted to room temperature |
| P_0 | tunnel total pressure |
| P'_0 | total pressure behind a normal shock wave |
| q | heat added per unit mass (J/Kg) |
| Q | non-dimensional heat added |
| R | resistance |

S collision cross section
 T temperature
 U flow velocity
 v velocity
 V voltage
 V'_i effective ionization potential
 w electrode dimension in direction of flow
 x distance from leading edge to electrode center-line in lower flat plate in inches
 y perpendicular distance from electrode surface

 α number of ion-pairs formed per electron per meter, in the direction of the electric field (1/m)
 γ number of electrons released by the cathode per positive ion arriving at the cathode
 δ average boundary layer thickness over lower electrode
 $\Delta()$ increment
 e dielectric constant
 $\left. \begin{array}{l} \kappa \\ \lambda \\ \eta \end{array} \right\}$ parameters defining density profile $\rho = \rho(y)$
 λ mean free path (mfp)
 ρ density between electrodes (Kg/m^3)
 ρ charge density (C/m^3)
 τ time

Subscripts

$()_a$ atmospheric value

| | |
|------------------|--|
| () _A | anode |
| () _b | breakdown value |
| () _C | cathode |
| () _e | electron |
| () _i | ion |
| () _n | neutral |
| () _o | tunnel total conditions, initial value |
| () _s | supply |
| () _t | transverse component |
| () _w | wall |
| () _∞ | free stream |

NOTE: In general, MKS units and their standard abbreviations are used when there is no clear convention established. However, those quantities that are peculiar to the wind tunnel and the equipment mounted therein are frequently left in their more familiar form. Also, quantities to be compared to static discharges are sometimes left in "practical" units.

I. INTRODUCTION

In general, it may be said that the low-density D. C. electrical discharge in a uniform gas stationary with respect to the electrodes is well understood.* Over half a century of active research and countless papers have left us with a number of authoritative reference works in the field.

An extensive treatment of the general problems of breakdown may be found in "Electrical Breakdown of Gases", by Meek and Craggs. (7)† Further exhaustive information on various factors important to gaseous discharges and the refined measurement thereof is found in "Basic Processes of Gaseous Electronics", by Loeb. (4) Fundamental collision processes that occur in both breakdown and sustained discharges are to be found in the detailed treatise, "Electronic and Ionic Impact Phenomena", by Massey and Burhop. (8) Simple introductory treatments are given by Cobine (2) and von Engle (1), while two volumes of "Handbuch der Physik", Gas Discharges I and II, Volumes XXI (9) and XXII (3), contain perhaps the most complete account of electrical discharge phenomena over the complete current range.

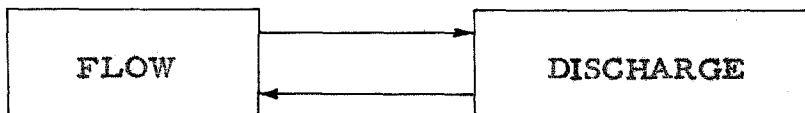
In contrast to the huge list of publications on "static" gaseous discharges, there is little relevant information on gas discharges in the presence of a high speed gas. (15, 16) Recently, however, the experimental study of electrical discharges in high speed flows has become

* Surface effects are still a problem.

† Numbers in parentheses denote references at the end of the text.

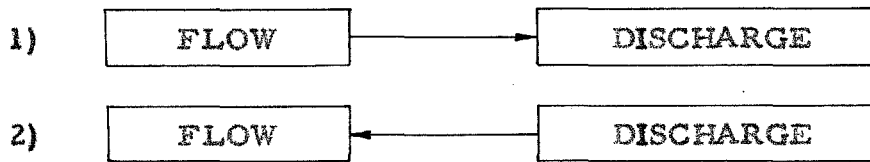
of topical interest by reason of the sharply increased attention given basic non-equilibrium interactions between charged particles and a high-speed neutral gas.

Consider the effect of the addition of a high-speed gas flow between the electrodes of a D. C. electrical discharge. The "well understood" static discharge becomes disrupted by the appearance of convection in a direction generally different from that of the electric field; in addition, the presence of the electrodes themselves and the discharge may cause severe non-uniformities in the flow field -- which in turn affects the discharge, and so on. Thus, in the general case, the flow affects the discharge and the discharge affects the flow.



From the theoretical point of view, this interaction is reflected by a complete coupling of the two groups of governing equations -- the conservation equations of each species and the electromagnetic relations including Ohm's law. Thus, at present, the general theoretical situation offers little hope. Experiments, on the other hand, can and have been made of situations involving this reciprocal interaction, but the large effect of the geometry both on the flow and on the discharge has generally limited the results to the particular device under study.

Less ambitiously, then, as a simpler approach we investigate regimes in which the interaction occurs essentially in one direction. The possibilities are:



It is easily seen that (1) is indeed possible, and it is the basis for the experimental investigation of this paper.

For example, since gaseous conduction of electricity may depend on a quite small percentage of all the particles in the gas, it is quite possible to change the discharge characteristics by a small change in the flow parameters, whereas even orders of magnitude change in the electrical circuit may not perceptibly perturb the flow. This should be the situation when current densities are very low and the dynamic impact (ρU_{∞}^2) of the flow is very high. If ρ (the flow density and thus the discharge density) is to be kept in the usual low density region of gas discharges, then U_{∞} , the flow velocity, must be high. Thus, high-speed flow effects on breakdown and sustained low-current discharges into the glow regime can be studied experimentally in a hypersonic wind tunnel with a negligible effect on the stream parameters, thus satisfying (1). (See IV. 1.)

It would be well to examine the significance of a superposed hypersonic flow upon conduction between two electrodes imbedded in two parallel flat plates with the electric field transverse to the flow. Consider first the case of inviscid, shock-free flow, where the velocity, density, and pressure of the gas are assumed identical from point to point. These assumptions are very significant, since they mean that the flow field is uniform, making the problem similar to

that of the static case where the condition of uniformity is also met. The only difference between the two cases is the existence of the fluid motion in the present problem. The effect of the motion of the gas relative to the electrodes is not obvious a priori. However, it cannot be significant if the velocity of the flow is much smaller than the transverse drift of the electrons and ions under action of the electric field. It is true that the electron drift velocity is much higher than that of the ions. On the other hand, since Coulomb forces make charge separation difficult, and since the ions are a necessary component of the breakdown mechanism, it would be more appropriate to compare the flow velocity with the ion drift velocities. This will be done in detail in a later section. In a flow of this type, it is possible that the progress of the electrons toward the anode remains unaltered by the stream if the density is low (of the order of 10^{-2} of atmospheric) and the electron-atom collision cross section is low; in other words, the fluid density remains (as in the static case) the important parameter as far as the electrons are concerned. The situation is different when it comes to the positive ions by virtue of their much larger transit time between the electrodes compared to the electrons. With a hypersonic transverse velocity component, the positive ions may have a tendency to be swept downstream and to escape the discharge area. If this tendency to escape the discharge region because of the convection of the free stream is stronger than the electrical effects tending to retard the ions, charge separation could occur. In self-sustaining discharges, this process will represent a net current leaving the discharge region, and a difference between anode

current and cathode current should appear. On the other hand, if the ions escape only by taking an equal number of electrons with them (escape in pairs), then restoring forces would not arise, but the overall "ionization efficiency" of the discharge should decrease since a smaller number of ions and electrons now arrive at the electrodes. We conclude that conduction between electrodes may be altered by the direct influence of the inviscid flow field on the ions and possibly by an indirect influence on the electrons.

Consider next the effect of viscosity. In this case, a boundary layer will grow on each electrode. Were we considering low speed flow, the boundary layers would result only in a non-uniformity in stream velocity. In hypersonic flow, however, the boundary layer also introduces large density gradients normal to the electrode surface because of the large temperature changes* in the viscous boundary layer. For a Mach number of 6 over an insulated surface, the fluid temperature adjacent to the surface is approximately six times larger, and the density six times smaller, than the free stream conditions†. Here, we encounter a phenomenon unknown in previous breakdown studies; the gas in the inter-electrode space has a strongly non-uniform density distribution, which should certainly affect the behavior of both ions and electrons.

* In the low density "cold" discharges under consideration, where the electrons receive the ionization energy from the electric field (non-equilibrium ionization), the effect of temperature in the gas upon the discharge is manifested only in its effect on the density (a mfp effect). See p. 69 of ref. 3, "The Glow Discharge at Low Pressure", by Gordon Francis.

† Of course, for a "sufficiently" cold wall, the wall density could be higher than the free stream value.

Finally, shock waves should be considered. In hypersonic flow, it is only with difficulty that the region between two near-planar electrodes can be made reasonably shock-free. Like the boundary layers, the greatest effect of the shocks should be the non-uniformities (in velocity, density, etc.) introduced into the flow field.

II. BREAKDOWN VOLTAGES

II. 1. Approach and Objectives

In a gaseous discharge, the production of charge carriers is usually accomplished by one of two methods, thermal agitation or the use of an electric field. In the first method, the gas is heated as a body so that particles at the high-energy end of the Maxwell temperature distribution attain energies exceeding the ionization potential of the gas molecules. In the second case, the gas is immersed in a strong electric field which provides ionization energy to a small number of electrons which are always present (from cosmic rays, for example); the additional electrons formed in turn make ionizing collisions and so on, thus creating an avalanche which leads to dielectric breakdown and one of the self-sustaining discharges.

With the presence of a high-speed gas, in order to fulfill the condition that there be an essentially one-way effect of the flow upon the discharge, the second case is appropriate -- where the electron energy is obtained by acceleration in an electric field. Of all the operating points on a typical voltage-current characteristic of a discharge, the single point of breakdown is especially appealing, since dielectric breakdown is one of the processes best understood in static gaseous discharges*. Since we are interested in a region where the

* For example, in the usual static gaseous discharge between flat plates, there is only one parameter (to a good approximation) that determines the breakdown voltage V_b -- the so-called Paschen similarity parameter. This is essentially ρd , the product of the constant density between the electrodes and the electrode separation. Hence, $V_b = V_b(\rho d)$ in the static case (see ref. 7, p. 82).

currents are initially of order microamperes or less, there is no question but that there is a one-way interaction occurring.

Accordingly, the objective of this work was the comparison of breakdown voltages obtained with and without motion of the gas between the electrodes. This comparison was done by studying experimentally the effect of a hypersonic flow on the long-established Paschen breakdown characteristic, which relates the breakdown voltage uniquely to the product of density and inter-electrode distance. Preliminary tests, as well as rough analyses based on elementary concepts of gaseous conduction, indicated the new important parameters introduced by the flow. Subsequently, further experiments were carried out in order to ascertain the role of these parameters.

II. 2. Description of Experiments

II. 2. 1. Wind Tunnel Description. The experiments were conducted in the GALCIT Hypersonic Wind Tunnel (Leg 1), which is of the closed return, continuously operating type. The tunnel has a nominal Mach number of 5.8, and the test section has a width of 5", a height of about 5 1/4", and a 29"-long test rhombus, as shown in figure 1. A fixed reservoir temperature of 225° F was chosen in order to apply extensive flow data taken at this temperature to the electrode configuration (conveniently) chosen. The tunnel has an available range of pressure from 14.4 to 104.4 psia, corresponding to free stream densities from $\rho_{\infty} = 0.0055$ to $\rho_{\infty} = 0.040 \text{ Kg/m}^3$. At room temperatures, these densities in turn correspond to pressures from $P = 3.5$ to $P = 25.3 \text{ mm Hg}$, which is

within the range of the low-density static glow discharges (pressures of a fraction of a mm Hg to several cm Hg) studied most extensively (see figure 6). Hence, it is seen that the hypersonic wind tunnel is well suited for discharge work. A complete description of the wind tunnel and compressor plant is found in references 10 and 11.

II. 2. 2. Electrode Geometry. The electrode and flat plate geometries used in this experiment were arrived at after prolonged experimentation with various configurations. The final configuration consisted of two circular 2-cm diameter copper electrodes[†] which were mounted in the following manner: one electrode was embedded in a 5" by 26" Lucite flat plate with provision for several electrode positions; the other was embedded in a smaller 3" by 5" Lucite flat plate supported by a steel beam that could be moved fore and aft to correspond to the lower electrode position (see figure 1).

The electrodes were contoured in the "Rogowski"⁽²⁾ fashion, which essentially gave them the shape of certain equipotential lines between flat plates with a voltage difference, and hence created a uniform electric field in the gap (for electrode separations no larger than a given value). A constant 2 cm separation was used, because this was the maximum that could be realized before arcing to the metal tunnel walls became objectionable. (Also see Section III. 3.) On the other hand, shock wave geometry became quite complicated for sig-

[†] Copper was chosen merely for convenience, since sputtering of electrodes was no problem here. In any case, the coating of "burnt oil" from the tunnel compressors and other impurities probably masked any identity of the electrode material.

nificantly smaller separations. The curvature of the electrodes required for a 2 cm separation did not significantly affect the flow field for work of this nature, as was demonstrated by total pressure traverses with the electrodes and with flat dummy plugs (see figure 2).

With the above arrangement, the effect of the shocks generated by the leading edges of the flat plates was small compared to the large density defects in the two boundary layers. Hence we have a configuration in which we may study the effect of large boundary-layer type density gradients upon breakdown voltages across a channel; as will be seen later, the total boundary-layer density defect is thought to be the most significant parameter in the present problem. Since the boundary layer on a flat plate at this Mach number has a thickness governed by the tunnel pressure and the distance from the plate leading edge⁽⁵⁾, we may cover a large range of boundary layer thicknesses in the channel by varying the tunnel pressure and by varying the electrode positions fore and aft.

II. 2. 3. Flow Geometry. Since the experiment has been arranged so that the interaction is one-way (flow → discharge), the complete flow situation is given solely by fluid-dynamical considerations. In practice, the electrodes were designed with flat plate configurations and the tunnel was operated under conditions identical to those prevailing when extensive fluid-dynamical measurements were made^{*}; therefore, assuming the leading edge shock from the upper plate is

* See references 5 and 12.

weak enough not to disturb the flow profiles, one may convert the pertinent flat-plate boundary layer profiles of references 5 and 12 to the present configuration.

The density and mean free path, both free stream and wall values, are plotted versus tunnel pressure in figure 3. The density profile between the electrodes and an approximation thereto is given in figure 4 with certain parameters labeled. The parameter $(\delta/d)(1+\kappa)$, which represents the relative distance across the electrodes disturbed by density gradients, is then plotted versus the product of tunnel density and electrode separation in figure 5. (The reason for this will appear later.) Figure 6 is a plot of free stream density versus P^* , which is the corresponding pressure in mm Hg at room temperature; this quantity is useful because most static discharge data is taken at room temperature with pressures measured in mm Hg.

II. 2. 4. Test Equipment. A D. C. power supply was used which has three filter stages and is rated at 2000 V D. C. and 250 mA (see figure 7). The ripple figure at no load (corresponding to just before breakdown) was about 0.2 V rms at 1000 V. The voltages at breakdown were automatically recorded on a Moseley Autograf Function Plotter. When static breakdown data were taken in the tunnel, the pressures were read on the oil manometer bank of the tunnel. Total pressure measurements (cf. figure 2) checking for the influence of the non-planar electrodes were also read from the manometer bank.

II. 2. 5. Test Procedure. First, the procedure consisted of measuring breakdown voltages across the hypersonic stream at various electrode positions and free stream densities. The copper

electrodes were wiped clean with acetone before each day's run and were then installed in the tunnel and allowed to come to a "uniform dirtiness" with oil from the compressors. It was found to take about an hour for the electrodes to settle down and give consistent voltage readings even after the tunnel had arrived at temperature equilibrium. The voltage readings at low densities went up about 5 per cent compared to reasonably clean electrodes just installed in the (warm) tunnel. This behavior points up a major unknown in the problem - the effect of the electrode surfaces upon breakdown; they are necessarily quite contaminated with impurities (such as compressor oil, and of course, oxides).

Secondly, breakdown measurements were made at several static (no flow) densities in the wind tunnel. The same "dirty" electrodes were kept in the same positions in the tunnel as for the dynamic tests (with flow). A range of static densities was obtained by closing the inlet valve of the tunnel, opening the exit valve, and pumping the tunnel down with the compressors. The above procedure was followed in order to subtract out, as far as possible, the effects of electrode contamination and possibly wind tunnel geometry in making a comparison of the static and dynamic breakdown results.

For the static case, the breakdown should follow the similarity law, $V_b = V_b(pd)$. Hence, to get even lower values of the product pd , the plate separation was also reduced.

II. 2. 6. Experimental Results. The breakdown voltages, V_b , both for the static case and the case with flow, including two electrode

positions, are plotted against the similarity parameter for the static case, ρd , in figure 8. For the dynamic data (with flow), the free-stream static density is used as the reference since it is easily found. Any other reference density, such as an average one between the electrodes, would generally be more cumbersome to compute, and in any case, would only shift the scale of the abscissa. It is noted that the static data follows the Paschen similarity, $V_b = V_b(\rho d)$, and we were justified in using smaller values of the electrode separation to get small values of ρd .

The striking result is that the dynamic breakdown data lies considerably below the static data. Of the two major expected causes of differences between static and dynamic data, presumably the effect of the velocity field would tend to raise the breakdown voltages, and the density defects in the boundary layers would tend to lower them. Since the experimental voltages are significantly lowered, we suspect that the velocity effect is smaller than the density effect.

In general, it is seen that one obtains lower breakdown voltages the further aft one goes on the flat plate because of increased boundary layer thicknesses. At this point, however, a new trend appears. There is a definite difference of breakdown voltages with a polarity reversal of the electrodes across the non-symmetrical boundary layers. We conclude that it is not just the total density defect that affects breakdown, but also the way it is distributed.

In order to establish experimentally the explicit effect of the velocity of the stream upon breakdown, the electrodes were progressively modified in order to obtain increasingly smaller values of the

ratio of electrode streamwise length w to electrode separation d ($= 2$ cm and held constant). [See the sketch on figures 9, 10.] This reduction in w/d presumably will tend to increase the breakdown voltages and emphasize the velocity effect. The shape of the electrodes was retained in order to maintain the same electric field, but their exposed streamwise length was progressively decreased using insulating cement. This procedure gave the electrodes more and more of an elongated shape transverse to the free stream (plan view).

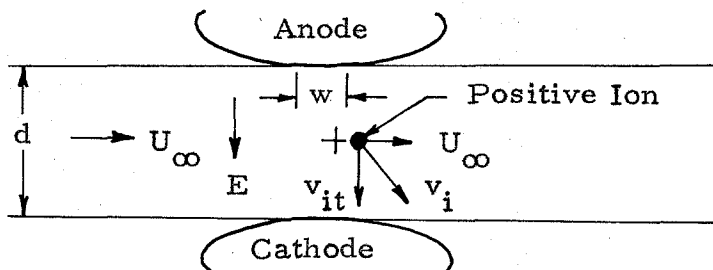
The results are plotted in figures 9 and 10. The trend is readily apparent despite the scatter. It appears that at the previously used gap-to-length ratio of unity, the velocity of the stream has a quite small effect upon breakdown compared to the density defects.

II. 3. Theoretical Considerations

II. 3. 1. Velocity Effects. Consider the effect that the velocity of the stream might have upon the discharge. For the reasons given in the introduction, attention is primarily focused upon the positive ions.

Examining the problem from a naïve point of view, imagine a single neutral molecule flowing parallel to the electrodes with a velocity U_{∞} . Assume the molecule is then ionized by a fast electron, becoming a singly-charged positive ion. This ion will retain its parallel velocity component U_{∞} , but in a very short time will attain an additional transverse average drift velocity of v_{it} , because of the electric field transverse to the stream velocity. The subsequent directed motion will be the vector sum of these two velocities (see

sketch). Very crudely, one might expect velocity effects to become very important where U_{∞}/v_{it} is of order w/d or larger, because then a significant portion of the positive ions would simply not reach the cathode and the avalanche process would not occur.



Positive ion velocity data⁽⁶⁾ for air indicate that for typical conditions under which the experiments were carried out, v_{it} is of the order of 2000 m/sec.* Alternately, the strong field approximation to the ion velocity v_{it} which may be used as a lower limit is given⁽²⁾ by:

$$v_{it} \sim \left(\frac{Ee\lambda_{in}}{m_i} \right)^{\frac{1}{2}} \sim \left(\frac{Ee\lambda_{nn}}{m} \right)^{\frac{1}{2}}, \quad (1)$$

where $\lambda_{in} \approx \lambda_{nn} =$ neutral mean free path,
 $m_i \approx m =$ mass of molecule.

* In the static case at room temperature, ion drift velocities are usually plotted versus a parameter E/P . In the general case, we want a quantity that is proportional to the average energy picked up in a mean free path. This is $E\lambda$ or E/ρ (for constant T this E/P). Thus, in order to use static data, the pressure at room temperature must be converted to density units or vice-versa. (See figure 6.)

For $E = 10^5$ V/m, $e = 1.60 \times 10^{-19}$ coul, $\lambda_{nm} = 3 \times 10^{-6}$ m
(typical value), $m = 48 \times 10^{-27}$ Kg;

$$v_{it} = \left(\frac{1.60 \times 3 \times 10^7}{48} \right)^{\frac{1}{2}} = 1000 \text{ m/s.}$$

This value is consistent with the values taken from experiment, and thus v_{it} appears to be of the same order as U_{∞} ($= 800$ m/s).

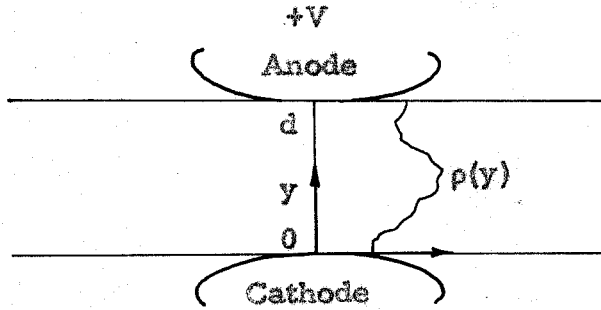
These two estimates of positive ion velocity were based upon free stream conditions. The effects of non-uniformities in the flow, such as the thick, low-velocity - low-density boundary layers, will all be such as to increase the ratio of transverse drift velocity to free stream velocity.

In summing up, for electrodes for which the ratio of length w to separation distance d is of order unity or greater, the positive ions can easily make their way across the gap, and the explicit effect of the stream velocity may very well be small compared to the effects of the large density gradients in the gap.

This conclusion leaves unexplained the surprising experimental fact that the velocity effect is small compared to the density effect for much smaller ratios of (w/d) than one might have reason to expect from a simple "hit or miss" argument involving the positive ions and the cathode. For, referring to the previous sketch, if breakdown can occur at the limit $U_{\infty}/v_{it} \approx w/d$, where U_{∞} and d are fixed and the pressure (density) is constant, and we take $v_{it} \sim E^n \sim V_b^n$, where $n < 1$, we have $V_b \sim (1/w)^{1/n}$. This estimated V_b becomes quite large at small w , contrary to the experimental results.

II. 3. 2. Density Gradient Effects.

In order now to examine the density gradient effects, consider two flat-plate Rogowski electrodes across a gas of arbitrary density profile $\rho = \rho(y)$ with a potential difference $V = Ed$ between them (see sketch).



Assume an electron is emitted from the cathode. This electron will accelerate toward the anode, ionizing the gas and releasing other electrons which are themselves free to accelerate in the electric field and thus also ionize the gas. If $n(y)$ is the number of electrons at a certain y , we have a number of ionizations

$$dn = n \alpha dy, \tag{2}$$

where

$$\alpha = \frac{\text{number of ion pairs formed}}{\text{electron-meter in direction of } E}.$$

Hence, with n_A electrons arriving at the anode per electron emitted at the cathode.

$$\int_1^{n_A} \frac{dn}{n} = \int_0^d \alpha dy.$$

$$\ln(n_A) = \int_0^d \alpha dy,$$

and

$$n_A = e^{\int_0^d \alpha dy} \quad (3)$$

These electrons cause $(n_A - 1)$ positive ions to impinge on the cathode (assuming single ionizations -- no recombination):

$$\text{number of positive ions impinging on cathode} = e^{\int_0^d \alpha dy} - 1. \quad (4)$$

Breakdown is said to occur when the ions, as given by (4), act to replenish the original electron which left the cathode through some physical mechanism. For the purposes of this argument, this mechanism is taken to be secondary emission due to positive ions arriving at the cathode. (See complete discussion in Loeb, ref. 4.) Thus, we arrive at a modification of the well known Townsend breakdown criterion:

$$\gamma \left(e^{\int_0^d \alpha dy} - 1 \right) = 1 \quad (5)$$

where γ is the number of electrons emitted at the cathode per incident ion.

Using the Townsend approximation for α (see Appendix A) of

$$\alpha = A_p(y) e^{-B_p(y)d/V_b}, \quad (6)$$

where V_b is the voltage at breakdown = Ed , the condition for breakdown becomes:

$$\gamma \left(e^{\int_0^d A \rho(y) e^{-B \rho(y) d / V_b} dy} - 1 \right) = 1. \quad (7)$$

Solving for the integral,

$$e^{\int_0^d \alpha dy} = \frac{\gamma+1}{\gamma}$$

or

$$\int_0^d \alpha dy = \int_0^d A \rho(y) e^{-B \rho(y) / V_b} dy = \ln \left(\frac{\gamma+1}{\gamma} \right). \quad (8)$$

At this point, we need to know the function $\rho = \rho(y)$. The profile given in figure 4 has several free parameters (i. e., δ/d , κ , λ , η) and can be adjusted to give a reasonable approximation to certain boundary-layer type flows such as the ones in the experiments.

The integral may now be evaluated and solved for a parameter combination which essentially represents the relative distance across the gap that is disturbed by density defects (see Appendix B). The result is:

$$\left(\frac{\delta}{d} \right) (1 + \kappa) = \frac{\ln \left(\frac{\gamma+1}{\gamma} \right)}{\frac{A(\rho_{\infty} d)}{\gamma - e^{-C}}} - e^{-C} \quad (9)$$

where

$$\gamma = \eta \lambda e^{-\lambda C} + \frac{e^{-CM}}{CN} \left[\left(M + N\eta + \frac{1}{C} \right) e^{-CN\eta} - \left(M + N + \frac{1}{C} \right) e^{-CN} \right],$$

and

$$M = \lambda - \left(\frac{1-\lambda}{1-\eta} \right) \eta,$$

$$N = \left(\frac{1-\lambda}{1-\eta} \right),$$

$$C = B(\rho_{\infty} d) / V_b.$$

In the limiting case of uniform density, $(\delta/d)(1 + \kappa) = 0$, and the numerator of the RHS must be zero. This result may be put in the form of the usual static breakdown, $V_b = V_b(\rho d)$ (see reference 1). Written out, this is

$$V_b = \frac{B(\rho d)}{\ln \left[\frac{A}{\ln(\gamma+1)/\gamma} \right] + \ln(\rho d)} \quad (10)$$

For air (see Appendix A),

$$A = 9.3 \times 10^5 \text{ m}^2/\text{Kg},$$

$$B = 2.323 \times 10^7 \text{ V m}^2/\text{Kg}.$$

Given a value of γ , we may plot this static curve. Now, γ is tabulated for various electrode materials⁽²⁾, but this data does not apply to the electrodes used in the present experiments: they are quite contaminated, and γ is known to vary greatly with the condition of the electrode surface⁽⁴⁾. However, γ can be estimated by curve-fitting equation 10 to the breakdown results already obtained in the static case. (See "Theoretical" curve and static data on figure 8.) This procedure resulted in a $\gamma \approx 0.001$, while Cobine⁽²⁾ lists $\gamma = 0.025$ for pure outgassed copper.

Having this estimate of γ , and using $\lambda = 0.17$, $\eta = 0.525$, $M = -0.747$, and $N = 1.747$ to curve-fit the boundary-layer density

defect, we may now proceed to compare the theoretical curves with the experimental data.

The equation for dynamic breakdown may be plotted as $(\delta/d)(1+\kappa)$ versus $\rho_{\infty} d$ for various values of V_b (see figure 11). Cross-plotting then gives $V_b = V_b(\rho_{\infty} d)$ for various values of $(\delta/d)(1+\kappa)$ (see figure 12). To compare this result with experiment, plots are now needed of $(\delta/d)(1+\kappa)$ versus $\rho_{\infty} d$ for the experiment, since in the tunnel $(\delta/d)(1+\kappa)$ changes with $\rho_{\infty} d$. For various distances of the lower electrode from the leading edge, this parameter has already been obtained from J. Kendall's work ⁽⁵⁾ and has been plotted in figure 5. We may now draw traces of $(\delta/d)(1+\kappa)$ versus $\rho_{\infty} d$ for various electrode positions on the other theoretical curves (figure 12). These, finally, are the proper "theoretical" curves to be compared to the experimental breakdown data.

II. 4. Comparison of Theory with Experiment

Comparing the static data in figure 8 with the static curve $(\delta/d)(1+\kappa) = 0$ in figure 12 (also recorded on figure 8), it is seen that the slope of the latter is slightly greater, which may well be attributed to the fact that the electrodes used do not approximate infinite planes very well, and actually tend to look more like the ends of rounded rods separated by a gap.

We see that the rough theoretical consideration of the density defect can account for a great deal of the difference between static and dynamic breakdown. This observation helps substantiate the previously noted experimental result that the indirect effects of the

high velocity (the large density gradients) cause considerably greater departure from the static breakdown characteristic than the velocity itself.

III. SUB-NORMAL GLOW CURRENTS

III. 1. Approach and Objectives

A typical static discharge characteristic is given in figure 13 (see reference 3). In Section II, the measurement of the breakdown voltage V_b as a function of ρd was described, where the discharge became self-sustaining, with current limited by the external circuit resistance. In addition to breakdown, the sub-normal and normal regimes of the flow discharge also hold promise of yielding useful information about various flow effects on the discharge (density defects, velocity effects) while still maintaining one-way interaction.

In the sub-normal glow regime following breakdown, the voltage falls with increasing current because of space charge effects. A positive ion sheath forms at the cathode, thus causing most of the potential drop across the discharge to occur in a region called the cathode fall region⁽¹³⁾. These large induced electric fields relieve the need for a large applied field, and so the overall discharge voltage decreases. As the current increases, the cathode fall decreases until it reaches a constant value. The current density at the cathode then remains constant with the area of the cathode covered by the discharge being proportional to the total current, i. e., the cathode area participating in the discharge increases as the overall current increases. (See "The Glow Discharge at Low Pressure by Gordon Francis [reference 3] for a complete discussion.)

Hence, if the currents are sufficiently small after breakdown into the sub-normal glow-discharge regime, the electric field may not yet be grossly distorted. If it is possible to make measurements of the discharge characteristics in this range of currents, the possibility exists of estimating the role of the stream velocity on breakdown and the low-current discharges.

One of the first things to examine is to what degree the free stream velocity acts differently upon the positive ions and the electrons, in the sense of imparting to the electrons and ions different mean streamwise velocities. We might expect a difference due to several things. First, the collision cross section of the free stream neutral particles with the positive ions is up to an order of magnitude greater than the collision cross section of the free stream neutral particles and the electrons⁽²⁾. (The classical result is $S_{ni} \approx 4\sqrt{2} S_{ne}$.) A second difference is that the electron, being much less massive than the positive ion will be imparted a higher velocity when contacted by a neutral. (Classically, for a one-dimensional elastic collision of a particle of mass m_2 by a particle of mass m_1 and velocity v_1 , the velocity of the m_2 particle after collision is given by $v_2 = 2m_1v_1/m_1 + m_2$ (see reference 2). Since $m_1 \approx m_2$ for positive ions and $m_1 + m_2 \approx m_1$ for electrons, the above result follows.) A third difference, however, and one that overwhelms the other two, is that the positive ions remain in the discharge region much longer than the electrons and are subjected to the force of the free stream for a much longer time than the electrons because of their much smaller mobility and thus much larger transit time $\Delta\tau$ between the electrodes.

Therefore, the total impulse $F\Delta\tau$ upon the ions is much larger than that on the electrons because $\Delta\tau$ is much greater, and not so much because of the differences in forces in the two types of collisions.

Granted that there is a significant difference in the effect of the free stream upon the electrons and ions, what is the result of this? In the absence of streamwise electric fields, * the characteristic particle paths of the ions compared to the electrons should be such that more ions than electrons would simply miss the appropriate electrode and so a net number of positive charges would be swept out of the discharge region. This effect would appear as a net difference between anode and cathode currents. With streamwise induced electric fields considered, however, one expects that such charge separation will be hindered, resulting in a "dipole" type of discharge with a net number of electrons more likely to be found on the upstream side and positive ions on the downstream side of the discharge (see A. C. Pipkin's paper, reference 14). Both of the above effects are present in varying degrees; that is, there is a tendency for the charges to separate due to aerodynamic forces that are opposed by the streamwise electric field created according to Poisson's equation.

To look for these effects experimentally, several things may be done. Measurements of anode and cathode currents along with Kirchhoff's Law will tell us whether a net current is leaving the discharge. In addition, as in the breakdown case (see Section II. 2. 6), the streamwise electrode dimension w can be decreased and the

* Streamwise electric fields cannot be large (of the same order of the applied field) if the charged particle density is very small.

effect studied on the anode and cathode currents and on the overall level of the voltage-current characteristics. (If the polarization of the discharge is appreciable, then this reduction of w should, in extreme cases, interrupt the discharge.) The overall voltage level should be checked, because of the possibility of decreased discharge efficiency even if the electrode currents prove equal by reason of the particles leaving in pairs. In other words, some of the energy obtained by the electrons from the applied field is wasted if after an ionizing collision some positive ions are swept out of the discharge region and take an equal number of electrons with them because of their mutual attraction. These "pair" losses may have the same effect as an increase in the recombination rate insofar as the discharge is concerned, because ionized particles are similarly removed from the discharge in pairs. It might be expected, then, that an increased voltage level would be necessary to maintain a given current level in the discharge under the above conditions if a parameter (such as electrode width) is varied.

III. 2. Description of Experiments

III. 2. 1. Electrode and Flow Geometry. The electrodes and flat plate supports used are the identical ones described in II. 2. 2, with the lower electrode fixed at the 17" position. Thus, the flow field is identical, and the information for the 17" electrode position in II. 2. 3 is unchanged. This should be a reasonable configuration for this work also, since at high pressures only about 30 per cent of the gas is disturbed by the boundary layers (refer to figure 5, the 17" curve). Hence, a large portion of the dynamic impact of the free stream is

felt across the discharge.

III. 2. 2. Stability Considerations. Since the sub-normal glow regime is characterized by a falling voltage with increase of current (like a negative resistance), there is no stable operating point on this curve using a supply that looks like a voltage source (low internal impedance compared to load impedance). To have a stable operating point on the voltage-current characteristic, we must make the power supply look more like a current source by means of large ballast resistors in series with the discharge (i. e., the power supply characteristic should cross the discharge characteristic in the manner shown in figure 13). The criterion for stability may be stated as $dV/dI + R > 0$ where dV/dI is the slope of the discharge characteristic at the point of intersection with the power supply characteristic (taken to be a pure voltage source in series with pure resistance R). That is, if the slope of the discharge $V-I$ characteristic may be considered a "resistance", the net circuit resistance must be positive for stable operation (see discussion in reference 2). This condition is sometimes known as Kaufmann's stability criterion.

Hence, the discharge will be started in the glow regime and then the current reduced and the ballast resistance increased as necessary until the $V-I$ characteristic shows that operation in the sub-normal glow regime is achieved.

III. 2. 3. Test Equipment. The experimental arrangement used is given in figure 14. The battery power supply was left completely "floating" with respect to the wind tunnel metal walls. (The effects of using a power supply held at a fixed potential with respect to the tunnel walls will be discussed later.) Fifty small 45V batteries were used as

voltage steps with six larger batteries being used for continuous adjustment between the steps. The total ballast resistance necessary to achieve the desired currents varied from 600 to 1100 M Ω . Two large 10 μ A movement meters were used to measure anode and cathode currents.

III. 2. 4. Test Procedure. In order to maintain equilibrium, the discharge remained on during a complete day of testing. Supply voltage, V_s , and cathode currents I_C were read at 0.1 μ A increments of anode current I_A at every 5 psi increment in the wind tunnel. Then

Discharge Voltage $V = V_s - RI_A - 100I_C$ volts (I_A, I_C in μ A), where $R = 500$ or 1000 .

For comparison purposes, this experiment was repeated in a bell-jar using the electrodes with the same degree of contamination they attained in the wind tunnel. Subsequently, the exposed area of the electrodes was narrowed with insulating cement to the shape given in figure 18. Both wind tunnel and bell-jar data were repeated for this configuration.

III. 3. Results and Discussion

The first result is that, at least to the degree of accuracy inherent in the meters (about 5 per cent maximum), there is no difference between anode current I_A and cathode current I_C for the complete range of conditions as represented in figure 15 (full-size electrodes used). This result implies that if a positive ion is blown out of the discharge region, it takes an electron with it and thus maintains charge neutrality, and/or that there is some mechanism allowing the positive ions to resist the bulk motion of the high-speed gas and remain in the

discharge area. One of the above possibilities should hold, since from simple mobility and geometry considerations, a substantial number of the positive ions are deflected by the stream sufficiently to miss the cathode (see discussion in Section II. 3).

As a consequence, the current plotted in figures 15 and 18 is just the discharge current. In figure 15, the low current data was limited at the higher densities by the increasing curvature of the discharge characteristics compared to those at lower densities, thus causing the operating point to become unstable. At the higher currents, the data range was limited by the total power supply voltage available, since the voltage drop across the ballast resistance begins to become quite large (around 1500 volts), being proportional to discharge current. The "Large Electrodes" curves on figure 16 are a cross-plot of some of the data in figure 15 showing the density (pressure) variation explicitly for constant current operation.

The fact that the anode and cathode currents were the same may not be a "result" of the experiments because of the floating power supply. In figure 17, the cathode was held at 0, -300, and -940 volts with respect to the tunnel, and the cathode currents were considerably smaller than the anode currents at the higher pressures. However, at least a significant portion of the current defect was a result of concentrated current paths that were formed between the walls and the electrodes, i. e., was not only a result of positive ion current lost downstream. These concentrated stray currents formed because of the proximity of the tunnel walls and their fixed potential. It is true that the walls are over 10 cm distant from the discharge, but since the boundary layers over the electrodes approach the tunnel walls, an alternate current path

between the metal walls and the electrodes may form in the very low density regions of the boundary layers (the density at the surface is about one-sixth of its free stream value). Hence, the effect of the stray electric fields produced by the tunnel is multiplied in importance since $E\lambda$ or E/ρ is really the important parameter (see the footnote in Section II. 3. 1).

On the other hand, with a floating power supply, if a current path should form with the wall, the charge carried would float the power supply with respect to the tunnel so as to decrease the stray electric fields. That is, the electrodes automatically are kept at such a potential with respect to the tunnel walls so as to minimize the tunnel's participation in the discharge. Unfortunately, a positive ion current leaving the discharge region also represents a net current between the discharge circuit and the tunnel since electrons for the ions' neutralization must eventually come from the tunnel. The result of this is that if ions are blown out of the discharge region initially, the electrode circuit will float more and more negative with respect to the tunnel walls until perhaps an "ion potential well" is formed in the discharge region of sufficient magnitude to overwhelm the flow velocity and equalize the electrode currents.

At this point, the qualitative appearance of the discharge (which was very faintly visible) deserves comment. At the lowest densities and highest currents, the visible discharge covered a significant portion of the electrodes, but as the density increased and current decreased, the electrode area covered by glow shrank and moved upstream. Furthermore, there was no particular visible effect of the

flow upon the discharge except through the changes of luminosity due to density effects (i. e., no visible sweeping or bending of the discharge downstream).

By examination of figure 15, the only portion of the curves that could allow an electric field without transverse space charge distortion is the portion at the lower currents, corresponding to the sub-normal glow discharge region where the V-I characteristics are beginning to rise to the breakdown values. This is in the 10^{-7} ampere region, as is evident from Poisson's equation in Appendix C. We emphasize the region where large electric field distortion has not set in so that we can have roughly the same electric fields that govern breakdown in order that results of this section may be applied to that problem.

The question arises as to whether the additional electrode area available over the effective visible area occupied by the glow is contributing to the experimental results. To examine this point, the electrodes were made an order of magnitude smaller in exposed stream-wise length -- from 2 cm to 0.2 cm in the configuration of figure 18, and the measurements were concentrated on the higher densities and 10^{-7} ampere region, where the effects should be most pronounced. The change of geometry was proven to have no effect upon the static discharge at the same general operating level by comparing the V-I characteristics of each geometry (see figure 19). (This means that the smaller electrode configuration still served as "infinite" electrodes so far as the static discharge was concerned.) In order to maintain a stable discharge, it was found necessary to use 1100 megohms total resistance in place of the 600 megohms. The results of the dynamic

experiments are plotted in figure 18, and this is cross-plotted on figure 16 ("Small Electrodes"). The anode and cathode currents remained identical (at least to within 5 per cent) over the range tested, but a much larger (factor of 2) voltage was needed compared to the "Large Electrodes" curves on figures 15 and 16. It is difficult to explain this magnitude of voltage difference between the two cases solely by means of an "ion potential well". An alternative is that a significant number of positive ion - electron pairs are now being blown out of the discharge, thus decreasing its "efficiency" with the result that a much larger voltage is now needed to maintain a given current. *

In general, the mechanisms at work in this section are largely unclarified. However, despite the problems involving the metal tunnel and floating supply, there can be no doubt that a strong interaction of the discharge with the flow has been observed.

See Section V. 2. Suggested Experiments, under Part V. Suggestions for Further Study.

* The possibility that fewer ion-electron pairs are produced by the smaller electrodes is contradicted by the comparison of the static data with the smaller and larger electrodes.

IV. NORMAL GLOW CURRENTS

IV. 1. Approach and Objectives

Having discussed the breakdown problem and sub-normal glow currents, we turn now to the microampere to milliamperere current levels found in the normal glow regime (see figure 13). At this point, the electric field is distorted, the potential "drop" has assumed a large value close to the cathode, and the current increases at constant voltage. Hence, the transverse electric field should be quite small across a long ("positive") column where the discharge meets the free stream exactly as in the static discharges (electric fields in static discharges in the positive column are approximately a few volts/cm). In this case then, the possibility exists that the discharge is much less "rigid" and will tend to yield more to the free stream.

With smaller electric fields, the transit times ($\Delta \tau$) of the ions and electrons will be greater and there will be more time for the flow to act on the discharge particles and give them a correspondingly larger impulse $F\Delta\tau$ (assuming the transverse forces F due to the air stream remain about the same).

Since the currents used in this part of the work were much higher than before, we have to calculate the maximum discharge current density that can be used without violating the condition that we have a one-way interaction of the flow upon the discharge.

Eventually, we reach a point where the Joule heating of the stream by the discharge is sufficient to change the parameters (e. g., density and velocity) of the stream significantly and to destroy the one-way

relationship. To check this point, we will compare the kinetic energy density of the free stream $\frac{1}{2}\rho_{\infty}U_{\infty}^2$ (Joules/m³) where ρ_{∞} is the free stream density (Kg/m³), and U_{∞} is the free stream velocity (m/s), with the Joule heat produced by the discharge JE (Joules/m³s), where J is the current density (A/m²), and E is the electric field strength (V/m), in the time that a free stream molecule travels the streamwise length of the electrode area w/U_{∞} (s).

Hence this condition becomes

$$JE(w/U_{\infty})/\frac{1}{2}\rho_{\infty}U_{\infty}^2 < 0.05 \quad (\text{say}), \quad (11)$$

or

$$J < 0.025 \rho_{\infty} U_{\infty}^3 / wE .$$

From the higher current values obtained in the low-intensity glow discharge experiments, we may estimate the quantities in the RHS as follows for three stagnation pressure levels, taken to be 20 psig, 50 psig, and 80 psig:

| Quantity | | 20 psig | 50 psig | 80 psig |
|---|----------------------|---------|---------|---------|
| ρ_{∞} | (Kg/m ³) | 0.0125 | 0.0245 | 0.036 |
| U_{∞} | (m/s) | 800 | 800 | 800 |
| w | (m) | 0.01 | 0.01 | 0.01 |
| E | (V/m) | 17,500 | 22,500 | 30,000 |
| $\frac{0.025\rho_{\infty}U_{\infty}^3}{wE}$ | (A/m ²) | 915 | 1390 | 1540 |

Hence, say, $J < 1000 \text{ A/m}^2$, or

$$J < 100 \text{ mA/cm}^2 \text{ for } \frac{JE(w/U_\infty)}{\frac{1}{2}\rho_\infty U_\infty^2} < 0.05. \quad (12)$$

We now check the change in the free stream parameters relevant to the discharge (i. e., density and velocity) for this value of J . To do this roughly, we use the differential form of the one-dimensional inviscid relations for a thermally and calorically perfect gas:

$$\begin{aligned} d(\rho U) &= 0 \\ \rho U dU &= -dP \\ c_p dT + U dU &= dq \\ \frac{dP}{P} &= \frac{d\rho}{\rho} + \frac{dT}{T} \end{aligned}$$

where

$$q = \frac{EJ \frac{w}{U_\infty}}{\rho_\infty} \quad (13)$$

is the heat added per unit mass and is considered very small compared to $U_\infty^2/2$.

These equations may be solved for dU/U , giving

$$\frac{dU}{U} = \frac{dq}{c_p T} \left(\frac{1}{1 - M^2} \right) \quad (14)$$

where M is the Mach number.

For $M \gg 1$ and the ratio of specific heats = 1.4 (for air)

we have

$$\frac{U_2 - U_\infty}{U_\infty} \approx -0.2 \Omega \quad (15)$$

and

$$\frac{p_2 - p_\infty}{p_\infty} \approx 0.2 Q \quad (16)$$

where $Q = EJw / \frac{1}{2}\rho_\infty U_\infty^3$ is the non-dimensional heat added. For

$$Q = \frac{EJw}{\frac{1}{2}\rho_\infty U_\infty^3} = 0.05, \quad (17)$$

$$\frac{U_\infty - U_2}{U_\infty} \approx 0.01 \quad (18)$$

and

$$\frac{p_2 - p_\infty}{p_\infty} \approx 0.01. \quad (19)$$

Hence, if we operate with current densities less than 100 mA/cm^2 , the parameter $Q = EJw / \frac{1}{2}\rho_\infty U_\infty^3$ will be less than 0.05, the density and velocity changes in the free stream will be less than a per cent or so, and essentially a one-way interaction will occur between the free stream and the discharge.

Knowing the current density limitations, it remains to pick the type of experiments that will yield useful results. First, obviously, we can make total current measurements at each electrode similarly to the sub-normal case. However, in addition, we have the possibility of measuring current distributions by use of segmented electrodes, now that currents are high enough and the discharge area large enough. Hence, we may compare current distributions in a

static discharge with the current distributions in the presence of the free stream at, say, given external current levels and discharge densities.

IV. 2. Description of Experiments

IV. 2. 1. Electrode and Flow Geometry. In order to measure current distributions over the electrodes, the electrodes were segmented as shown in figures 20 and 21. Each electrode proper was made of five copper segments 1/16" thick in a 'Rogowski'⁽²⁾ shape as seen from the stream direction with the edges rounded. These electrodes were spaced 1/32" apart and insulated from each other with Micarta spacers. To prevent high-electric-field end effects, half-Rogowski electrodes, suitably rounded in the same manner as the segments, were likewise positioned at each end. This arrangement was mounted in lucite flat plates of the shape shown in figure 20 with suitable supports. Insulating cement was used around the electrodes to cover the end pieces completely and leave a portion 1×0.1 cm exposed of each electrode. Hence, an active electrode streamwise length of about 1.1 cm resulted with a total active discharge region area of about 1.1 cm^2 and an area of 0.55 cm^2 at the electrodes proper. The electrode leads were then attached from below the flat plates and led out through the supports. The separation was maintained at 2 cm for all of the tests (see figure 21). The flat plate geometry was chosen so as to have reasonably thin boundary layers and to cause a minimum disturbance of the stream at this separation (see figure 30). For purposes of rough calculation, the disturbances of the stream

across the gap (e. g., shock waves) can thus be ignored and any assessment of the gross effects of the stream velocity upon the discharge will be made using free stream values of velocity and density.

IV. 2. 2. Test Equipment. The test equipment and circuit used are shown schematically in figure 21. A fully-floating voltage source of stepped batteries was used as a power supply (see Section III). A Simpson 260 meter was calibrated to read the voltage of the batteries, draining a maximum of 50 μ A in the process, and the discharge voltage was calculated using the total current and known ballast resistors. A choice of ballast resistors was mounted on a pinboard as was the switching arrangement for the electrode segments. A Simpson 269 meter was used to read total currents, while a Keithley model 600A fully-floating battery-powered electrometer was used to read the segment currents. For convenience, the current scales were employed, and these caused a change in potential of at most 0.01 volt (full scale) in the electrode being measured compared to the others. The current was measured by pinning the electrometer across the closed switch to the appropriate electrode, opening the switch to sample the current, closing the switch, changing the electrometer to another electrode, etc. This process does not disturb the discharge.

A bell-jar, pressure pump, and Wallace-Tiernan gauge (0.1 to 20 mm Hg) were used in the static tests (see figure 22).

IV. 2. 3. Static Tests. In order to check the electrode geometry and to offer a comparison with wind tunnel tests, extensive tests were made in a bell-jar (see figure 22). The static pressures that correspond to low wind tunnel densities across the electrodes lie in

the 2- to 8-mm Hg range of bell-jar pressure. This fact was verified by the correspondence (between static and dynamic tests) of the voltage levels at equal currents in the high sub-normal glow regime. Accordingly, measurements were made at static densities of 2, 4, and 8 mm Hg with total currents covering five orders of magnitude from 10^{-7} amperes to 10^{-2} amperes, all well within our established one-way interaction criterion of $J < 100 \text{ mA/cm}^2$.

First, voltage-total current measurements were made over the complete ranges noted above. Secondly, current distribution measurements at both anode and cathode were made at decade current intervals. Thirdly, anode no. 1 (the first anode segment from an upstream direction) was operated and the current distribution at several total current levels was read at the cathode. The process was reversed, and anode distributions were recorded with cathode segment no. 1 activated.

IV. 2. 4. Results and Discussion of Static Tests. The voltage-total current data were plotted in figure 23. At the low currents, the discharge voltage is coming down from the breakdown value, being controlled and made stable by the large, 1000 M Ω ballast resistor. At a current level of about 10^{-6} amperes, we identify the sub-normal to normal glow transition by the flattening of the voltage curves. In this region, the faint glow was very uniform and increased in intensity up to about 10^{-4} amperes, after which it became non-uniform and tended to concentrate on just one or two electrode segments (see current distributions in figure 23). After reaching new minimums around 10^{-3} amperes, the voltage began increasing, and at 10^{-2} amperes the

glow had become noticeably uniform again. The rather unusual two modes in the normal glow regime must be attributed in some manner to the electrode geometry. Therefore, we confine our attention to the first mode with its remarkably uniform properties covering two orders of magnitude in current from $1\mu\text{A}$ to $100\mu\text{A}$.

Several anode and cathode current distributions were taken at each pressure and total currents of 1, 10, and $100\mu\text{A}$. These are plotted in figures 24 and 26. It was not possible to take data consistently at 8 mm Hg because of minor instabilities, but the appearance of the glow was very uniform and qualitatively very similar to the glow at 2 and 4 mm Hg for each of the three currents.

To find out the sensitivity of the glow to changes in conditions at one electrode, static runs were made with just the number one segment of one electrode operated, with the distribution read at the other as shown in figures 25 and 27. This experiment demonstrated a rather pronounced insensitivity of the cathode current distribution to the anode position or size. The anode, however, was very sensitive to the cathode position or size. Accordingly, an attempt was made in the dynamic case using the number one segment (upstream) of the cathode to see if the flow shifts the static-type anode distribution.

All of the curves mentioned above show considerable reproducibility for the particular pair of electrodes constructed, although they would be different for another pair.

IV. 2. 5. Dynamic Tests. After the completion of the bell-jar tests, the electrodes were mounted in the wind tunnel in the manner shown in figures 28 and 29. The flow patterns (Schlieren) are given

in figure 30 for four pressures.

In order to check the voltage-current characteristics found in the static tests from 1 to 100 μ A (see figure 23), the discharge voltage and anode and cathode currents were measured over this range for tunnel pressures of 0, 20, 40, and 60 psig. As in the sub-normal glow tests, the total anode and cathode currents were sensibly the same, certainly being within 5 per cent of one another for all electrode combinations. Furthermore, as in the static tests, the V-I characteristics were very uniform (see figure 31).

Having identified the same working range in the static and dynamic tests, the same measurements that were done in the static case were carried out in order to see what, if any, variation exists between the two cases. Accordingly, current distributions were made with all of the electrode segments functioning at various tunnel pressures and current levels (see figures 32, 34, 36, 38). (For the conversion from free-stream pressure or density to bell-jar pressure, see figure 6.) Again, as in the static case, the number one segment of one electrode was switched on by itself and the current distribution read at the other for various currents and pressures (see figures 33, 35, 37, 39).

During these tests, it was found that the current distribution corresponded to what one would expect qualitatively from the appearance of the emitted visible light. Hence, several different combinations of electrodes were tried at 0 psig and $I = 1 \mu$ A; the voltage change for a constant 1μ A current was noted and the glow sketched, giving an interesting visual indication of the current paths and their

relationship to electrode position (see figure 40).

IV. 3. Results and Discussion

Comparing the dynamic and static voltage - total current curves over the range 1 to 100 μ A (figures 23, 21), we see that they are similar (both sets are flat), but that the voltage variation with pressure is considerably smaller in the dynamic case than in the static case. (From figure 6, the density correspondence of the free-stream total pressure and bell-jar pressure is 0 psig => 3.5 mm Hg, 20 psig => 8.3 mm Hg, 40 psig => 13 mm Hg, 60 psig => 17.8 mm Hg.) Furthermore, the voltage curves go through a minimum in the 0 - 20 - 40 psig range. The data taken at 0 psig and 20 psig in the wind tunnel may be properly compared with the static data taken, and the other pressures used to attempt to find qualitative trends with pressure (density).

Comparing figures 24 and 26 with figures 32 and 34, we find an unmistakable flow effect, with the current paths tending to be "blown" to the rear of the electrode area, increasing smoothly on the cathode, and concentrating mainly on segment 5 of the anode. To check the tendency of the glow to be swept downstream, the number one anode and cathode segments were operated in turn, and the current distribution read at the cathode and anode respectively. As in the static case, the cathode current distribution did not change significantly with anode choice, as can be seen by comparing figures 32 and 34 with figures 33 and 35. However, the static distribution at the

anode with cathode segment number one operating, given in figures 25 and 27, is changed considerably by the influence of the flow, with the maximum current moving downstream compared to the static case and the discharge being inclined at an angle with the vertical. Operating only the second cathode segment essentially shifted the anode pattern down one segment. Interestingly, the "discharge angle" is of the same order of magnitude that one would derive from an estimate of ion velocities in conjunction with the free stream velocity (see Section II. 3). If we accept the assumption that the free stream acts directly on the ions to a much greater extent than it does directly on the electrons, then a possible explanation for this downstream inclination is the following: the ions that are formed in the body of the discharge tend to be swept downstream and their electric fields tend to deflect the electrons downstream from their "straight line" travel across the discharge (i. e., from anode number one to cathode number one). Even if this is the case, a problem of what happens to the positive ions remains in view of the fact that little, if any, net current leaves the discharge ($I_A \approx I_C$). A consistent explanation, at least, is that those positive ions that are not pulled to the cathode by an electric field (see the "ion potential well" argument in Section III. 3) take electrons from the deflected swarm with them as they leave the discharge by means of their electric fields. The net result is that there is a lack of electrons at the anode per unit time prevented from impinging on the cathode by the free stream. Externally, this would appear as an efficiency effect and increase the voltage necessary for a given current with flow over the static case; the

voltages are significantly higher, at least at the low densities.

At the higher pressures (densities) and higher currents, this downstream angle seemed to decrease, with the current turning up mainly at the number one anode. In addition, however, other effects arose which invalidates the results of these high pressure measurements. These are recorded in the distributions and sketches of the visible glow, figures 36, 37, 38, 39.

One possible explanation for, or at least contributing to, this behavior is that (as noted previously) the 40 psig and 60 psig tunnel total pressures correspond to free stream densities of 13.0 and 17.8 mm Hg, respectively (see figure 6). This is far above the range, particularly at the higher currents, where stable measurements could be made in the static case. (In the static case, 8 mm Hg pressure proved just high enough so that reliable data could not be taken; see Section IV. 2. 4.) Consequently, no static counterparts to these data exist for comparison purposes. In addition, as in the static case at the higher densities, the final distribution depended upon how the electrode segments were turned on (a hysteresis effect), so that several modes of operation were possible. The distributions plotted were the ones usually obtained when the discharge was initially struck across the electrode segment configuration shown. This behavior is in contrast to the results at the lower pressures, which were completely independent of how the discharge was turned on and the "path" used to arrive at the final electrode segment configuration by switching the various electrode segments.

Another possible contributor to the unusual results at high densities is the formation of an "ion potential well" (see Section III. 3) and thus an "electron potential barrier" at high currents and pressures. * The presence of this electron barrier would explain some of the current distributions (see the $100\mu\text{A}$ distributions and sketches at 40 and 60 psig on figures 36 and 38, respectively).

It appears that the data taken at 0 psig and $1\mu\text{A}$ is relatively free from the several objectionable effects mentioned in the two previous paragraphs. Accordingly, the 0 psig, $1\mu\text{A}$ operating condition was used to get a visual indication of the position of the electron current for various electrode segment geometries (the visible glow roughly confirmed the measured electrode current distributions for all of the configurations in figures 23 through 27 and figures 32 through 39).

The discharge characteristics as a function of the relative positions of anode and cathode are shown on figure 40. The prevailing tendency indicated in these sketches is for the voltages (at constant current) to decrease (i. e., discharge is more "efficient") when the cathode is moved upstream relative to the anode. In addition, at both ends (upstream and downstream) of the electrodes, the glow seems to bend, following what looks like an electric field curvature (at first, the impulse is to think of the downstream curva-

* From an examination of figure 17, the discharge will probably float more and more negative as higher pressures are reached; that is, an "ion potential well" or "electron potential barrier" will grow. At the low densities, this barrier effect will be much smaller.

ture as being similar to a loaded column, an analogy useful in some arc work with transverse flows⁽¹⁵⁾, but the explanation offered is more probable). If we accept the thesis that the curvature is simply an electric field effect, a possible explanation for the decreased voltages noted above for forward movement of the cathode "emitter" is as follows: the electrons emitted at the cathode are directed into the free stream velocity at the forward end, thus helping the discharge particles to compensate for the free stream velocity by giving them a "head start"; whereas at the rear, the electric field has a component along the free stream direction, and electrons started along these field lines create ionizations that are in a disadvantageous position with respect to the electrodes.

V. SUGGESTIONS FOR FURTHER STUDY

V. 1. Analysis

In principle, the analysis of the experimental results of the preceding sections should be facilitated by the absence of severe chemical, thermal, and electromagnetic effects. The theoretical objective is to find the current paths as a function of the electric and fluid-mechanical parameters. Specifically, one would like to know the ion and electron number densities, $n_{i,e}$, the mean velocities, $\vec{v}_{i,e}$, and the electric field \vec{E} in and around the discharge region.

Of the pertinent equations, we might write first a drift equation for each species

$$\vec{v}_i = k_i(E) \vec{E} + \vec{U}_\infty \quad (20)$$

$$\vec{v}_e = k_e(E) \vec{E} + \vec{U}_\infty \quad (21)$$

where diffusion terms are ignored, being very small compared to the other terms.*

In addition, we have Poisson's equation governing the changes in the applied electric field due to space charges, some of which may be caused by the stream tending to separate the ions and electrons:

$$\nabla \cdot \vec{E} = \frac{\rho}{\epsilon_0} = \frac{e}{\epsilon_0} (n_i - n_e) \quad (22)$$

A continuity equation for each specie may be written

$$\nabla \cdot (n_i \vec{v}_i) = \dot{n} \quad (23)$$

* Free diffusion of the charged particles is insignificant compared to the stream velocity for small mean-free-path high Mach number flows.

$$\nabla \cdot (n_e \bar{v}_e) = \dot{n} \quad (24)$$

where \dot{n} is the net number of ion pairs created per unit volume per second. These equations are not easy to solve as they stand even if appropriate boundary conditions could be formulated (see Ward⁽¹³⁾ for discussion of a simpler though similar problem with no flow). The problem reduces to solving a highly non-linear partial differential equation of higher order. One therefore seeks to find out what approximations can be used to the equations and boundary conditions and still not render them trivial or irrelevant.

V. 2. Suggested Experiments

The problem of positive-ion current loss from the discharge remains, both for the sub-normal and normal glow regimes. [See Mettler's thesis (16).] An experiment that may clarify this situation could use a doubly-switched battery power supply such that the tunnel potential is always midway between the anode and cathode potentials. Then the stray current problem may be attacked, say, by the use of a larger facility (such as the Jet Propulsion Laboratory hypersonic wind tunnel) and/or the use of a series of support geometries that should change any stray current paths, while still maintaining the electrode and local flow geometry. A "limiting" geometry surrounding the discharge may be obtained such that stray currents would not be significant. If this procedure is possible, then the current difference between the electrodes (if any) which may be attributed to a net number of positive ions blown out of the discharge region, could be studied as a function of the discharge and stream parameters.

The objective remaining is the more detailed description of the electron and ion concentration and the current paths in the discharge gap. In particular, the streamwise distribution of the current density (cf. Section IV) is in need of clarification.*

It might be helpful to choose different geometries for subsequent experiments. For example, conduction between two thin, parallel cylinders normal to the stream seems to have some attractions, such as a uniform flow field and a known electric field (at least for limiting cases of neutrality or extremely small charge density). The study of the conductance of such an electrode system should give information on the bending of the current path due to the flow. Essentially, what one is striving for experimentally is to formulate the problem and get results that are in some sense at least qualitatively independent of the exact geometry used and the particular condition of the electrode surface. (An example is the breakdown - density gradient phenomena in Section II.) This criterion becomes of even more importance if more complex segmented electrodes are used and as finer details are sought.

If there is reason to believe that one is viewing a "general" phenomenon, the charged-particle population and the gain/loss mechanism in the gap should finally be studied with more sophisticated techniques such as optical filters, spectroscopy, and possibly Langmuir probes. The success of these techniques is rather

* More information is needed on the interaction of two critical "layers"; the viscous boundary layer and the discharge electrode layer.

crucially dependent upon the possibility of obtaining some theoretical results to use as a guide and basis of comparison.

VI. CONCLUSIONS

(1) Within the range of parameters investigated, it is possible to cause dielectric breakdown and to maintain self-sustained discharges with the presence of a hypersonic stream of air flowing transversely to the two electrodes.

(2) The density gradients in the viscous boundary layers help reduce the breakdown voltages considerably below the values they would have in the presence of a uniform static gas at free stream density.

(3) The dynamic (velocity) effect upon breakdown is smaller than might be expected from simple geometrical considerations at various densities and reduced electrode widths, until the extreme limit of small electrode streamwise width and high density is reached.

(4) At high densities in the sub-normal glow regime, much higher voltage - current characteristics (for equal currents) are obtained when the ratio of electrode exposed streamwise width to separation is reduced, yet the static voltage - current characteristics are closely maintained.

(5) In the normal glow regime, pronounced downstream shifts of current paths due to the free-stream velocity are observed when current distributions (obtained with segmented electrodes) are compared to the static bell-jar distributions at similar densities. The most impressive case was obtained when just the most upstream cathode segment was activated and the distribution read at the anode segments. In the static case, most of the current turned up at the

opposite (upstream) anode, but with flow the current bump was shifted downstream and the discharge formed a characteristic angle with the flow direction.

(6) In general, the discharges in the hypersonic stream were considerably more stable and could be examined successfully at much higher average densities than bell-jar discharges.

REFERENCES

1. von Engel, A.: Ionized Gases, Oxford at the Clarendon Press, London (1955).
2. Cobine, J. D.: Gaseous Conductors, Dover, New York (1955).
3. Handbuch der Physik, Vol. XXII, Springer Verlag, Berlin (1956).
4. Loeb, L. B.: Basic Processes of Gaseous Electronics, University of California Press, Berkeley and Los Angeles (1955).
5. Kendall, James M., Jr.: "An Experimental Investigation of Leading-Edge Shock-Wave — Boundary-Layer Interaction at Mach 5.8", Journal of the Aeronautical Sciences, Vol. 24, No. 1, pp. 47-56 (January 1957).
6. Brown, Sanborn C.: Basic Data of Plasma Physics, The Technology Press of the Massachusetts Institute of Technology, and John Wiley and Sons, Inc., New York (1959).
7. Meek, J. M., and Craggs, J. D.: Electrical Breakdown of Gases, Oxford at the Clarendon Press, London (1953).
8. Massey, H. S. W., and Burhop, E. H. S.: Electronic and Ionic Impact Phenomena, Oxford at the Clarendon Press, London (1952).
9. Handbuch der Physik, Vol. XXI, Springer Verlag, Berlin (1956).
10. Eimer, M., and Nagamatsu, H. T.: "Direct Measurement of Laminar Skin Friction at Hypersonic Speeds", GALCIT Hypersonic Wind Tunnel Memorandum No. 16 (July, 1953).
11. Baloga, P. E., and Nagamatsu, H. T.: "Instrumentation of GALCIT Hypersonic Wind Tunnels", GALCIT Hypersonic Wind Tunnel Memorandum No. 29 (July, 1955).
12. Korkegi, R. H.: "Transition Studies and Skin Friction Measurements on an Insulated Flat Plate at a Hypersonic Mach Number", GALCIT Hypersonic Wind Tunnel Memorandum No. 17 (July, 1954).
13. Ward, A. L.: "Effect of Space Charge in Cold Cathode Gas Discharges", The Physical Review, Vol. 112, No. 6 (December, 1958).

14. Pipkin, A. C.: "Diffusion from a Slightly Ionized Region in a Uniform Flow", Physics of Fluids, Vol. 4, No. 10 (October, 1961).
15. Thiene, P. F., Chambers, J. E., and von Jaskowsky, W.: "An Experimental Investigation of the Behavior of an Arc Positive Column in the Presence of Forced Convection", Plasmadyne Corporation Report No. T-4TNO31-334, Santa Ana, California (1961).
16. Mettler, R. F.: "The Anemometric Application of an Electrical Glow Discharge in Transverse Air Streams", Ph. D. Thesis, California Institute of Technology, Pasadena, California (1949).

APPENDIX A

Derivation of α

In this paper, the classical Townsend approximation is used for α , the first ionization coefficient. Its derivation and limitations have been thoroughly discussed elsewhere^(1, 2); however, for an arbitrary gas density, $\rho = \rho(y)$, it assumes a slightly different form and will be re-derived here for convenience.

Briefly, it is assumed that the electrons do not gain energy by collision, that the electrons move only in the direction (y) of the field, and that the probability of ionization is zero for energies less than eV_i' , and is unity for energies greater than eV_i' where V_i' is an effective ionization potential and e is the electron charge.

An electron is assumed to start a path with an energy very small compared to eV_i' . The least distance that the electron has to move to gain enough energy for ionization from a uniform field E is then

$$l = V_i' / E . \quad (A-1)$$

The probability that the distance travelled by the electron is larger than l follows from the statistical distribution of mean free paths⁽²⁾,

$$\frac{n_l}{n_0} = e^{-l/\lambda_{en}} \quad (A-2)$$

where n_l/n_0 is the relative number of electrons travelling a distance greater than a given length l before collision, and λ_{en} is the electron-neutral mean free path.

If the average number of free paths per meter, $(1/\lambda_{en})$, is

multiplied by the probability of the path being of ionizing length, the probable number of ionizing collisions per electron per meter in the direction of the electric field is obtained:

$$\alpha = \frac{1}{\lambda_{en}} e^{-l/\lambda_{en}} = \frac{1}{\lambda_{en}} e^{-V_i'/E\lambda_{en}} \quad (\text{A-3})$$

But $1/\lambda_{en} = A\rho$, where A is a constant $= [m^2/Kg]$, and ρ is the gas density $= \rho(y)$. Also, for a uniform E , at breakdown, $E = V_b/d$, where V_b is the breakdown voltage and d is the electrode separation.

Finally, with $B = AV_i'$,

$$\alpha = A\rho(y)e^{-B\rho(y)d/V_b} = \left| \frac{\text{number of ion pairs formed}}{\text{electron-meter in direction of } E} \right| \quad (\text{A-4})$$

The values and ranges of validity of A and B have been determined by a number of experiments (see refs. 1, 2). For air, in MKS units,

$$A = 9.3 \times 10^5 [m^2/Kg] \text{ and } B = 2.3 \times 10^7 [V m^2/Kg]. \quad (\text{A-5})$$

APPENDIX B

Integration of the Breakdown Equation

The breakdown condition may be written in the form:

$$\int_0^d \alpha dy = \int_0^d A \rho(y) e^{-\frac{B \rho(y) d}{V_b}} dy = \ln \left(\frac{Y+1}{Y} \right) \quad (B-1)$$

Using the density profile $\rho = \rho(y)$ given in figure 4, we may integrate the above expression as follows:

$$\begin{aligned} \int_0^d \alpha dy &= \int_0^{\eta\delta} \alpha_1 dy + \int_{\eta\delta}^{\delta} \alpha_2 dy + \int_{\delta}^{d-\kappa\delta} \alpha_3 dy + \int_{d-\kappa\delta}^{d-\eta\kappa\delta} \alpha_4 dy + \int_{d-\eta\kappa\delta}^d \alpha_5 dy \\ &= (1+\kappa) \int_0^{\eta\delta} \alpha_1 dy + (1+\kappa) \int_{\eta\delta}^{\delta} \alpha_2 dy + \int_{\delta}^{d-\kappa\delta} \alpha_3 dy \end{aligned} \quad (B-2)$$

Let

$$C = \frac{B \rho_{\infty} d}{V_b}. \quad \text{Thus, } \alpha = A \rho e^{-C(\rho/\rho_{\infty})}. \quad (B-3)$$

Evaluating the integrals,

$$\int_0^{\eta\delta} \alpha_1 dy = \alpha_1 \eta\delta = \left(\frac{\delta}{d}\right) A (\rho_{\infty} d) \eta \lambda e^{-\lambda C} \quad (B-4)$$

$$\int_{\eta\delta}^{\delta} \alpha_2 dy = \delta \int_{\eta}^1 \alpha_2 d\xi = \delta \int_{\eta}^1 A \rho_{\infty} (M+N\xi) e^{-C(M+N\xi)} d\xi \quad \text{where } \xi = \left(\frac{y}{\delta}\right).$$

$$\int_{\eta\delta}^{\delta} \alpha_2 dy = \left(\frac{\delta}{d}\right) A (\rho_{\infty} d) M e^{-CM} \int_{\eta}^1 e^{-C N \xi} d\xi + \left(\frac{\delta}{d}\right) A (\rho_{\infty} d) N e^{-CM} \int_{\eta}^1 \xi e^{-C N \xi} d\xi$$

Now

$$\int_{\eta}^1 e^{-CN\xi} d\xi = \frac{e^{-CN\xi}}{-CN} \Big|_{\eta}^1 = \frac{1}{CN} (e^{-CN\eta} - e^{-CN})$$

and

$$\begin{aligned} \int_{\eta}^1 \xi e^{-CN\xi} d\xi &= \frac{\xi e^{-CN\xi}}{-CN} \Big|_{\eta}^1 + \frac{1}{CN} \int_{\eta}^1 e^{-CN\xi} d\xi \\ &= \frac{e^{-CN}}{-CN} + \eta \frac{e^{-CN\eta}}{CN} + \frac{1}{C^2 N^2} (e^{-CN\eta} - e^{-CN}) \end{aligned}$$

Hence:

$$\int_{\eta\delta}^{\delta} \alpha_2 dy = \left(\frac{\delta}{d}\right) A(\rho_{\infty}^d) \frac{e^{-CM}}{CN} \left\{ N\eta e^{-CN\eta} - Ne^{-CN} + \left(M + \frac{1}{C}\right) (e^{-CN\eta} - e^{-CN}) \right\}. \quad (B-5)$$

$$\int_{\delta}^{d-\kappa\delta} \alpha_3 dy = \delta \int_1^{\frac{d}{\delta} - \kappa} A\rho_{\infty} e^{-C} d\xi = \left(\frac{\delta}{d}\right) A(\rho_{\infty}^d) e^{-C} \left(\frac{d}{\delta} - \kappa - 1\right). \quad (B-6)$$

Substituting (B-4), (B-5), and (B-6) into (B-2), we have:

$$\begin{aligned} \int_0^d \alpha dy &= (1 + \kappa) \left(\frac{\delta}{d}\right) A(\rho_{\infty}^d) \eta \lambda e^{-\lambda C} \\ &+ (1 + \kappa) \left(\frac{\delta}{d}\right) A(\rho_{\infty}^d) \frac{e^{-CM}}{CN} \left[N\eta e^{-CN\eta} - Ne^{-CN} + \left(M + \frac{1}{C}\right) (e^{-CN\eta} - e^{-CN}) \right] \\ &+ \left(\frac{\delta}{d}\right) A(\rho_{\infty}^d) e^{-C} \left(\frac{d}{\delta} - (1 + \kappa)\right) = \ln\left(\frac{\gamma+1}{\gamma}\right), \end{aligned}$$

or,

$$\left(\frac{\delta}{d}\right) (1 + \kappa) \left[\eta \lambda e^{-\lambda C} + \frac{e^{-CM}}{CN} [\sim] \right] + e^{-C} - \left(\frac{\delta}{d}\right) (1 + \kappa) e^{-C} = \frac{1}{A(\rho_{\infty}^d)} \ln\left(\frac{\gamma+1}{\gamma}\right).$$

Solving for the parameter $(\delta/d)(1+\kappa)$,

$$\left(\frac{\delta}{d}\right)(1+\kappa) = \frac{\ln\left(\frac{\gamma+1}{\gamma}\right) - A(\rho_{\infty}d)e^{-C}}{A(\rho_{\infty}d)\left[\eta\lambda e^{-\lambda C} + \frac{e^{-CM}}{CN} [\sim] - e^{-C}\right]}$$

Finally,

$$\left(\frac{\delta}{d}\right)(1+\kappa) = \frac{\frac{\ln\left(\frac{\gamma+1}{\gamma}\right)}{A(\rho_{\infty}d)} - e^{-C}}{\gamma - e^{-C}} \quad (\text{B-7})$$

where

$$\gamma = \eta\lambda e^{-\lambda C} + \frac{e^{-CM}}{CN} \left[\left(M + N\eta + \frac{1}{C}\right)e^{-CN\eta} - \left(M + N + \frac{1}{C}\right)e^{-CN} \right]$$

and

$$M = \lambda - \left(\frac{1-\lambda}{1-\eta}\right)\eta$$

$$N = \left(\frac{1-\lambda}{1-\eta}\right)$$

$$C = \frac{B(\rho_{\infty}d)}{V_b}$$

The best curve fit to the experimental boundary layer density profiles occurs for $M = -0.747$ and $N = 1.747$ (see fig. 4).

APPENDIX C

Calculation of Sub-Normal Glow Current Level

To calculate the magnitude of the largest currents tolerable in order to avoid large space charge electric fields across the gap, we use Poisson's equation,

$$\frac{dE}{dy} = \frac{\rho}{\epsilon} \quad (\text{all MKS units})$$

where E is the electric field, y here is the distance measured from the anode, $\rho = \rho_i - \rho_e$ is the excess charge density, and $\epsilon \approx \epsilon_0$ is the dielectric constant for air. Now $\rho_i - \rho_e \approx \rho_i$, since space charge electric fields are mostly caused by positive ions.* Hence $\rho \approx \rho_i \approx J_i/v_{it}$ where J_i is the positive ion current density, and v_{it} is the average ion drift velocity transverse to the electrodes.

Then

$$\frac{dE}{dy} \approx \frac{J_i}{\epsilon_0 v_{it}}$$

We know J_i at most = J , and v_{it} is at least of order U_∞ (see discussion in Section II. 3).

Thus, we take $J_i = 100,000 I$ where I is amperes discharge current, and $v_{it} = 1,000$. For J_i , we have tentatively assumed that the area of the smaller electrodes (0.1 cm^2) is just covered by the discharge. Then

$$\frac{dE}{dy} \approx \frac{100,000 I}{8.87 \times 10^{-12} \times 1000} \approx 10^{13} I \frac{\text{volts/meter}}{\text{meter}}$$

* See p. 213, ref. 2.

For less than a 10 per cent change in E over a distance like a boundary layer thickness (assuming $E = 5 \times 10^4$ V/m, b. l. t. = 0.005 m),

$$\frac{dE}{dy} < \frac{5 \times 10^3}{0.005} = 10^6$$

and

$$10^{13} I < 10^6 \quad \text{or} \quad I < 10^{-7} \text{ amperes.}$$

Hence, if we work in the 0.1 microampere region of the discharge, then large electric field distortion is avoided. For a qualitative indication of space charge effects upon the electric field, see fig. 6 of Ward⁽¹³⁾.

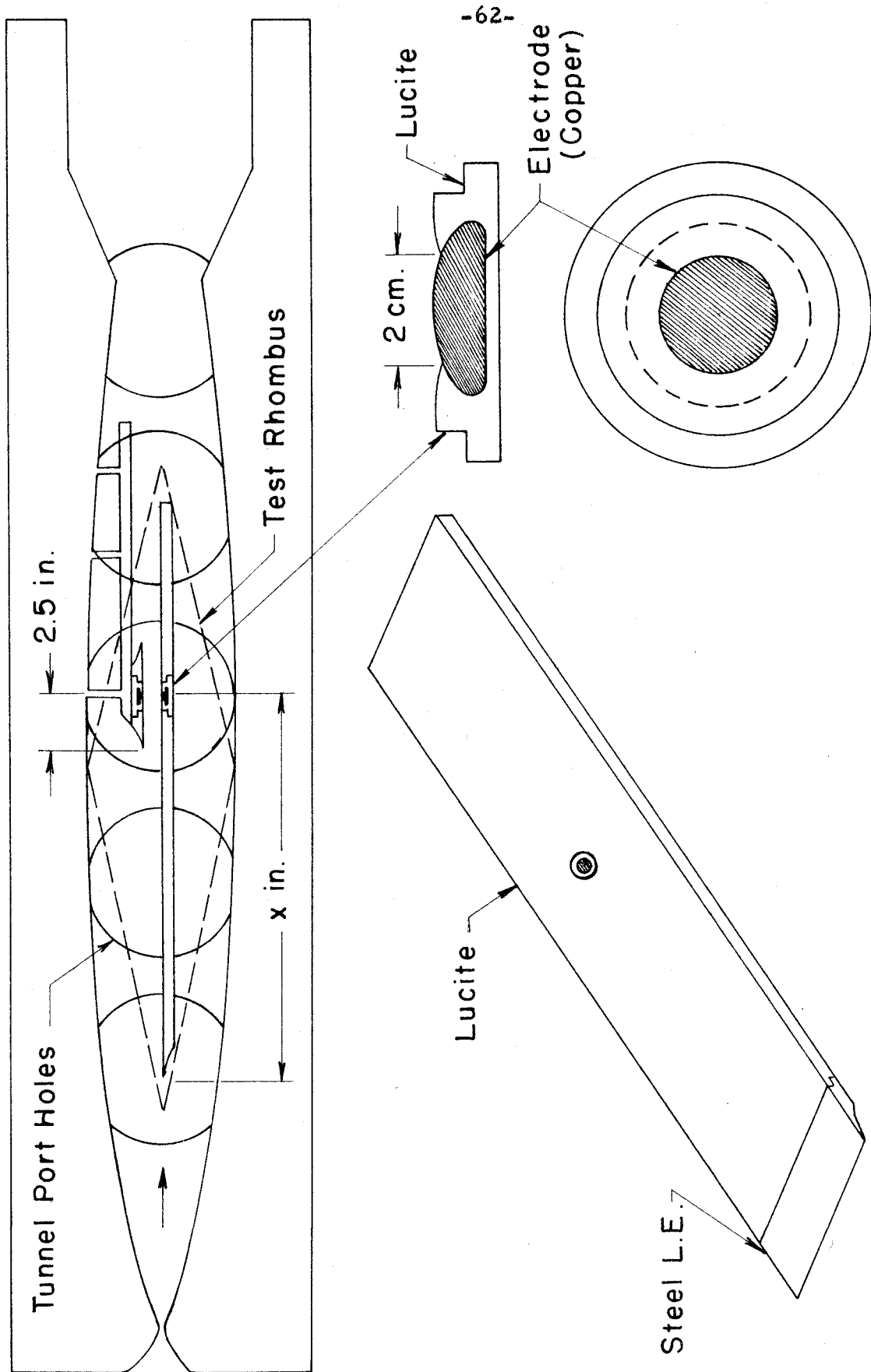


FIG. 1 - ELECTRODE GEOMETRY

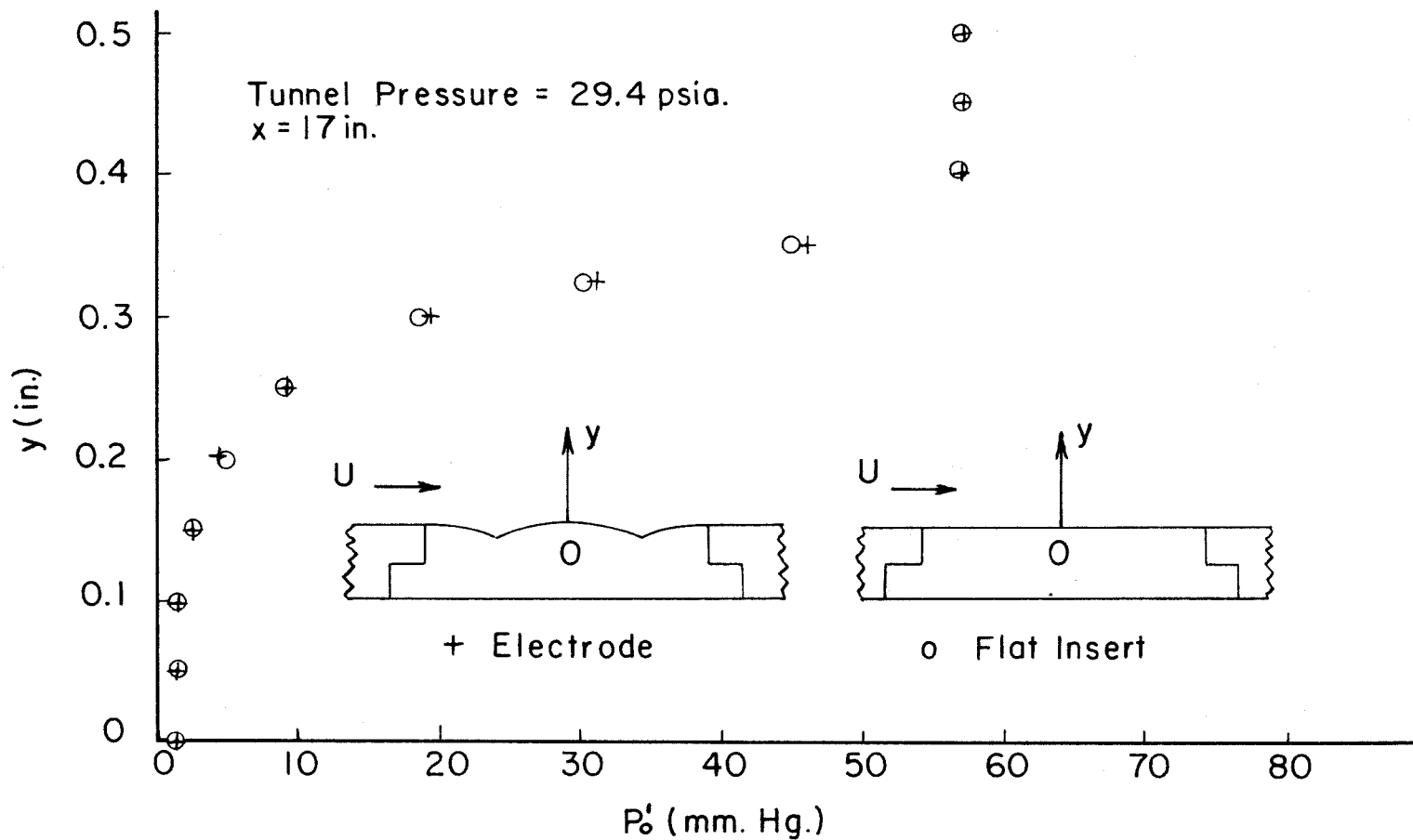


FIG. 2- TYPICAL TOTAL PRESSURE TRAVERSE ON ELECTRODE AND ON FLAT INSERT

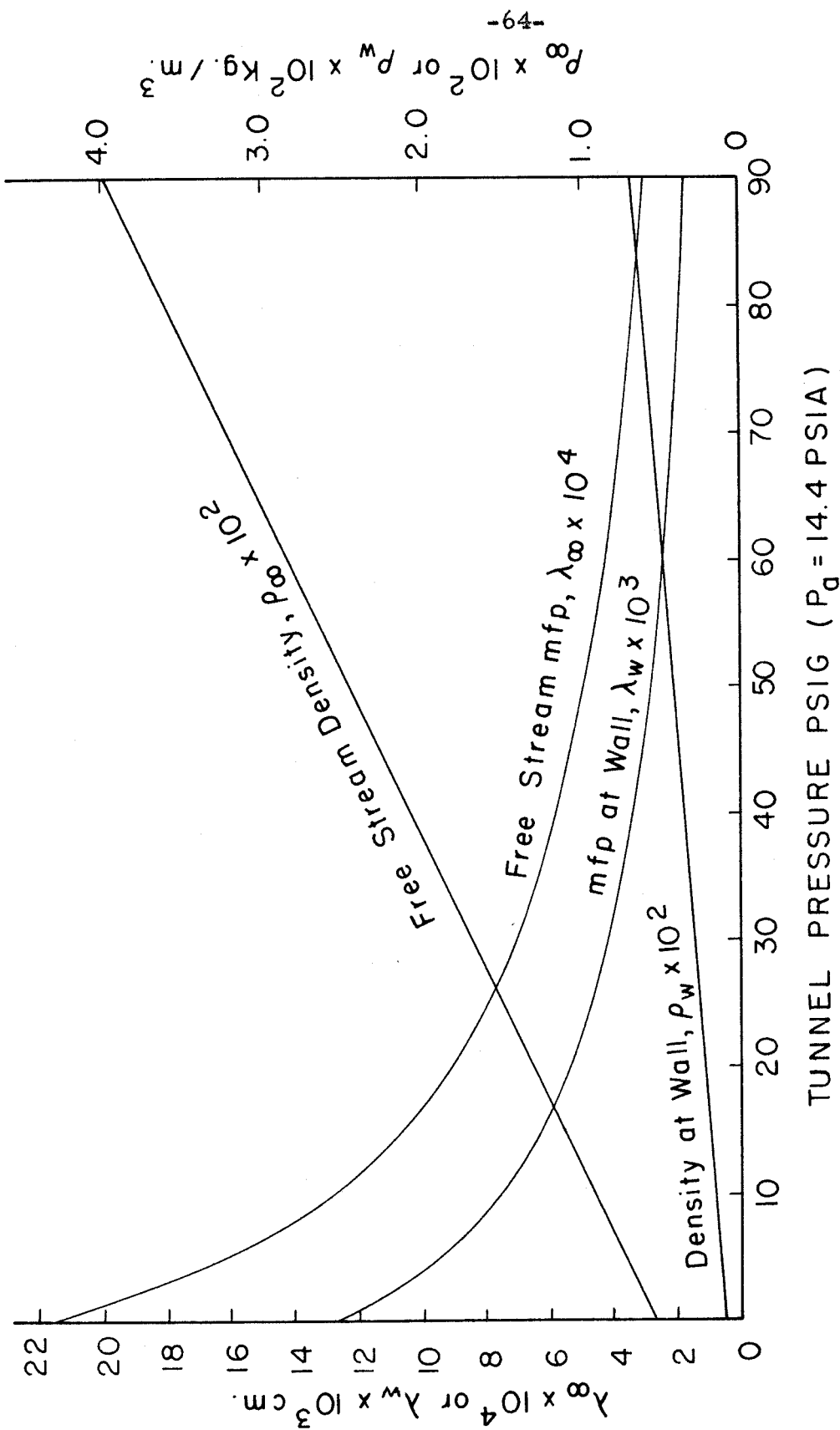


FIG. 3 - DENSITY AND NEUTRAL-NEUTRAL MEAN FREE PATH AS FUNCTIONS OF TUNNEL PRESSURE

APPROXIMATION

Region 1. $y = 0$ to $y = \eta\delta$
 $\rho/\rho_\infty = \rho_w/\rho_\infty = \lambda.$

Region 2. $y = \eta\delta$ to $y = \delta.$

$$\rho/\rho_\infty = M + N \left(\frac{y}{\delta}\right).$$

$$M = \lambda - \left(\frac{1-\lambda}{1-\eta}\right) \eta.$$

$$N = \left(\frac{1-\lambda}{1-\eta}\right).$$

Region 3. $y = \delta$ to $y = d - \kappa\delta$

$$\rho/\rho_\infty = 1.$$

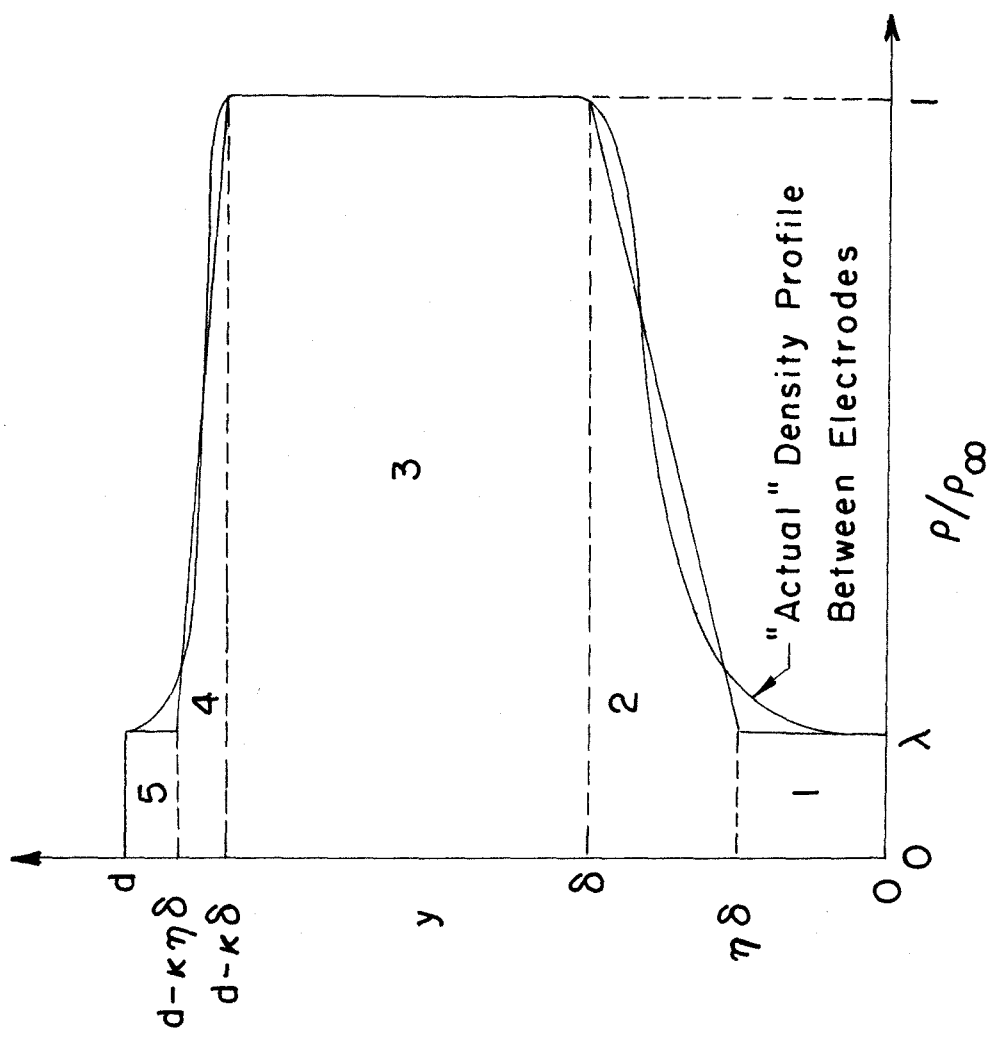


FIG. 4 - DENSITY PROFILE BETWEEN ELECTRODES

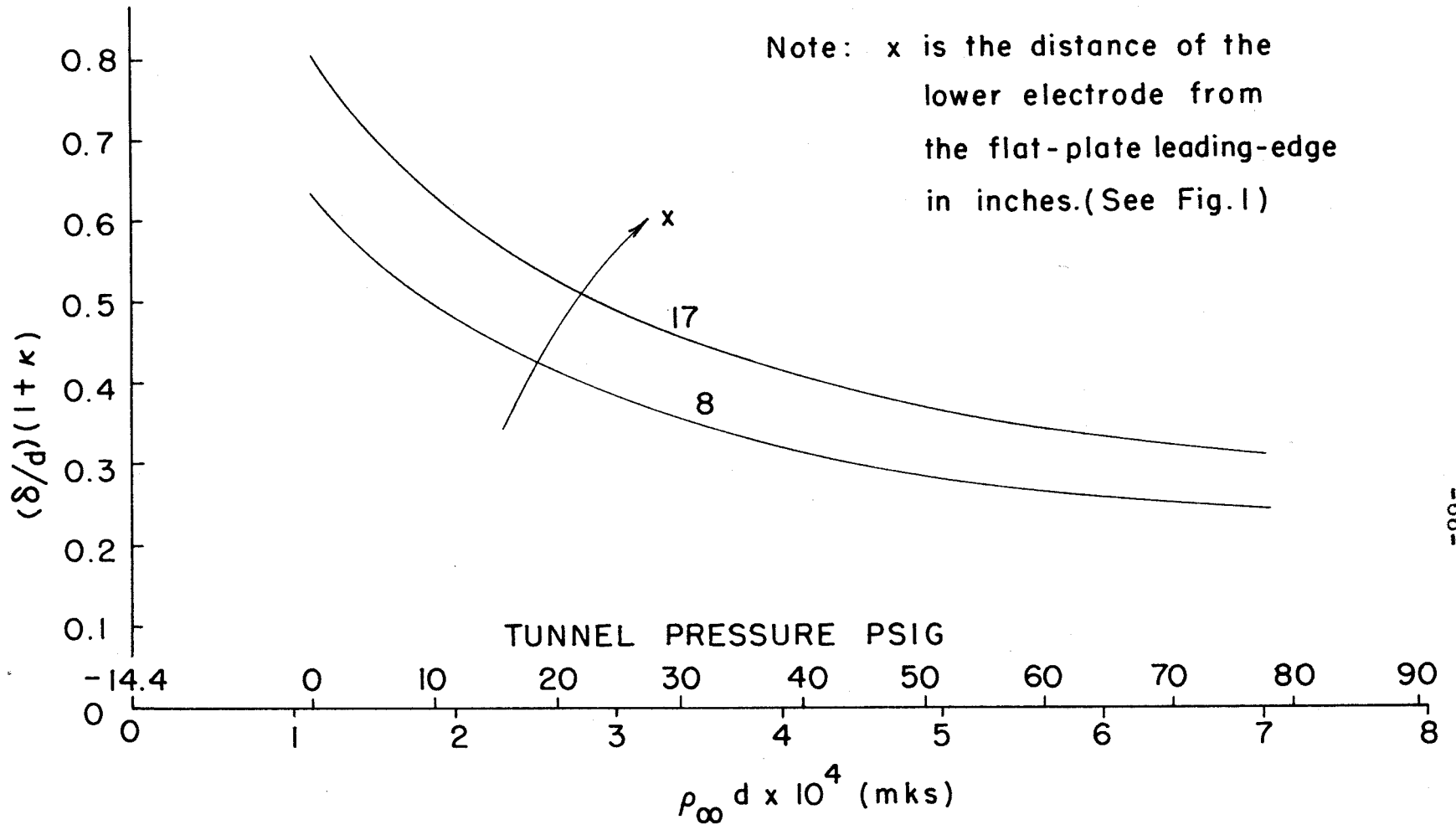


FIG. 5 - FRACTION OF ELECTRODE SEPARATION DISTURBED BY DENSITY GRADIENTS AS A FUNCTION OF THE PRODUCT OF FREE-STREAM DENSITY AND ELECTRODE SEPARATION

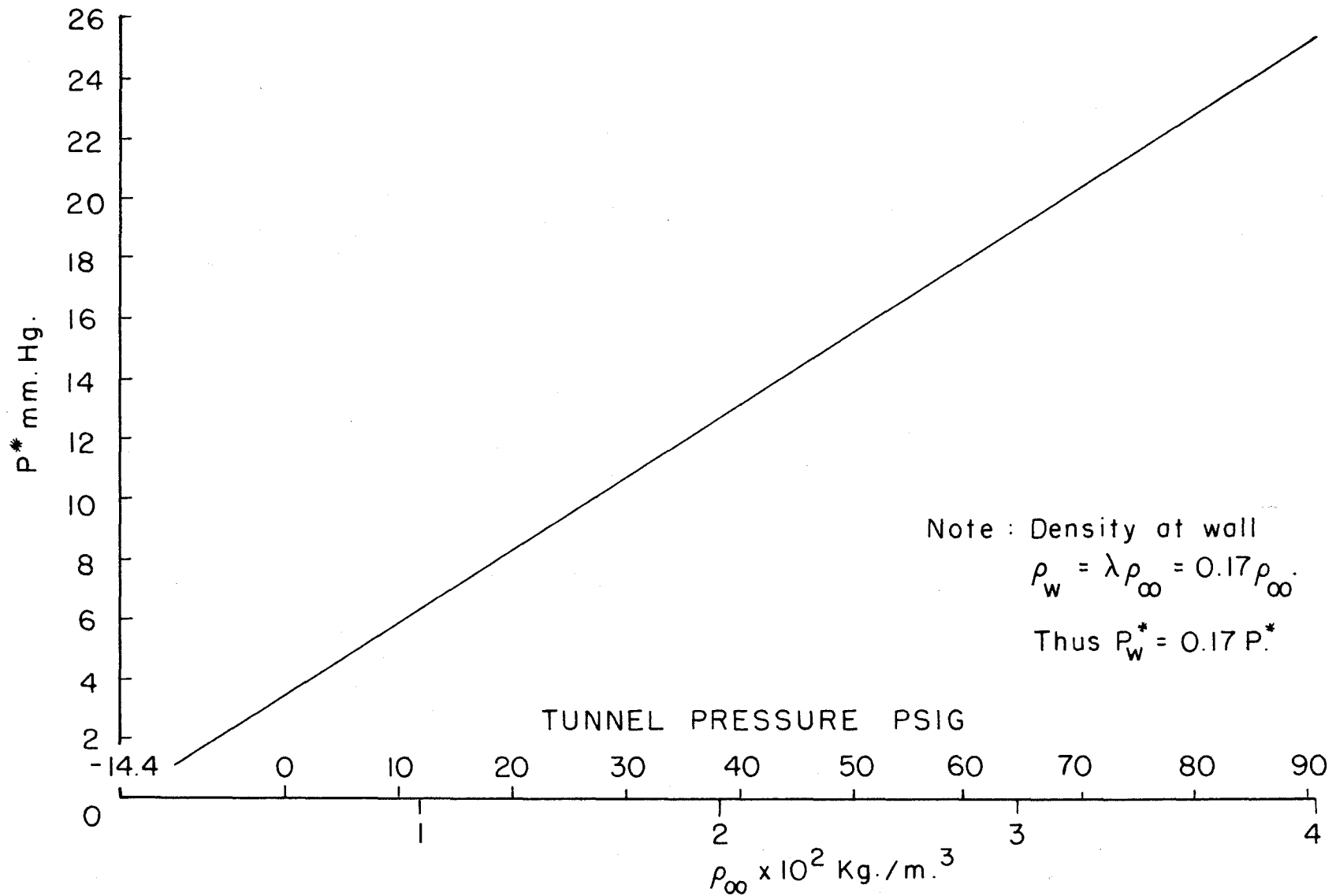


FIG. 6 - PRESSURE AT ROOM TEMPERATURE AS A FUNCTION OF FREE-STREAM DENSITY

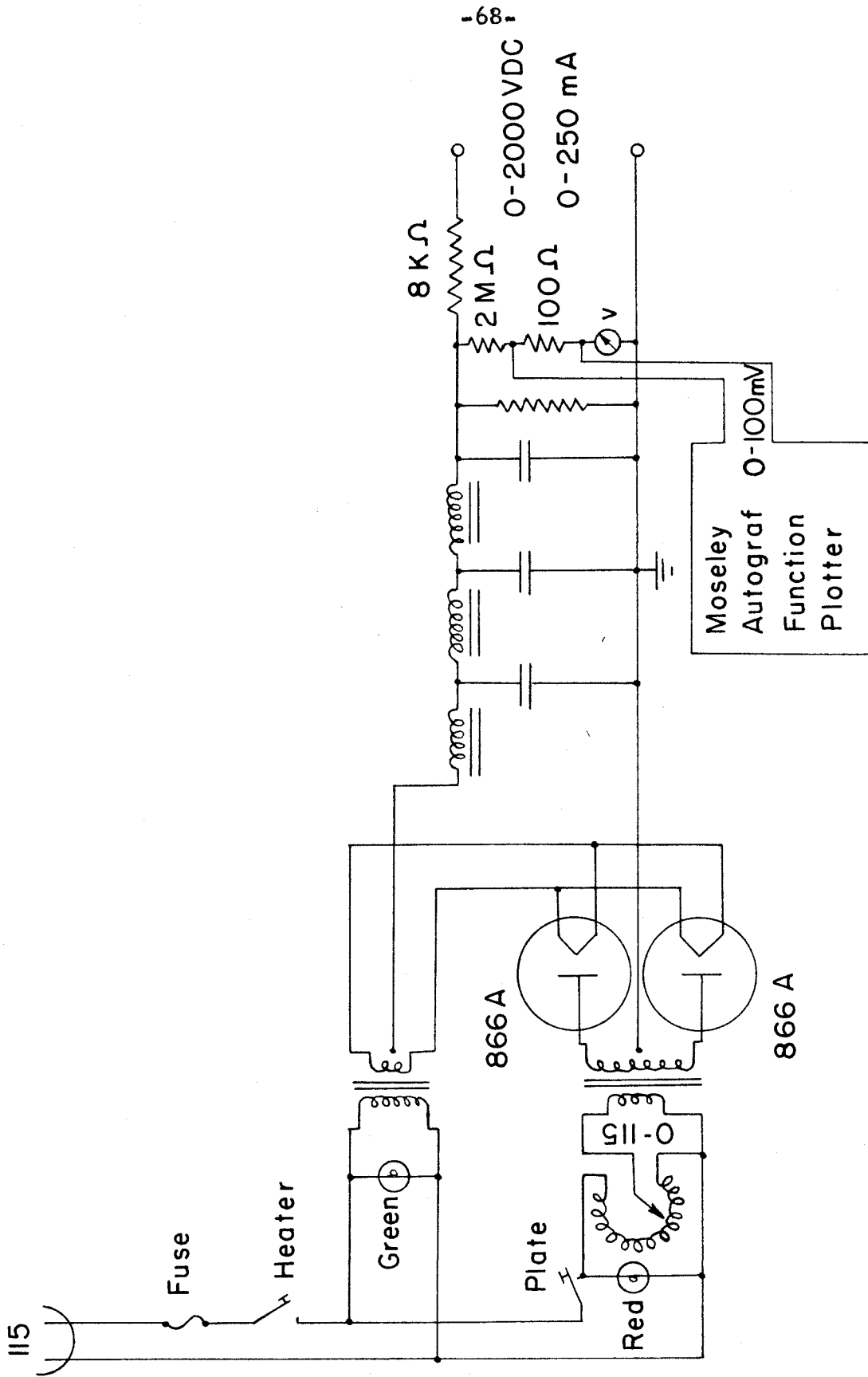


FIG. 7 - DIAGRAM OF POWER SUPPLY AND RECORDING CIRCUIT

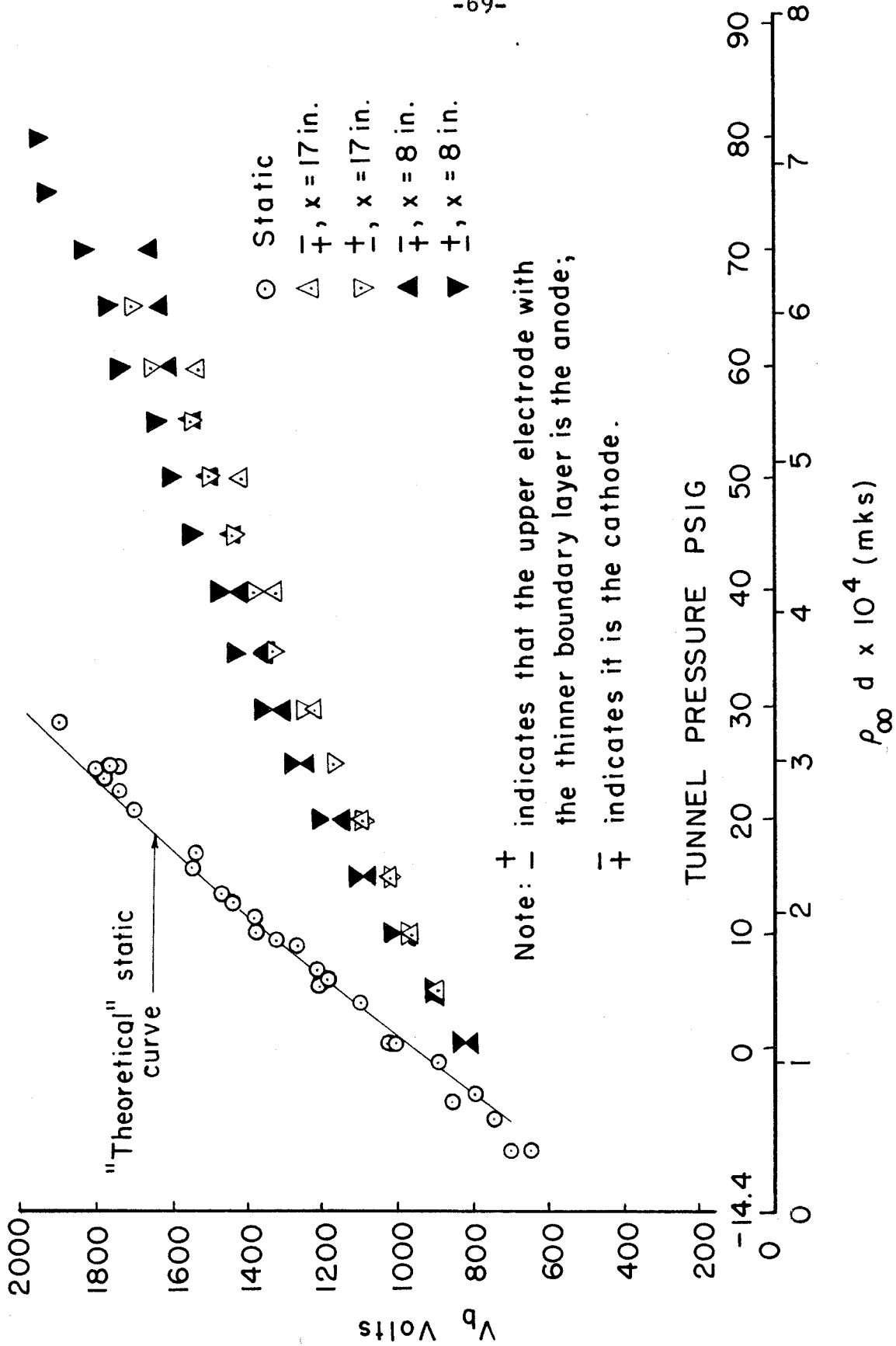


FIG. 8 - EXPERIMENTAL BREAKDOWN VOLTAGES

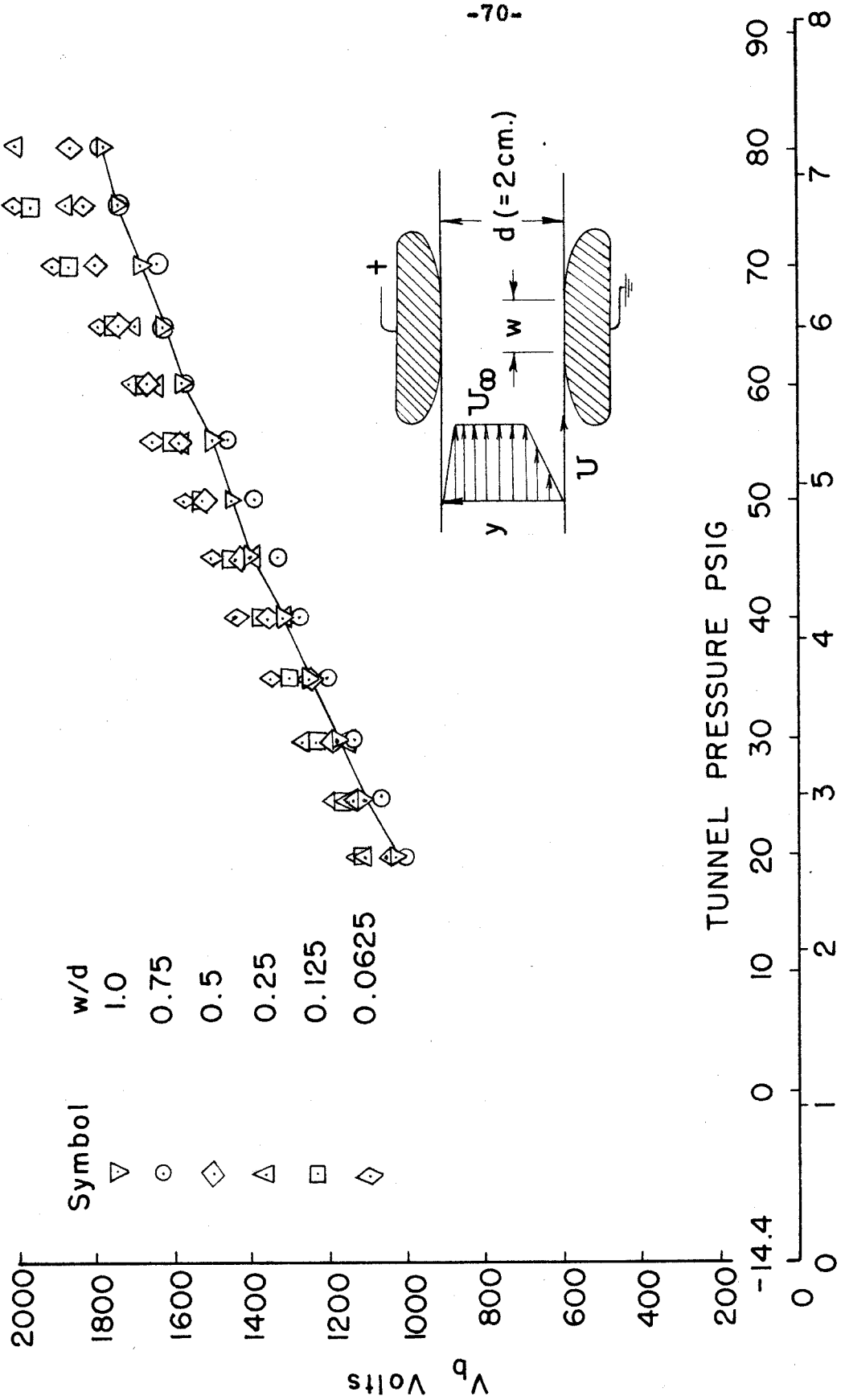


FIG. 9 - EFFECT OF THE RATIO OF ELECTRODE STREAMWISE LENGTH TO SEPARATION UPON BREAKDOWN

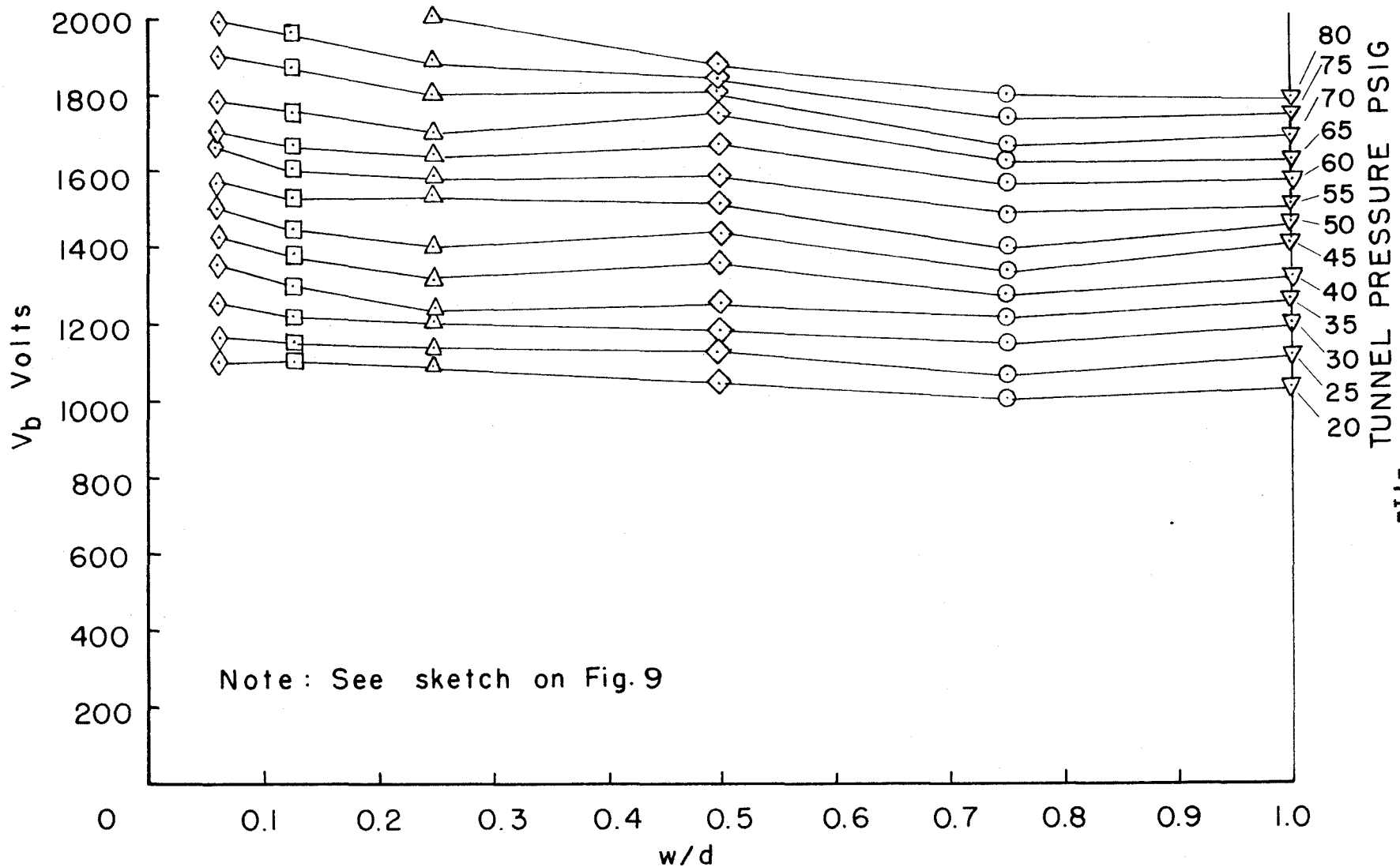


FIG.10-BREAKDOWN VOLTAGE AS A FUNCTION OF THE RATIO OF ELECTRODE STREAMWISE LENGTH TO SEPARATION

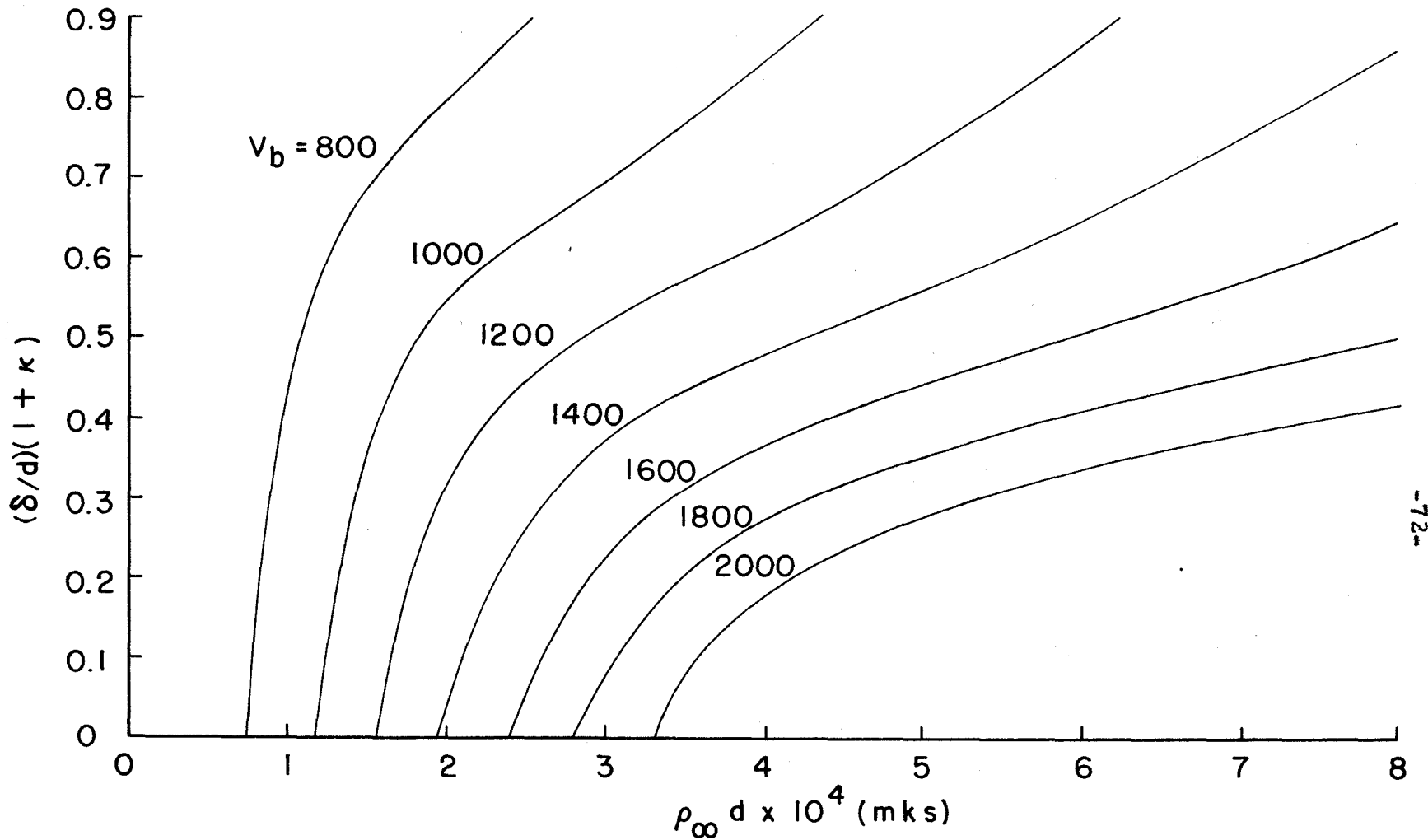


FIG. II- FRACTION OF ELECTRODE SEPARATION DISTURBED BY DENSITY GRADIENTS AS A FUNCTION OF THE PRODUCT OF FREE-STREAM DENSITY AND ELECTRODE SEPARATION WITH BREAKDOWN VOLTAGE AS A PARAMETER

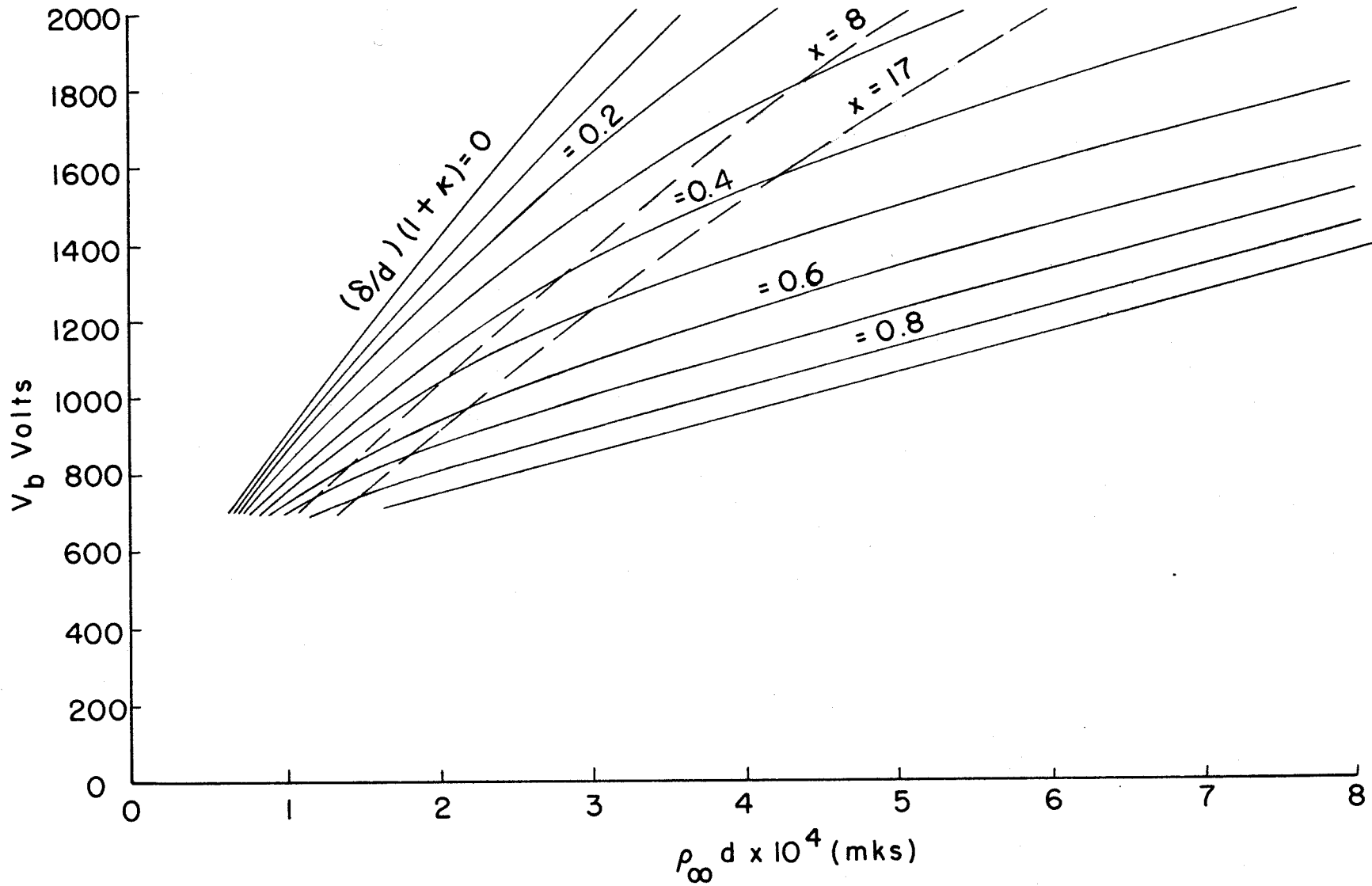


FIG. 12 - THEORETICAL BREAKDOWN VOLTAGES

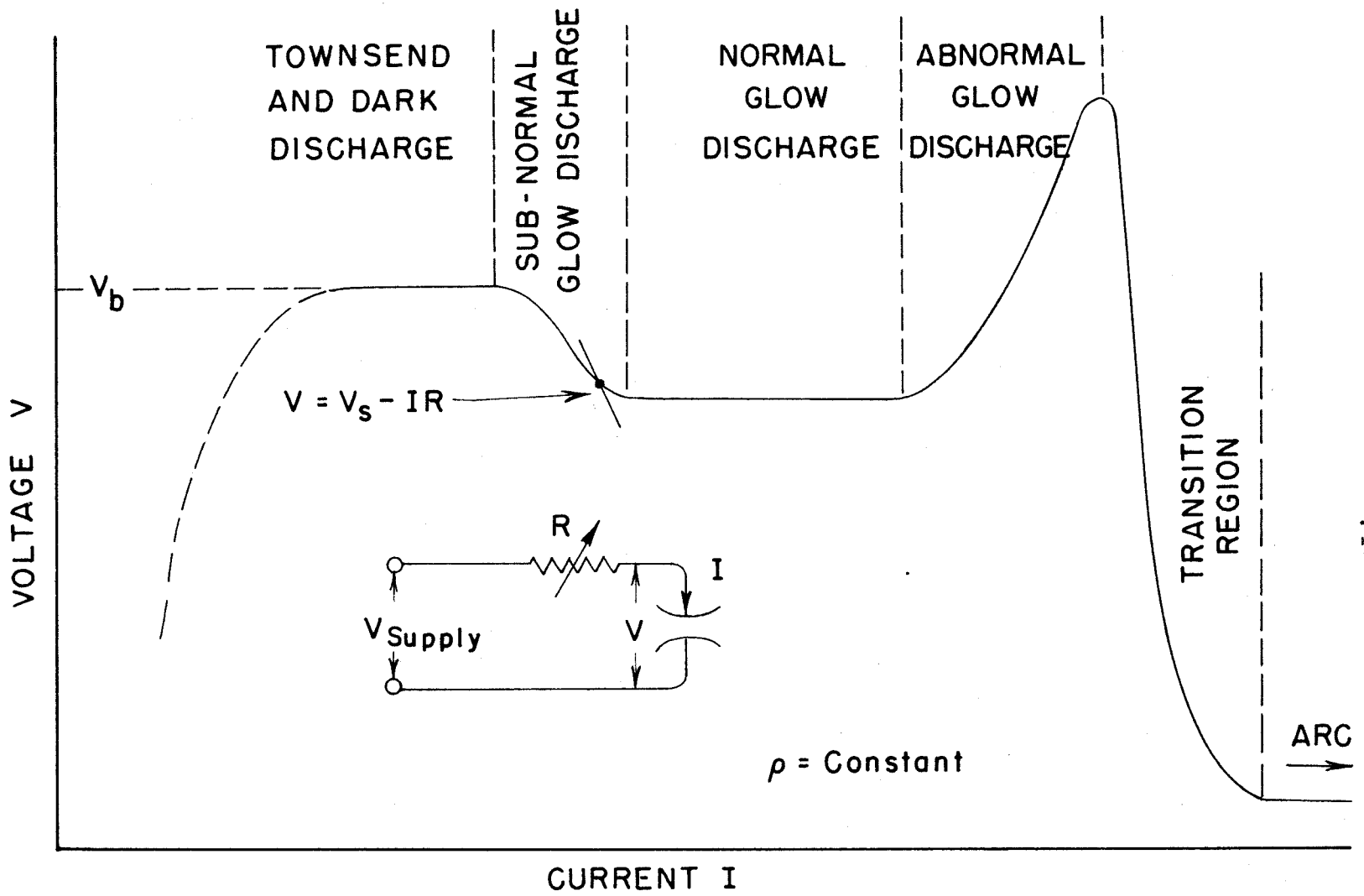


FIG. 13 - TYPICAL VOLTAGE-CURRENT CHARACTERISTIC OF A DISCHARGE

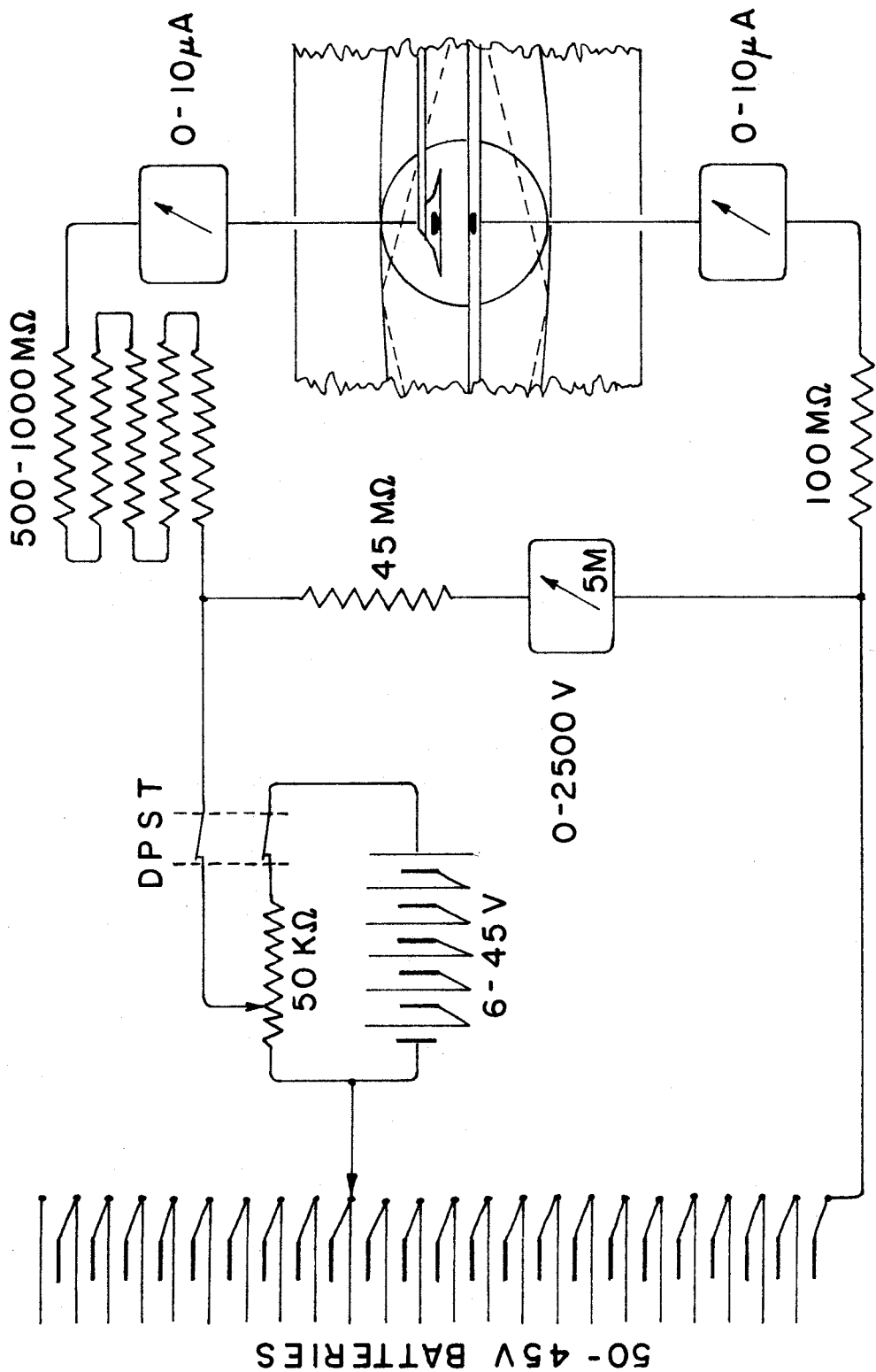


FIG. 14 - EXPERIMENTAL ARRANGEMENT FOR MEASURING GLOW CURRENTS

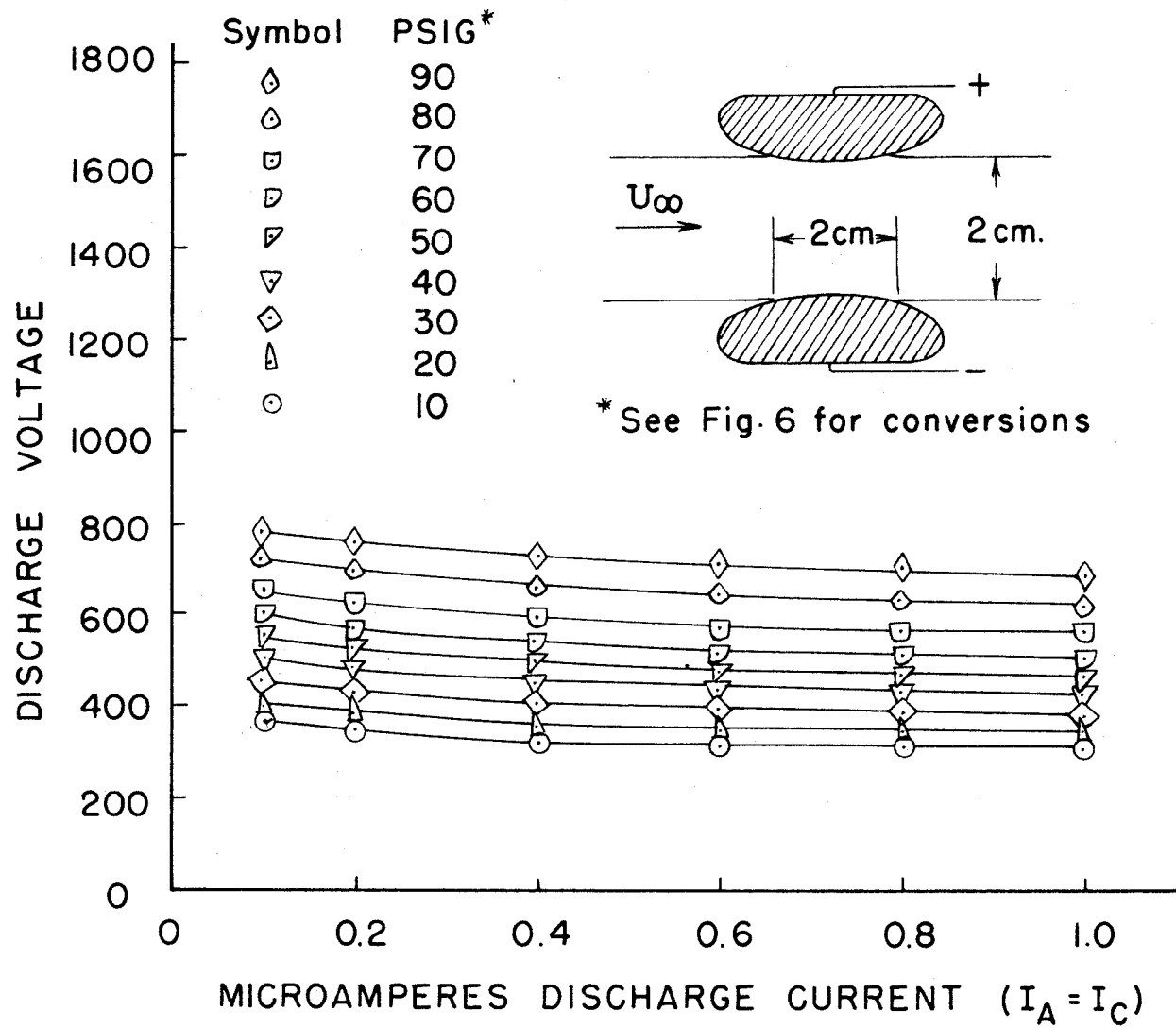


FIG. 15 - VOLTAGE-CURRENT CHARACTERISTICS OF LARGE ELECTRODES

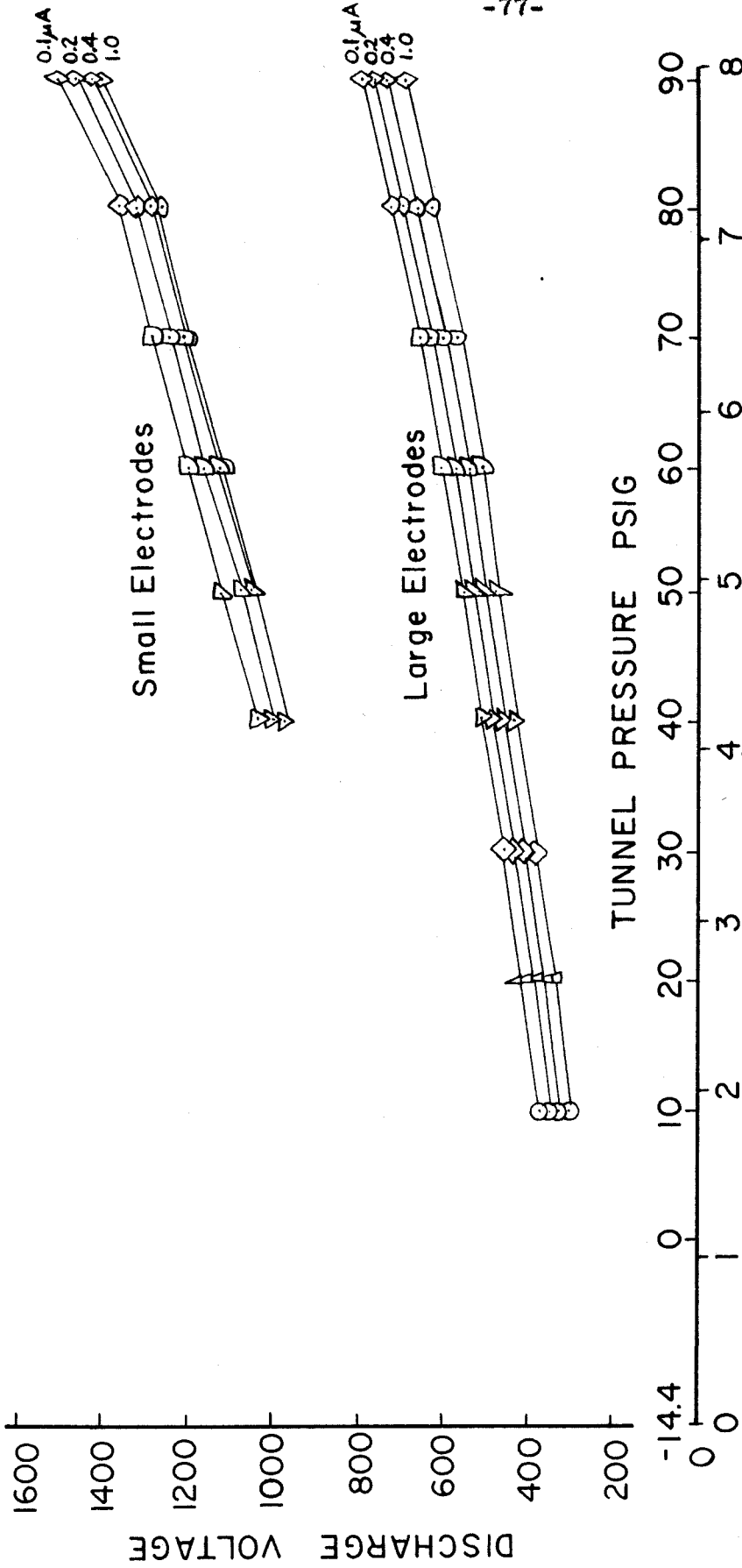
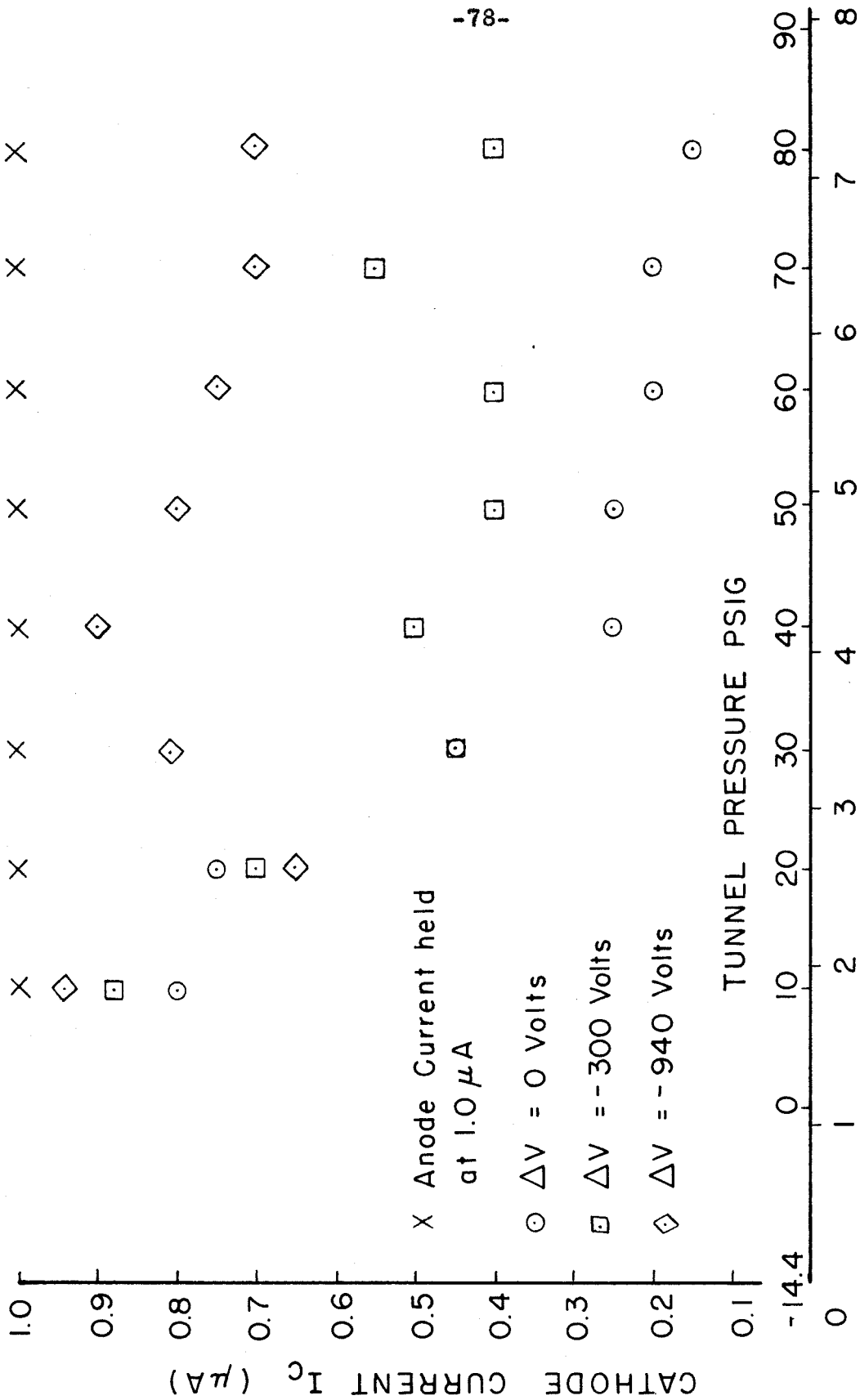


FIG. 16 - VOLTAGE AS A FUNCTION OF DENSITY WITH CURRENT AS A PARAMETER



$\rho_{\infty} d \times 10^4$ (mks)

FIG.17 - CATHODE CURRENTS MEASURED WITH CATHODE HELD AT VARIOUS FIXED POTENTIALS RELATIVE TO THE WIND TUNNEL

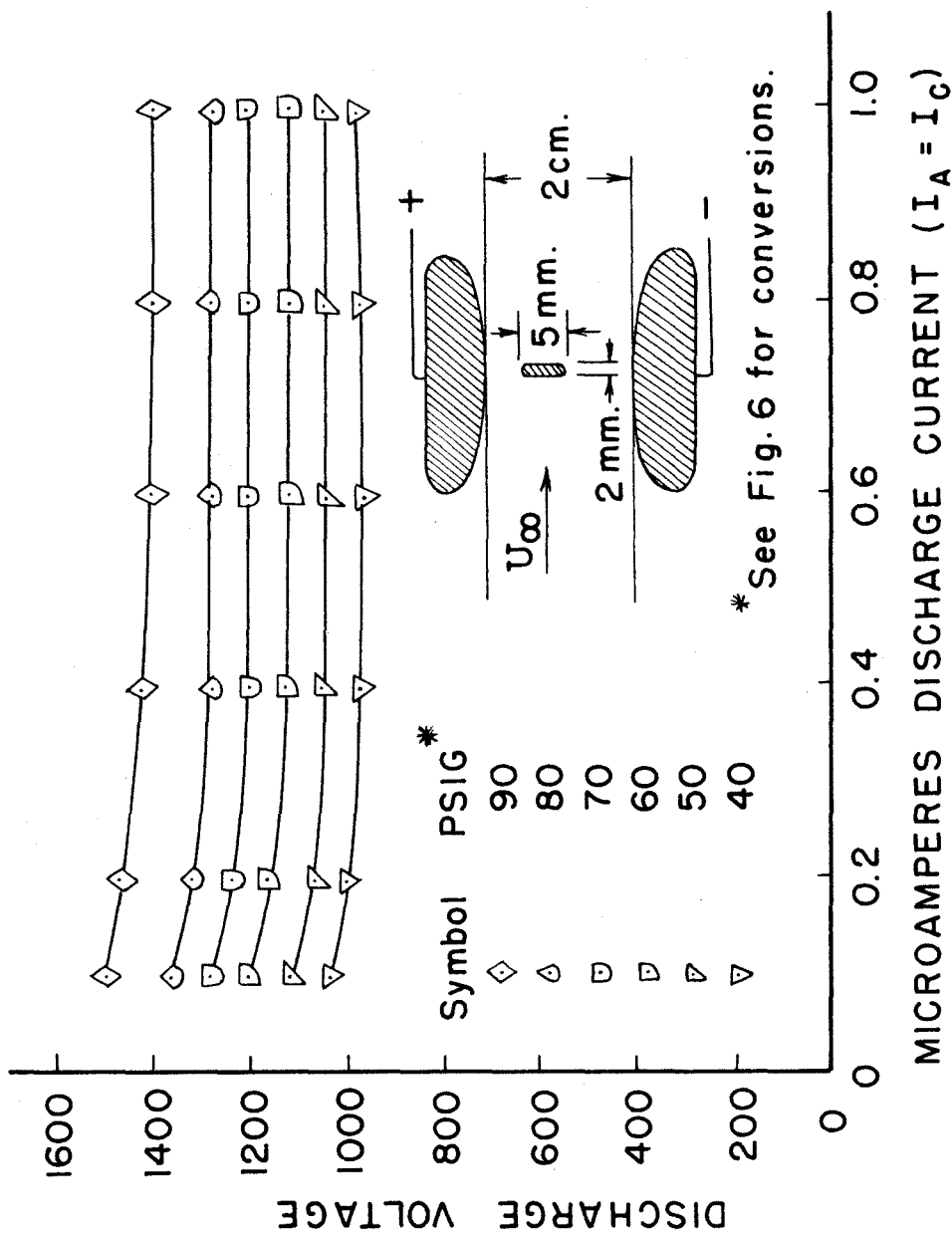


FIG. 18 - VOLTAGE - CURRENT CHARACTERISTICS OF SMALL ELECTRODES

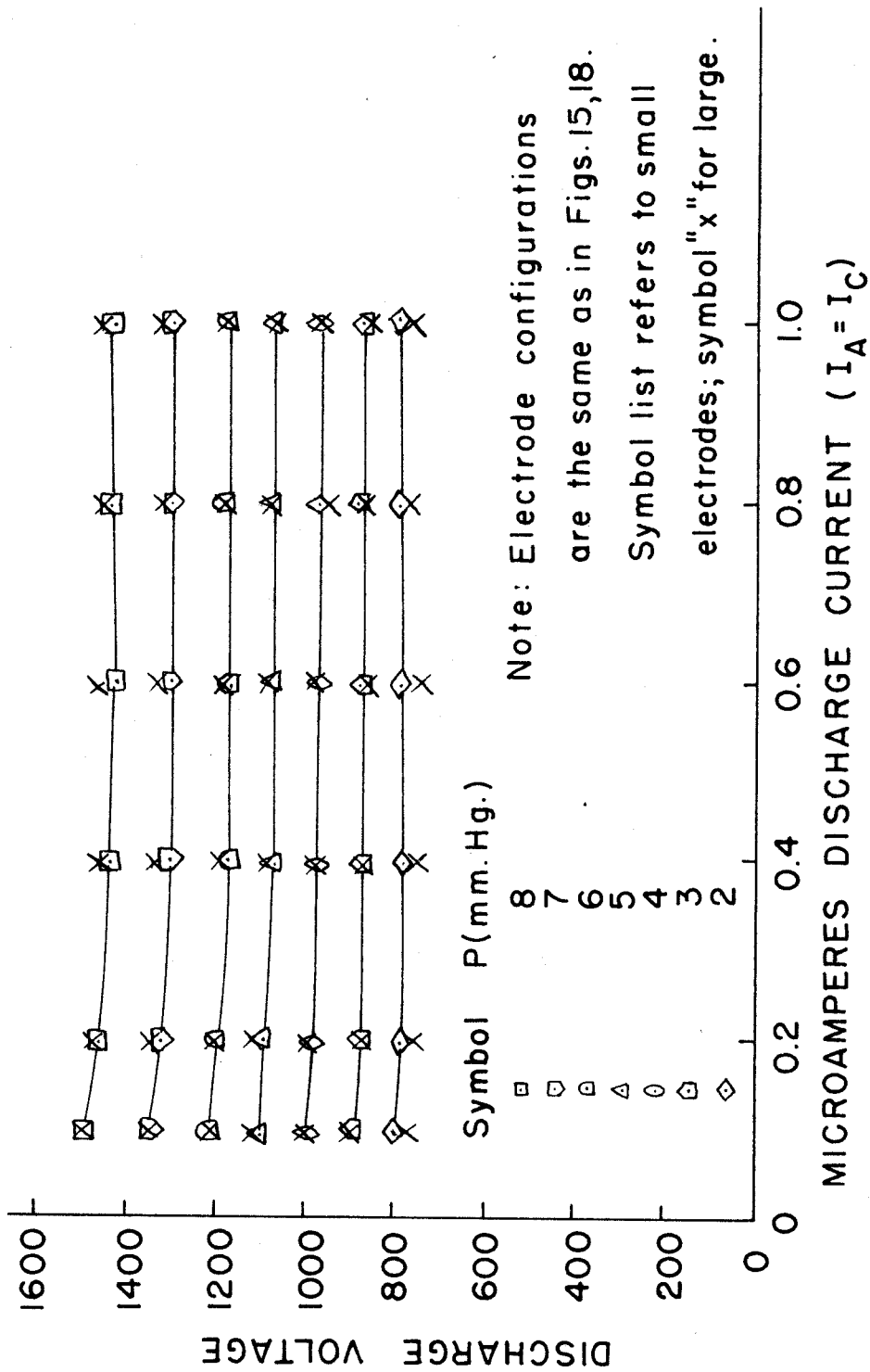


FIG. 19 - COMPARISON OF STATIC VOLTAGE-CURRENT CHARACTERISTICS BETWEEN LARGE AND SMALL ELECTRODES

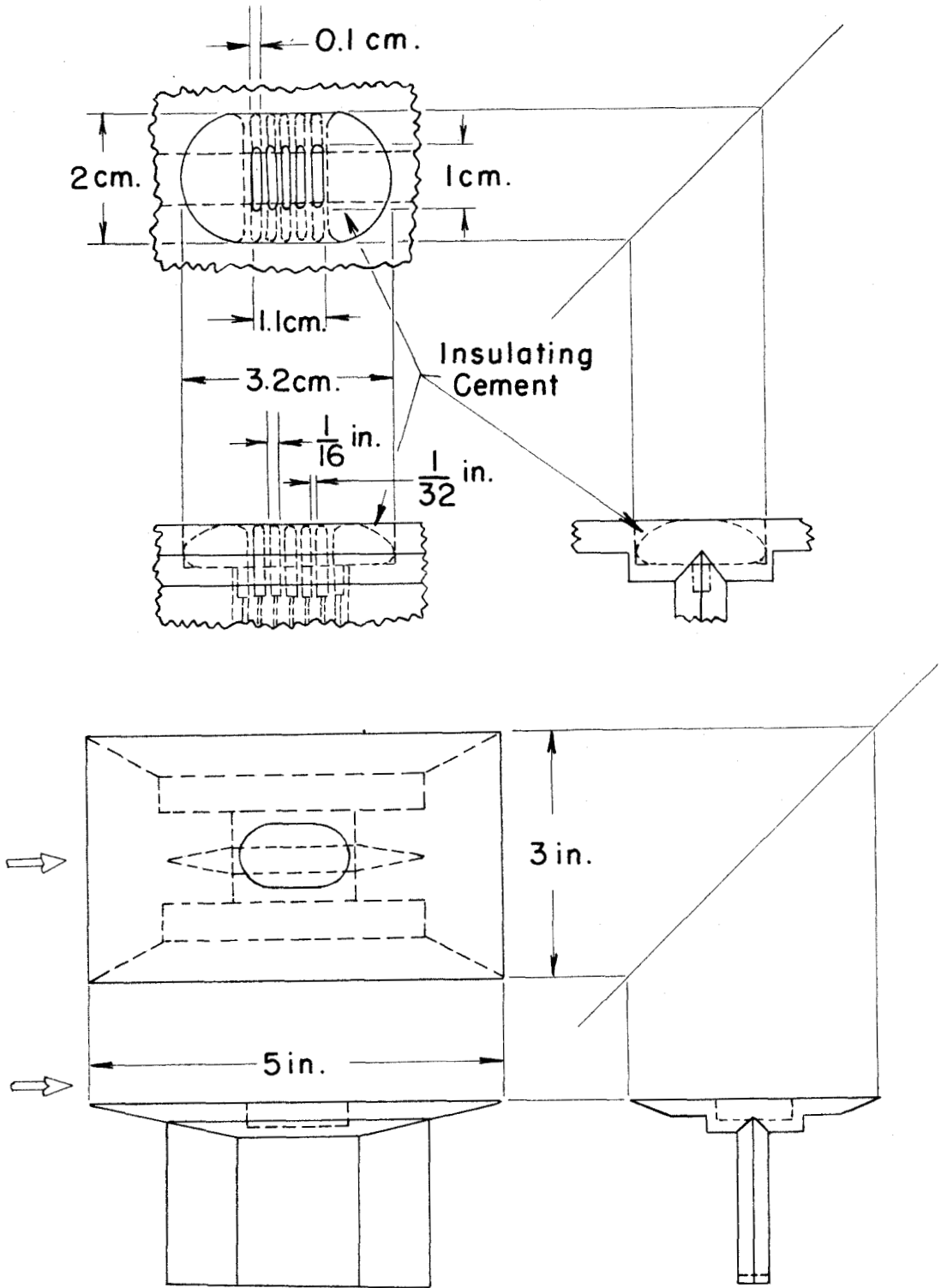


FIG.20-SEGMENTED ELECTRODE DETAILS

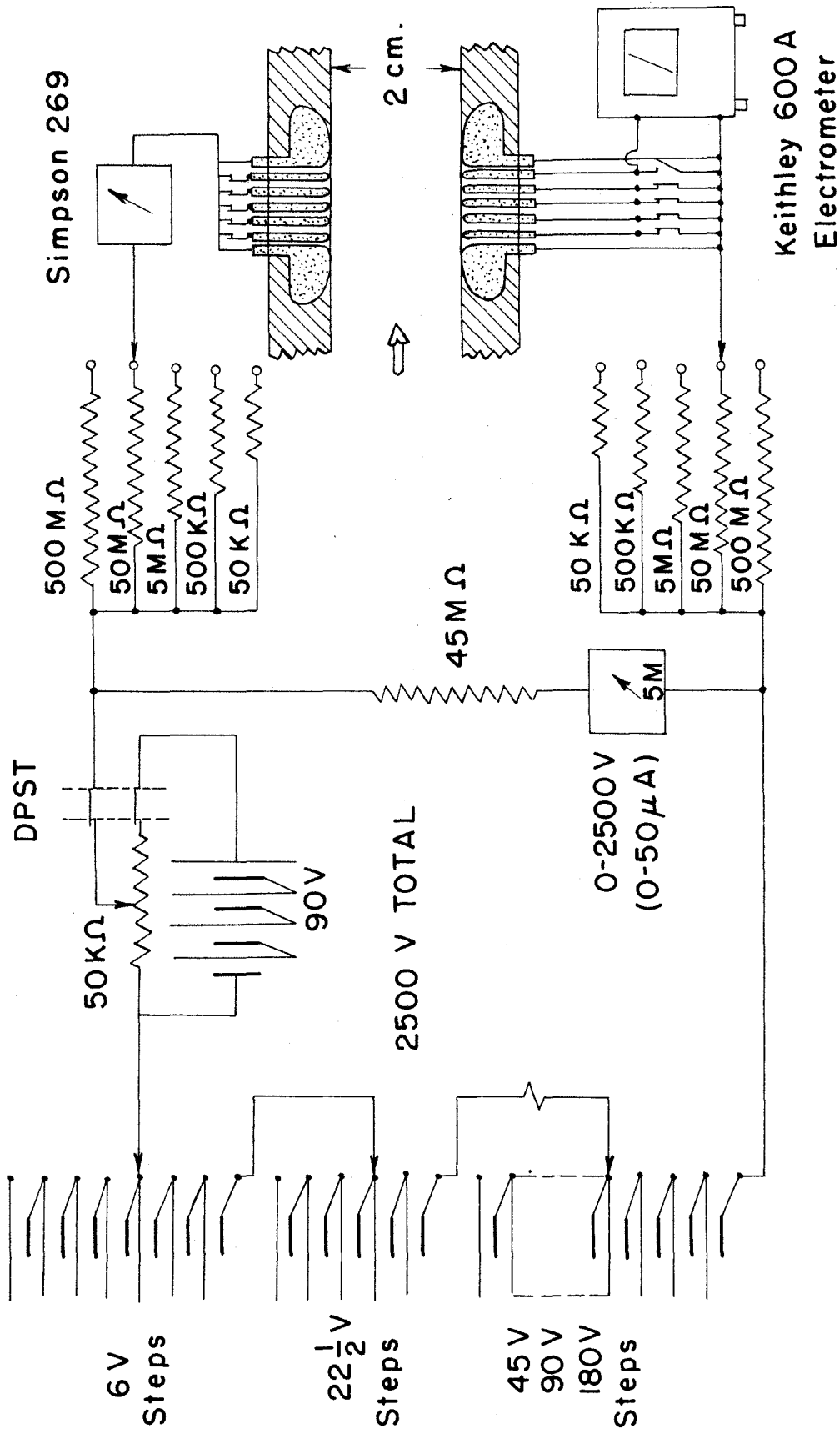


FIG. 21 - MEASURING CIRCUIT

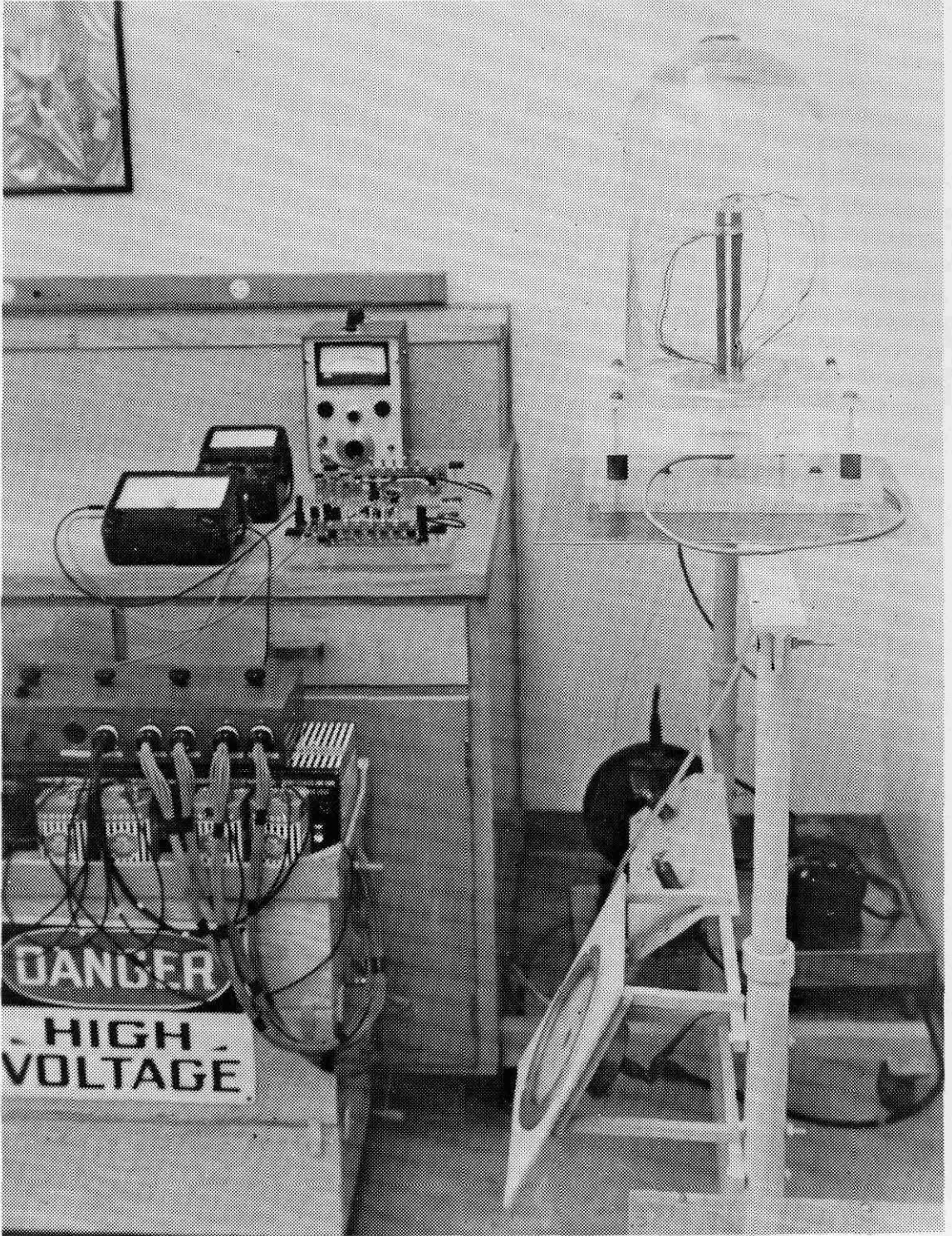


FIG. 22 - STATIC TEST APPARATUS

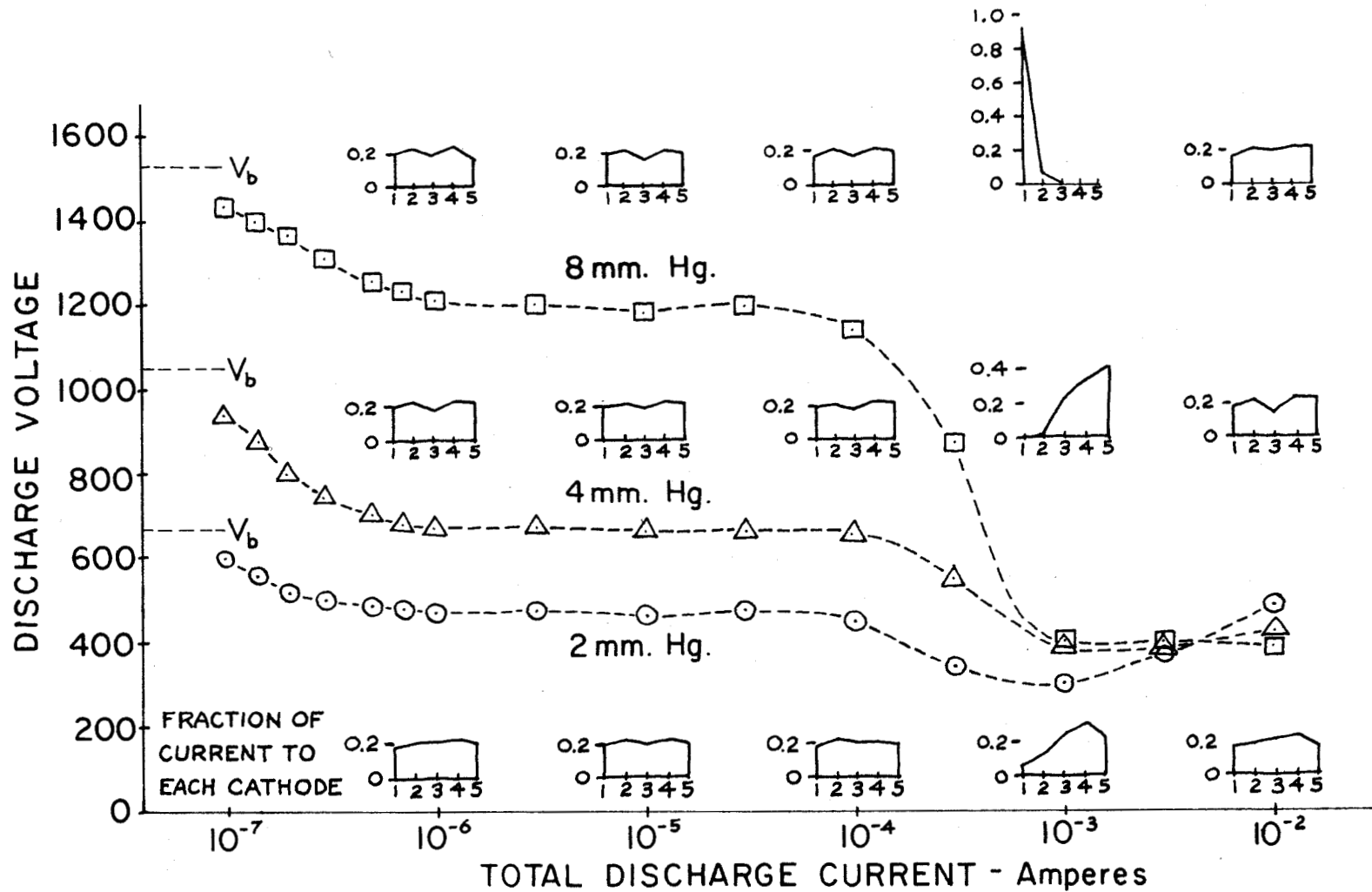


FIG. 23 - STATIC VOLTAGE - TOTAL CURRENT CHARACTERISTICS OF SEGMENTED ELECTRODES

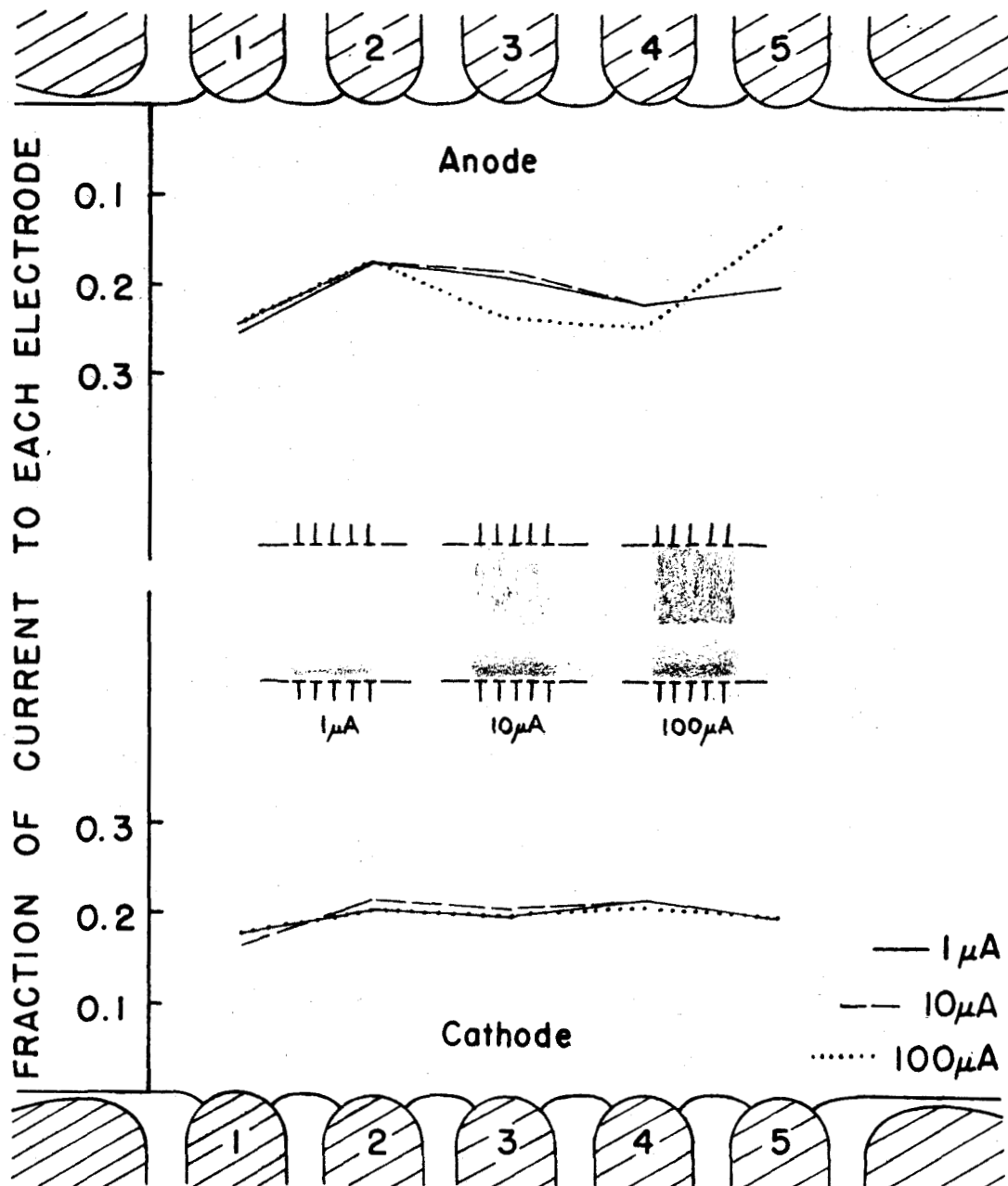


FIG. 24- CURRENT DISTRIBUTIONS AT ANODE AND CATHODE. P = 2 mm. Hg.

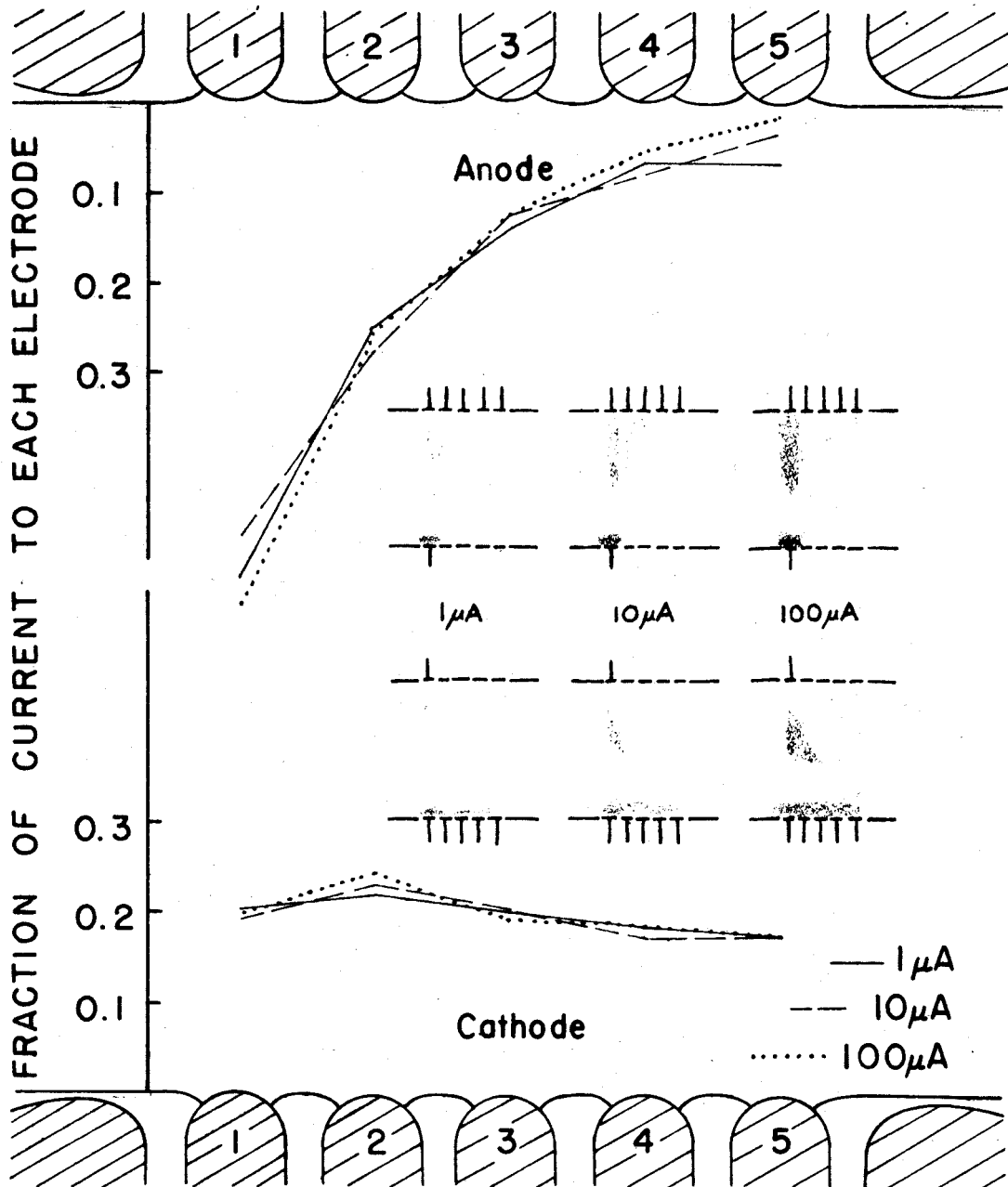


FIG. 25 - CURRENT DISTRIBUTION AT EACH ELECTRODE WITH NO.1 OPPOSITE ELECTRODE SEGMENT OPERATING. P = 2 mm. Hg.

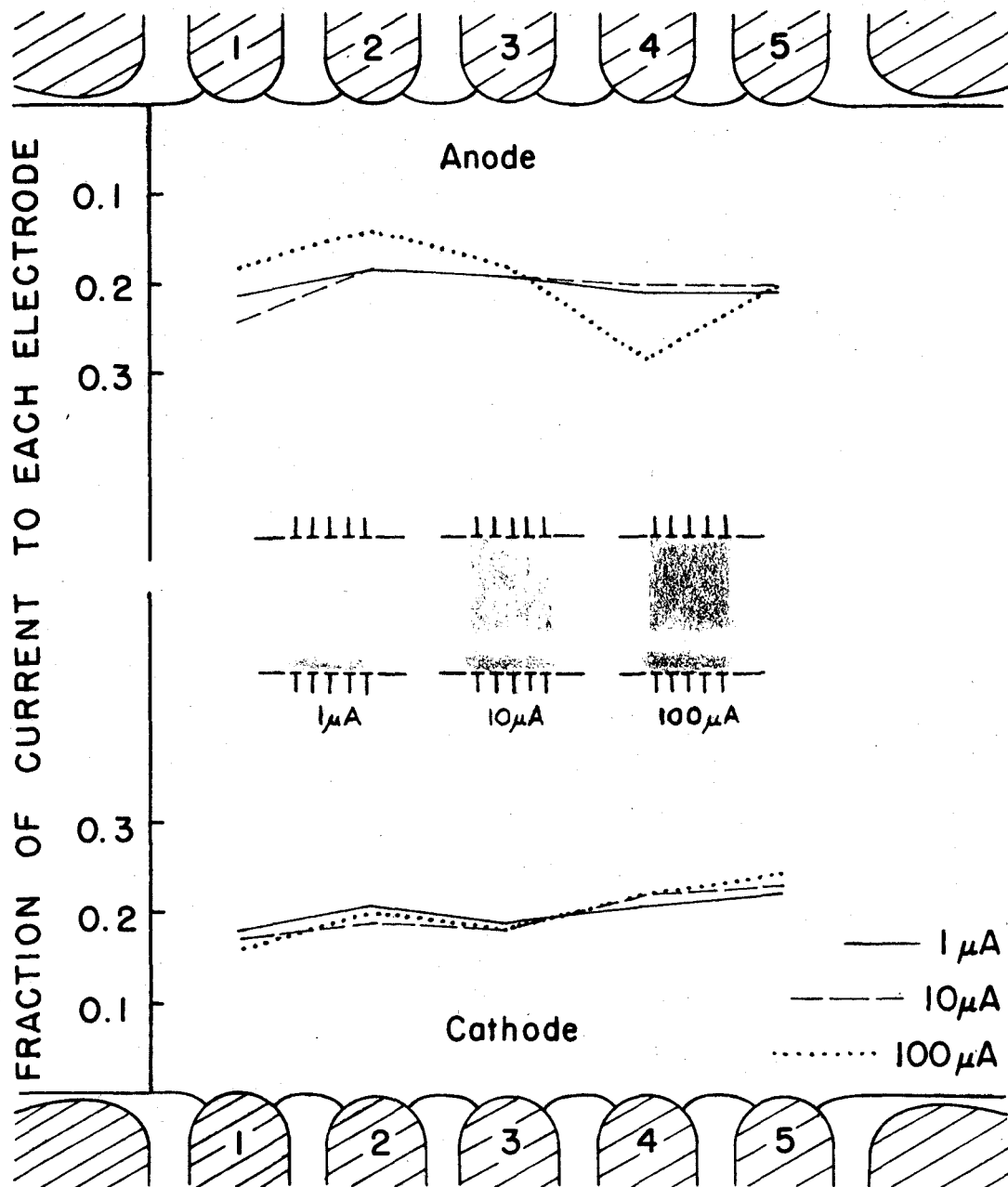


FIG. 26 - CURRENT DISTRIBUTIONS AT ANODE AND CATHODE. P = 4mm. Hg.

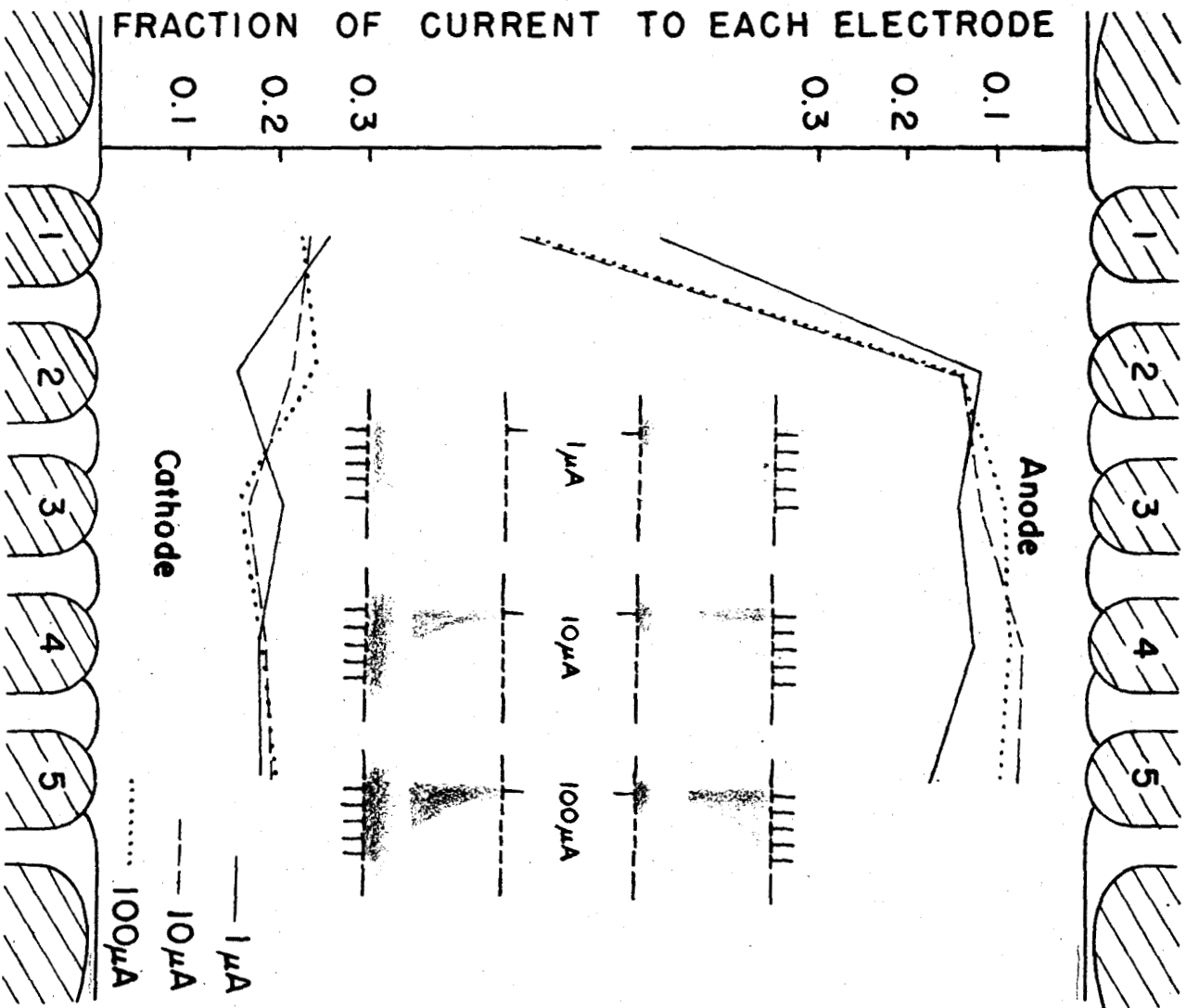


FIG. 27 - CURRENT DISTRIBUTION AT EACH ELECTRODE WITH NO. 1 OPPOSITE ELECTRODE SEGMENT OPERATING. P = 4 mm. Hg.

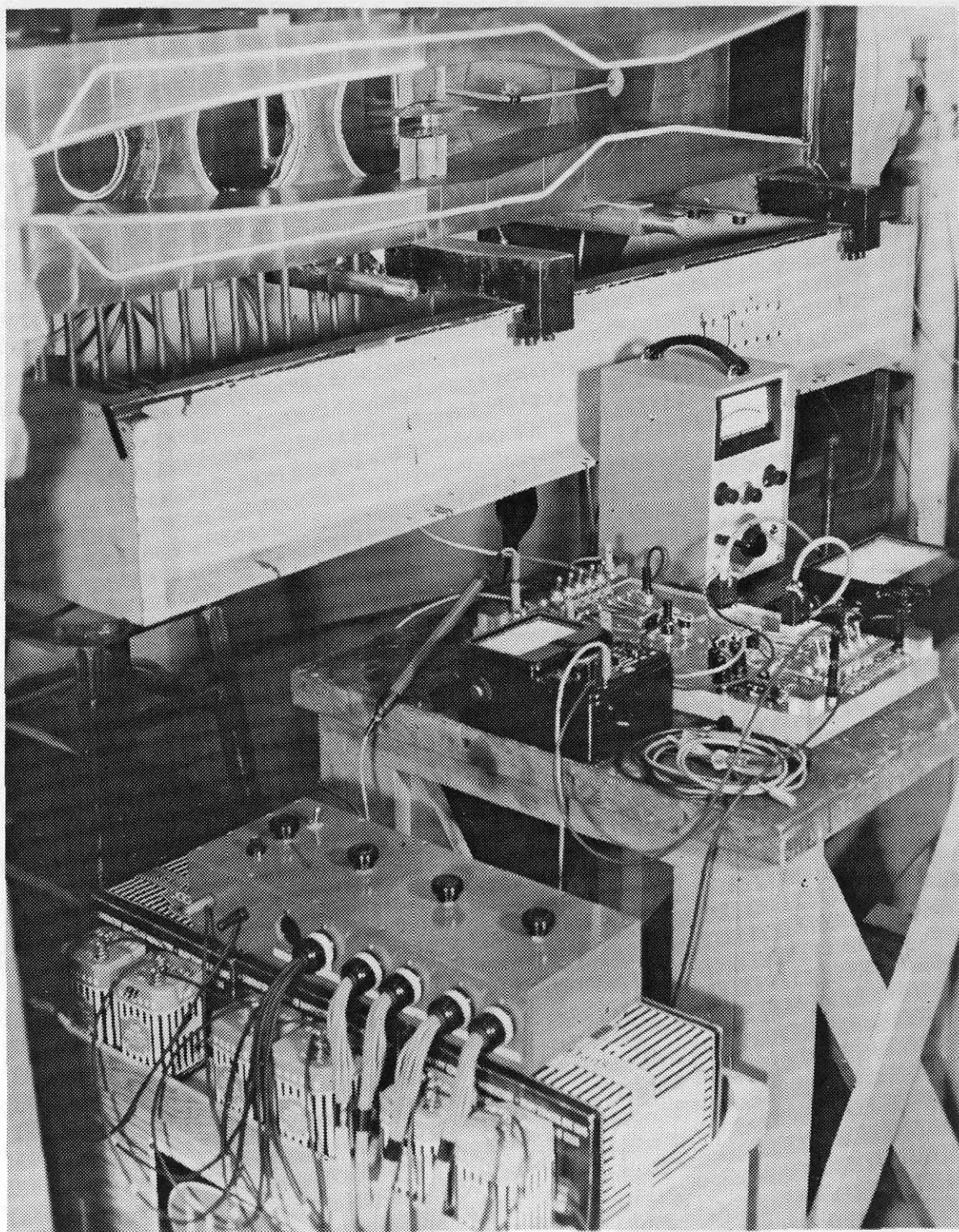


FIG. 28 - DYNAMIC TEST APPARATUS

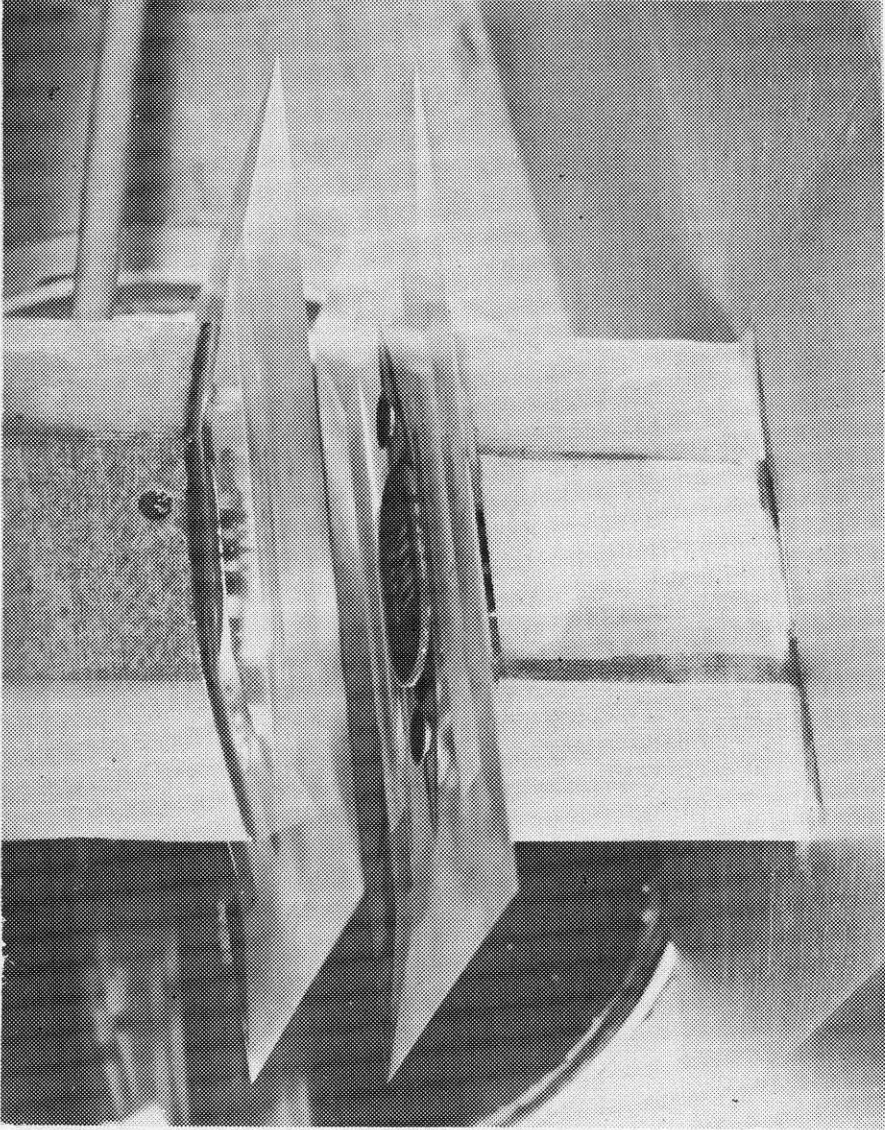


FIG. 29 - DYNAMIC ELECTRODE INSTALLATION

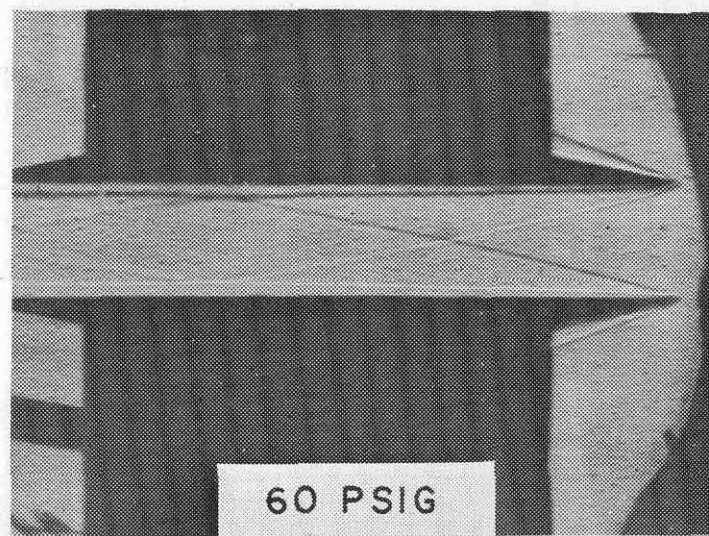
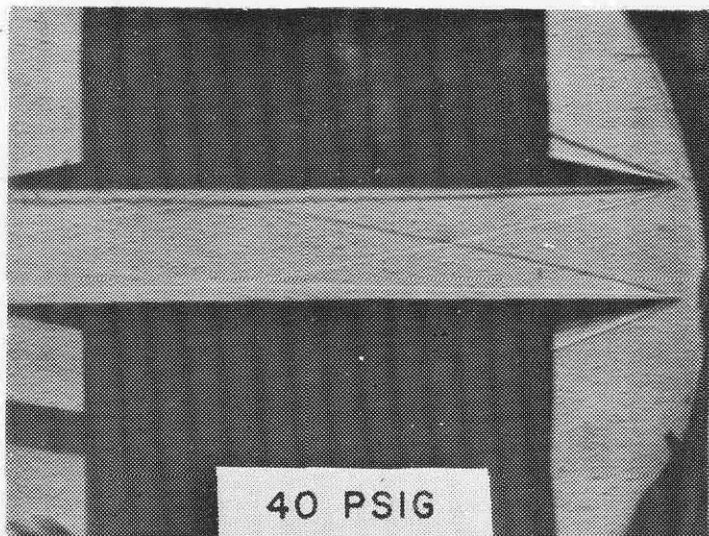
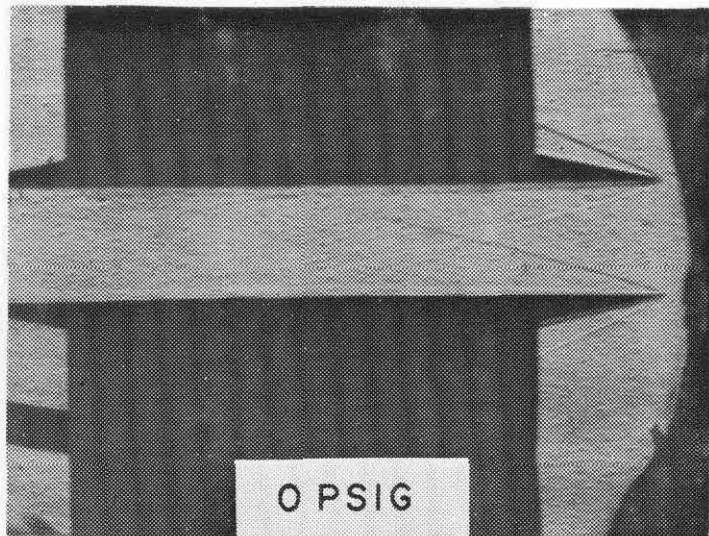


FIG. 30 - SCHLIEREN FLOW PICTURES

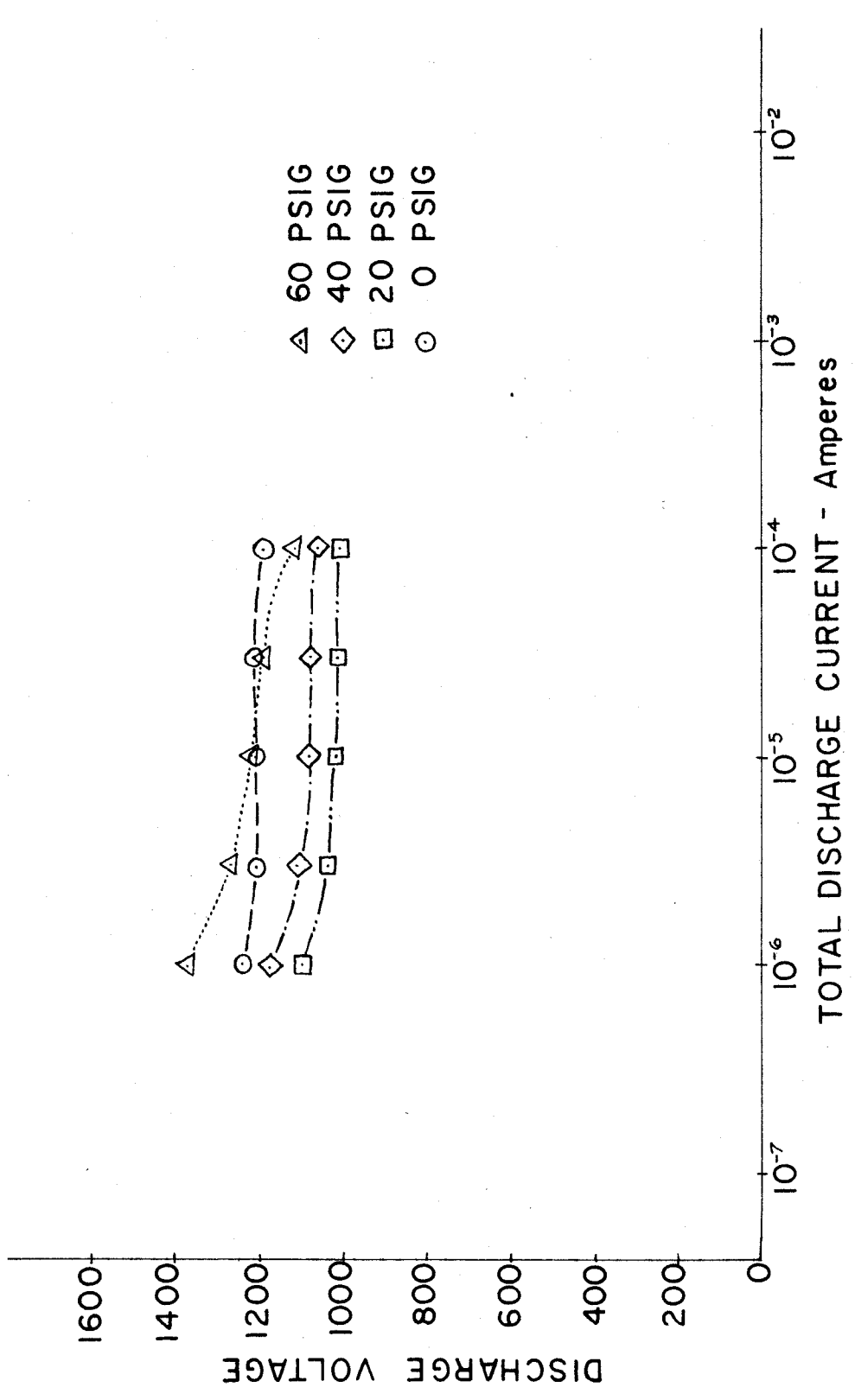


FIG. 31 - DYNAMIC VOLTAGE - TOTAL CURRENT CHARACTERISTICS OF SEGMENTED ELECTRODES

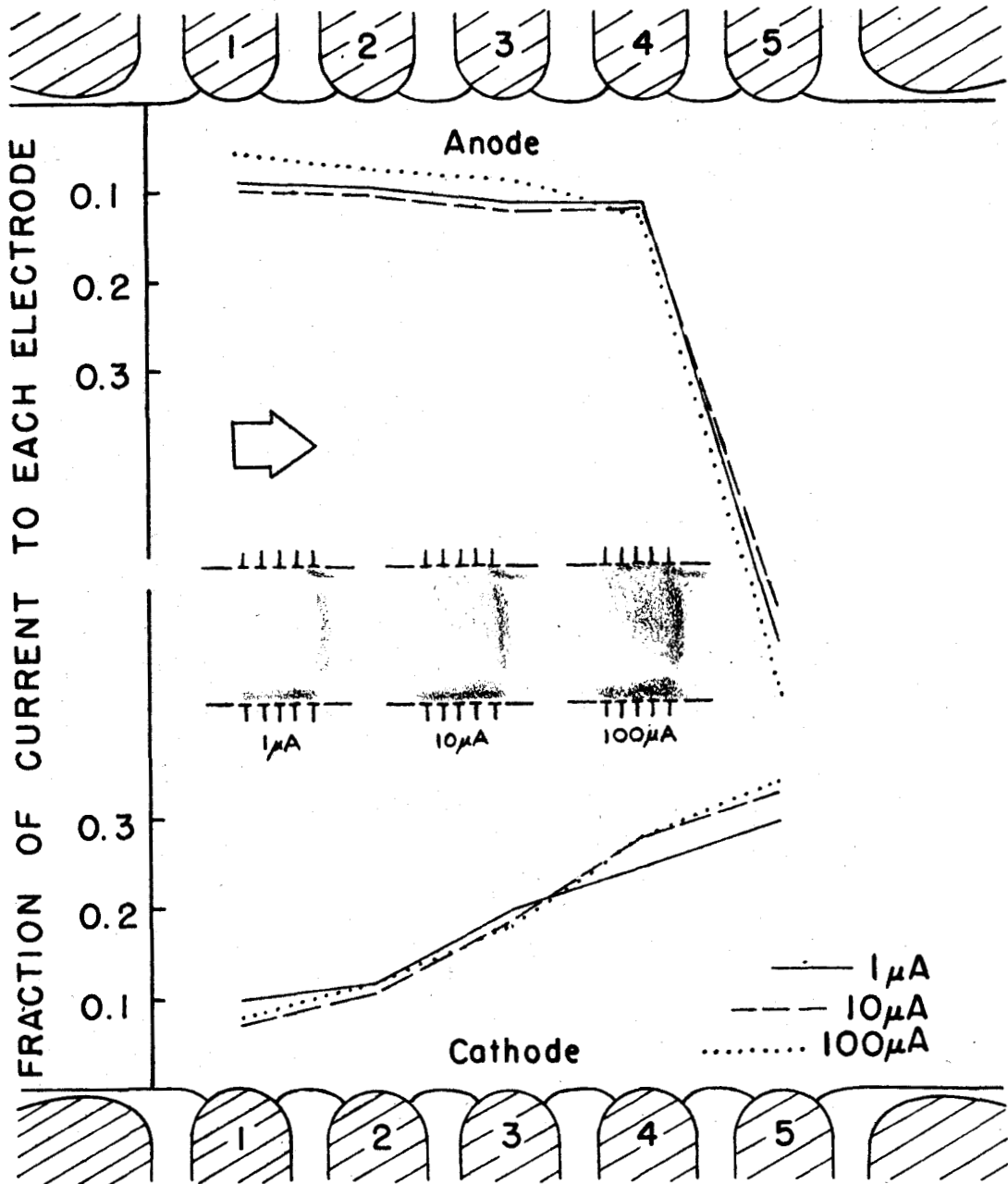


FIG. 32 - CURRENT DISTRIBUTIONS AT ANODE AND CATHODE. $P_b = 0$ PSIG.

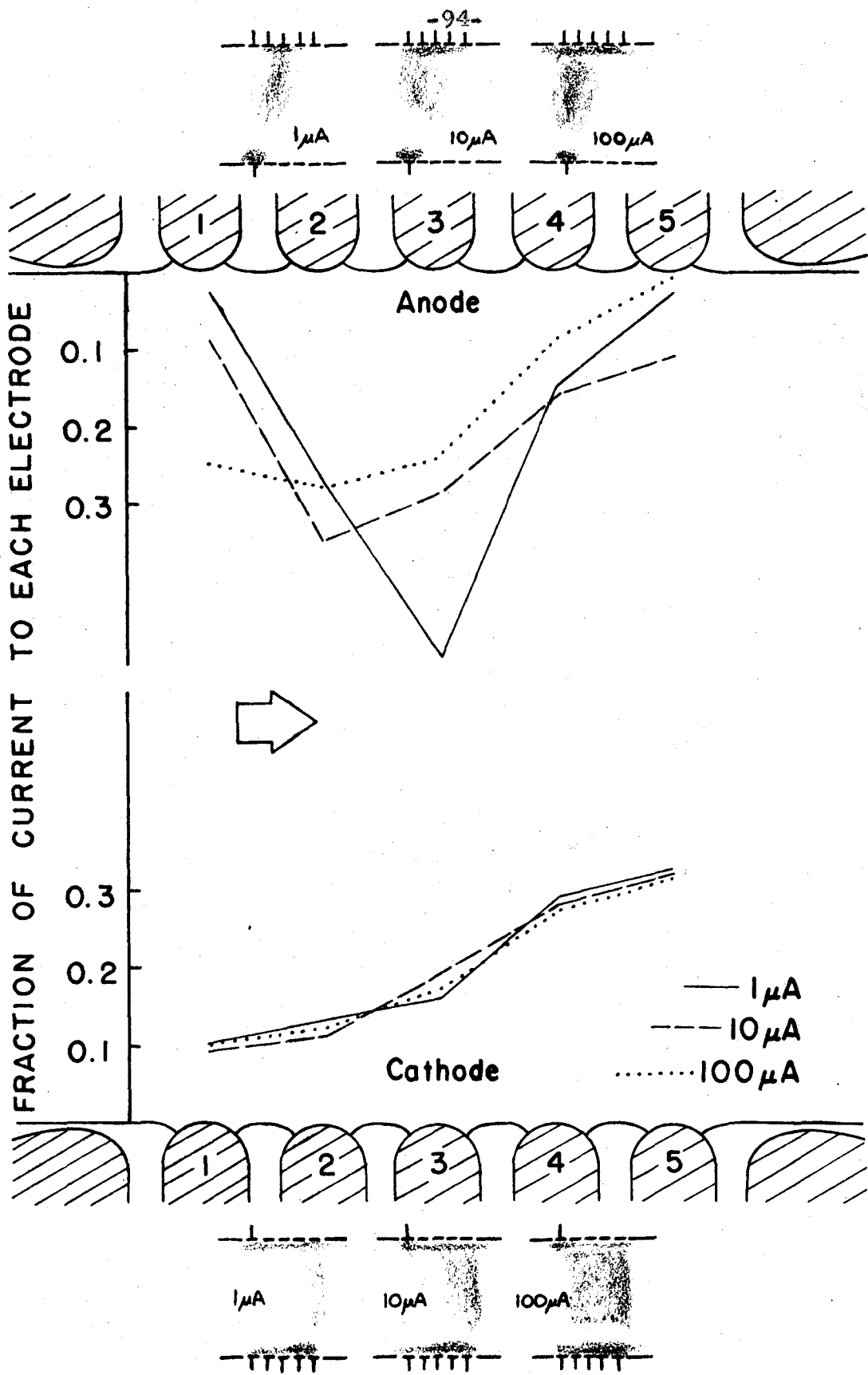


FIG. 33 - CURRENT DISTRIBUTION AT EACH ELECTRODE WITH NO.1 OPPOSITE ELECTRODE SEGMENT OPERATING. $P_0 = 0$ PSIG.

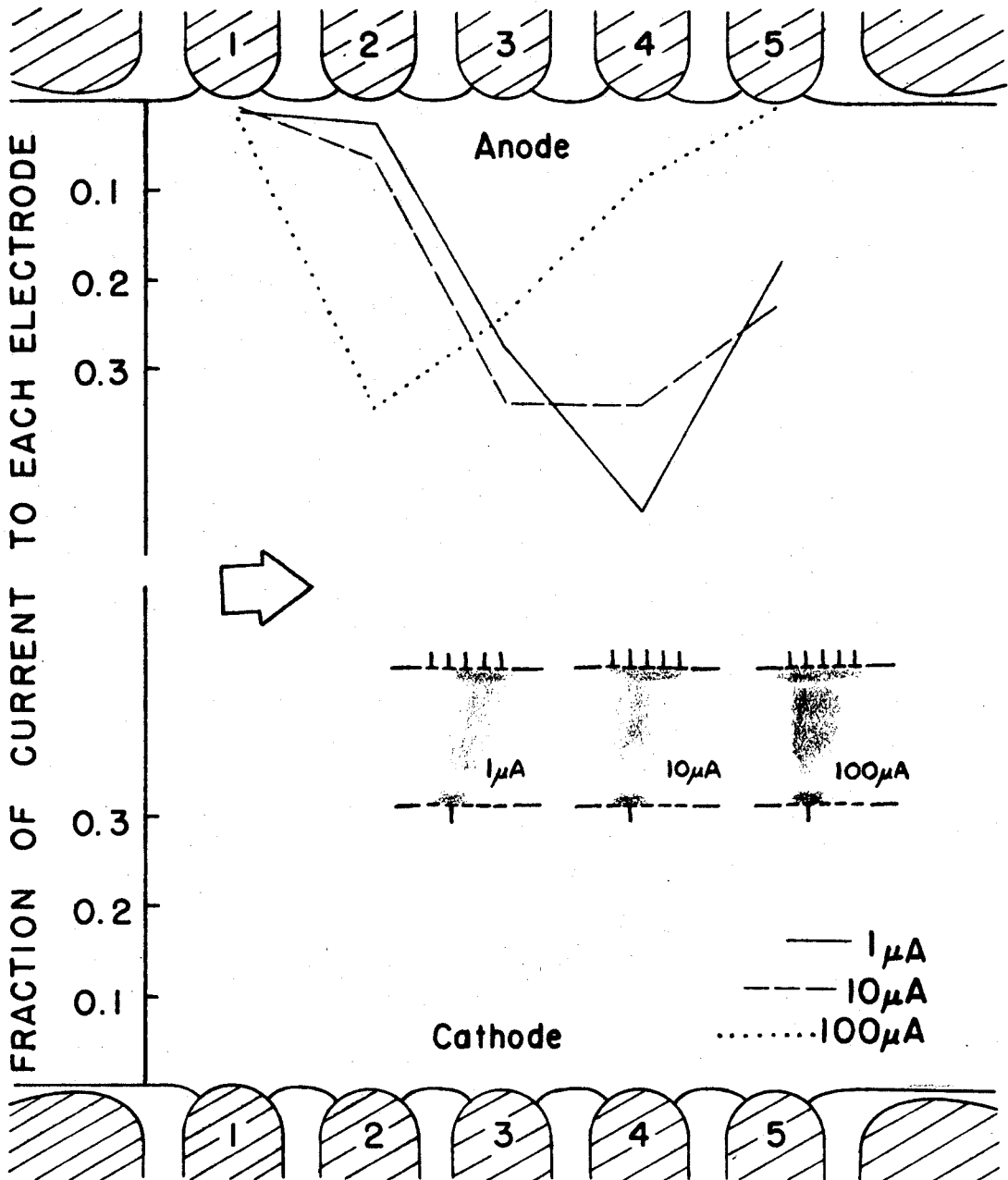


FIG. 33B - CURRENT DISTRIBUTION AT THE ANODE WITH NO. 2 CATHODE SEGMENT OPERATING. $P_0 = 0$ PSIG.

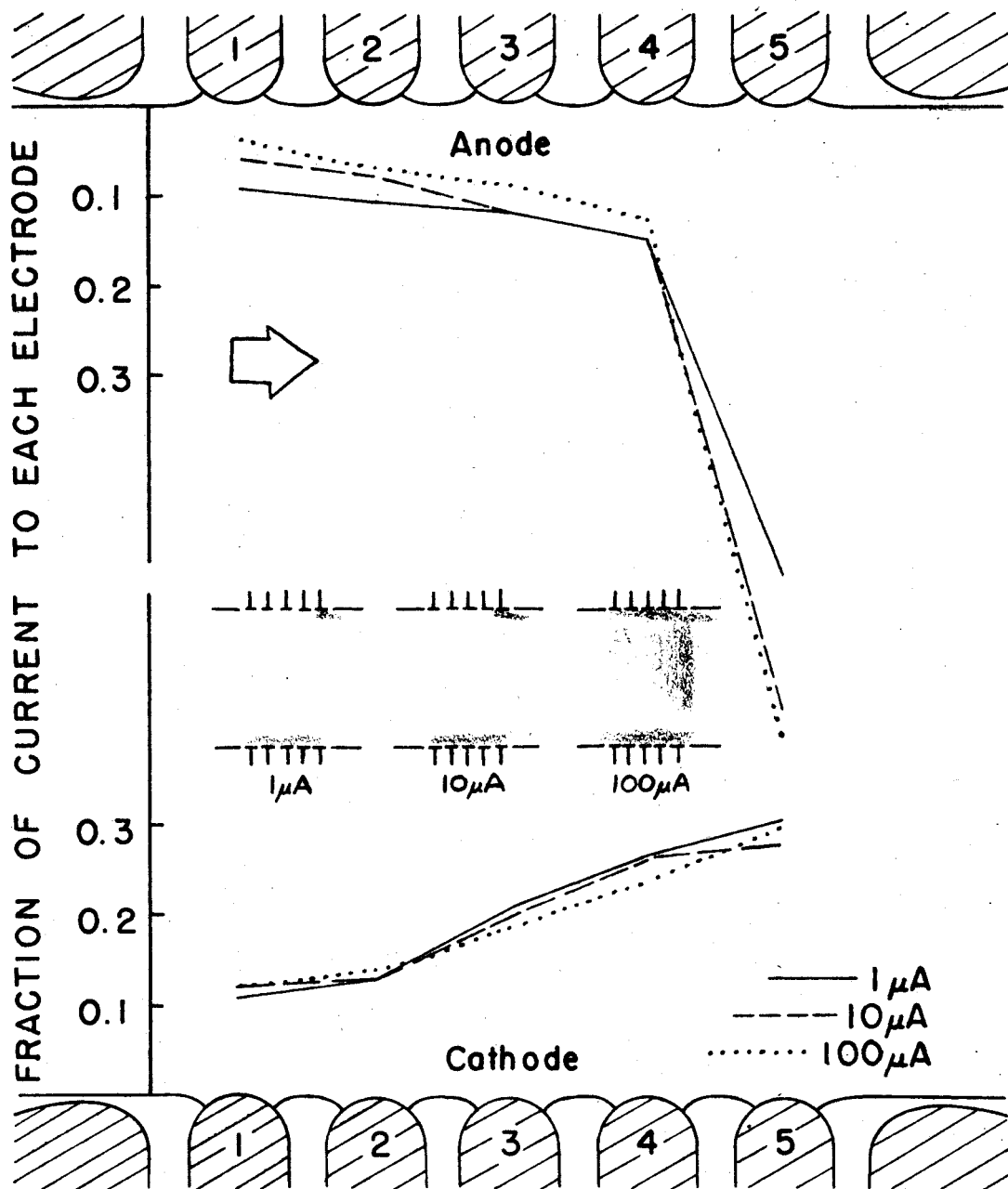


FIG. 34 - CURRENT DISTRIBUTIONS AT ANODE AND CATHODE. $P_0 = 20$ PSIG.

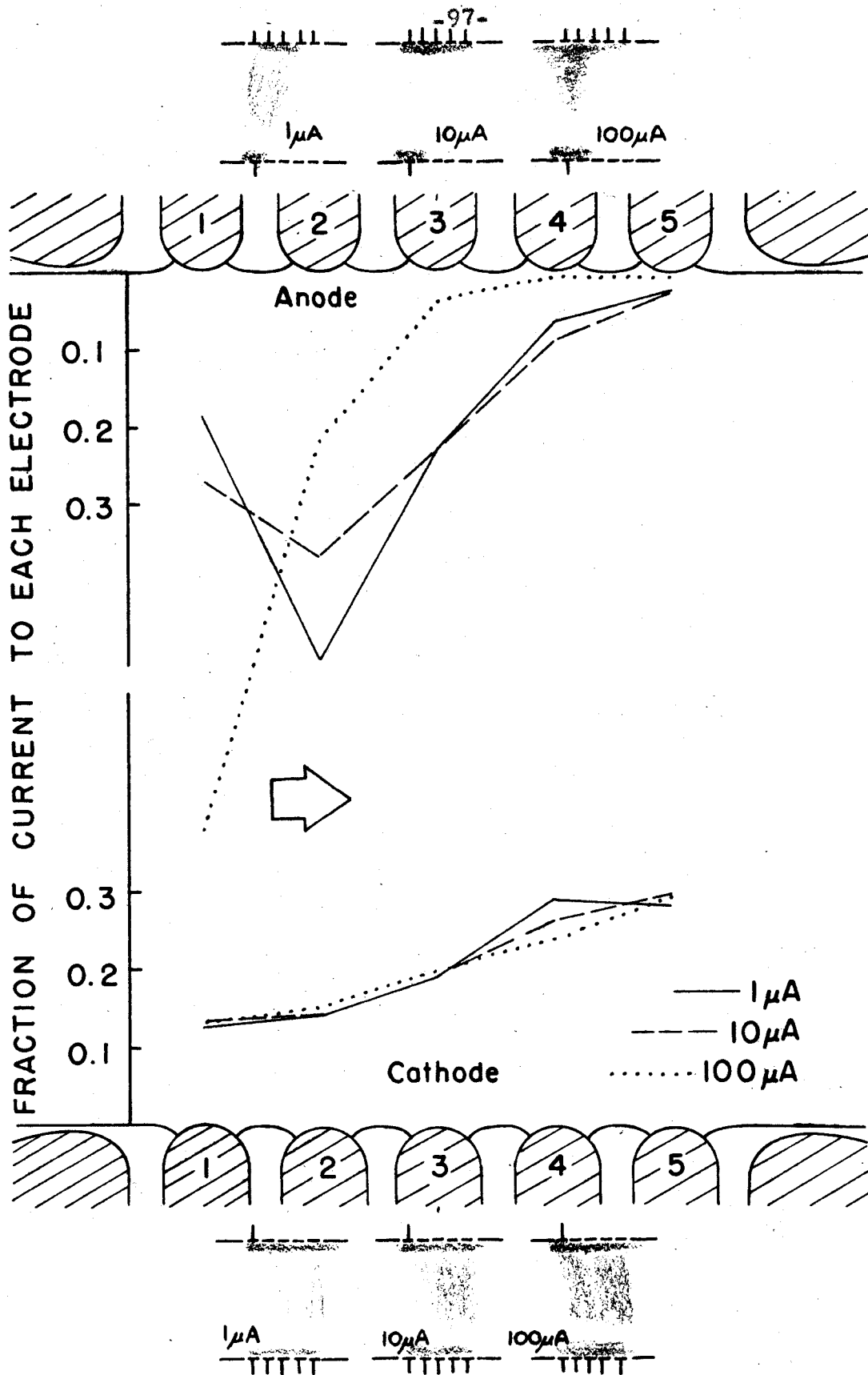


FIG. 35 - CURRENT DISTRIBUTION AT EACH ELECTRODE WITH NO.1 OPPOSITE ELECTRODE SEGMENT OPERATING. $P_0 = 20$ PSIG.

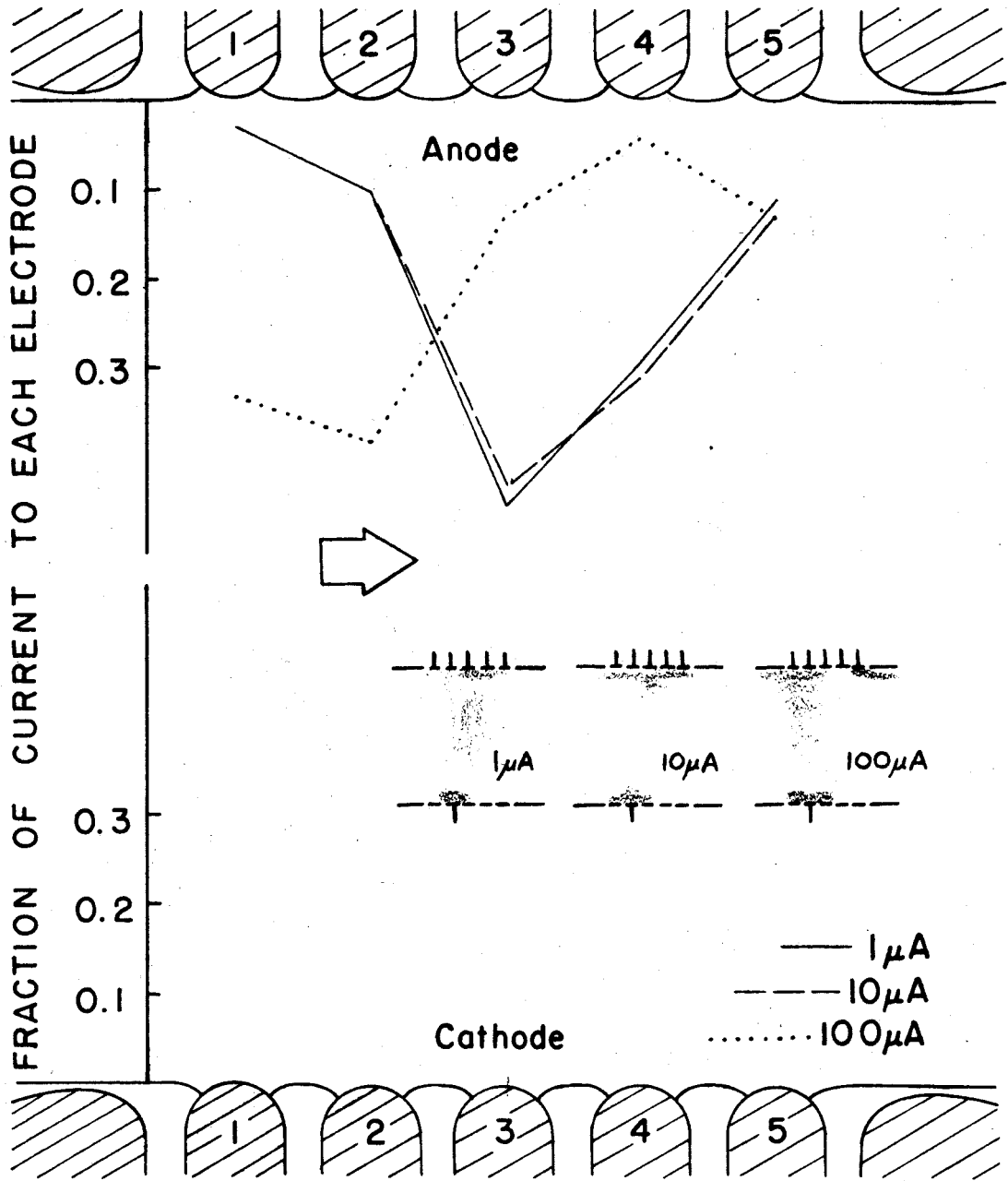


FIG.35B - CURRENT DISTRIBUTION AT THE ANODE WITH NO.2 CATHODE SEGMENT OPERATING. P₀ = 20 PSIG.

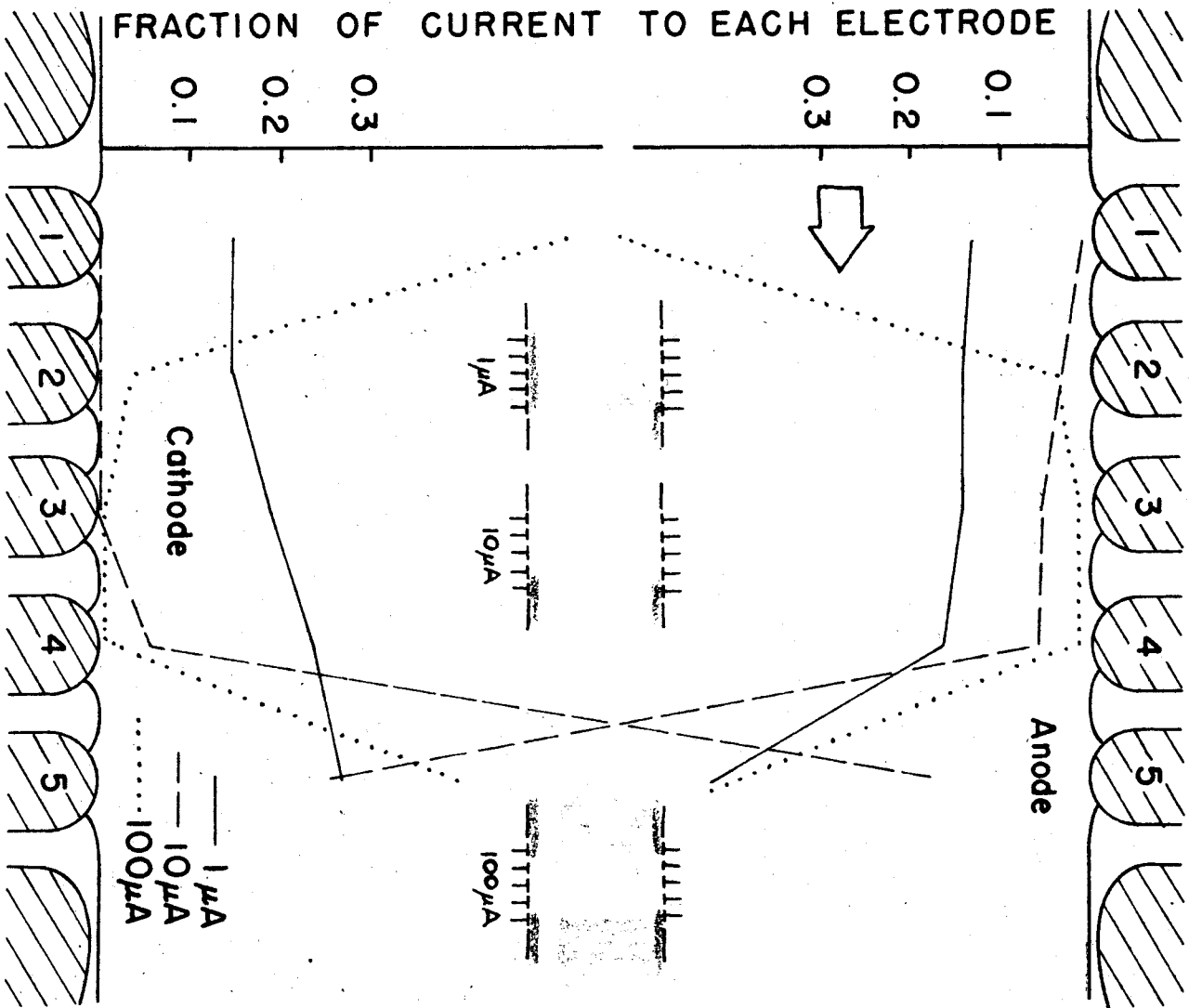


FIG. 36 - CURRENT DISTRIBUTIONS AT ANODE AND CATHODE. $P_0 = 40$ PSIG.

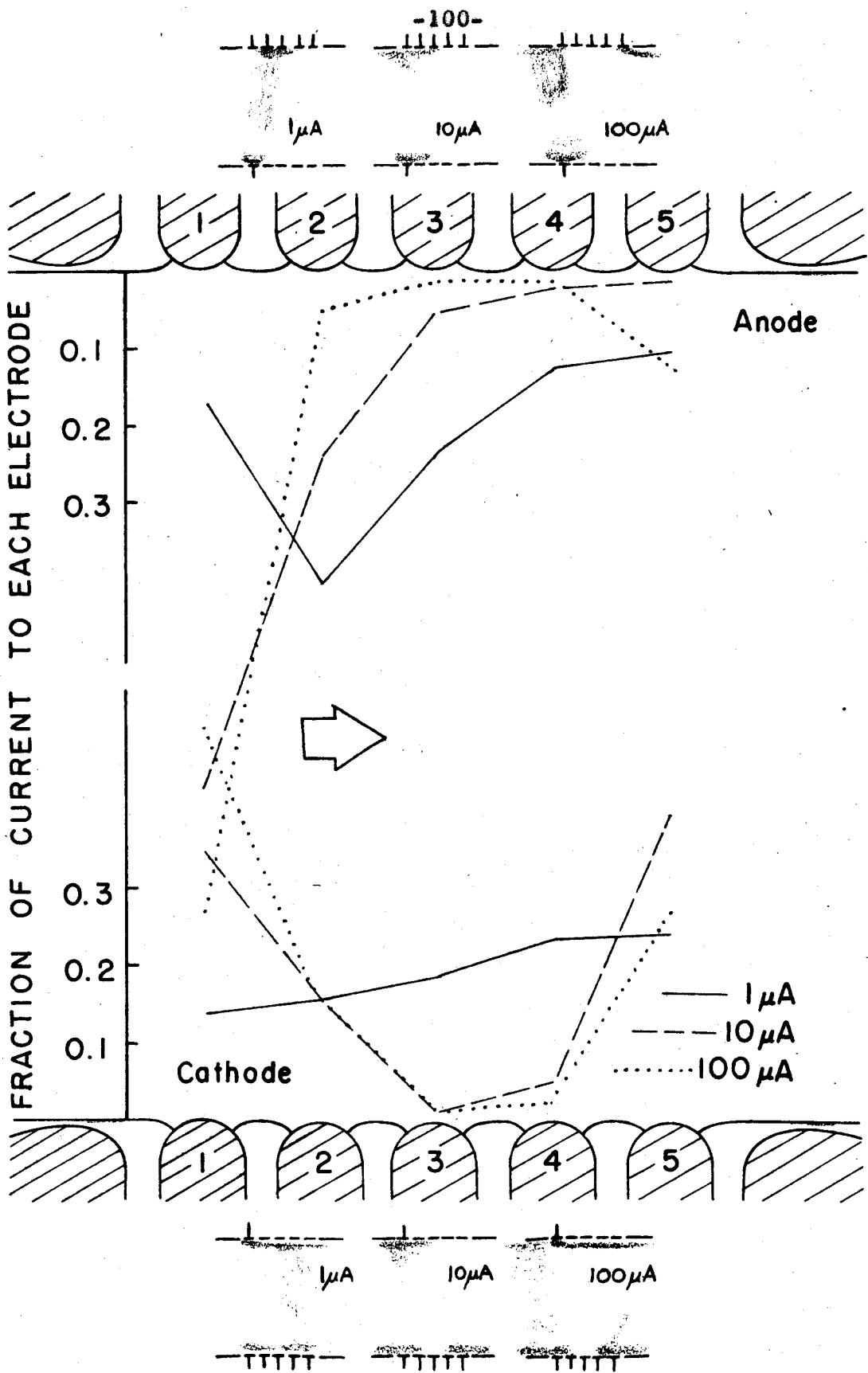


FIG. 37 - CURRENT DISTRIBUTION AT EACH ELECTRODE WITH NO.1 OPPOSITE ELECTRODE SEGMENT OPERATING. $P_0 = 40$ PSIG.

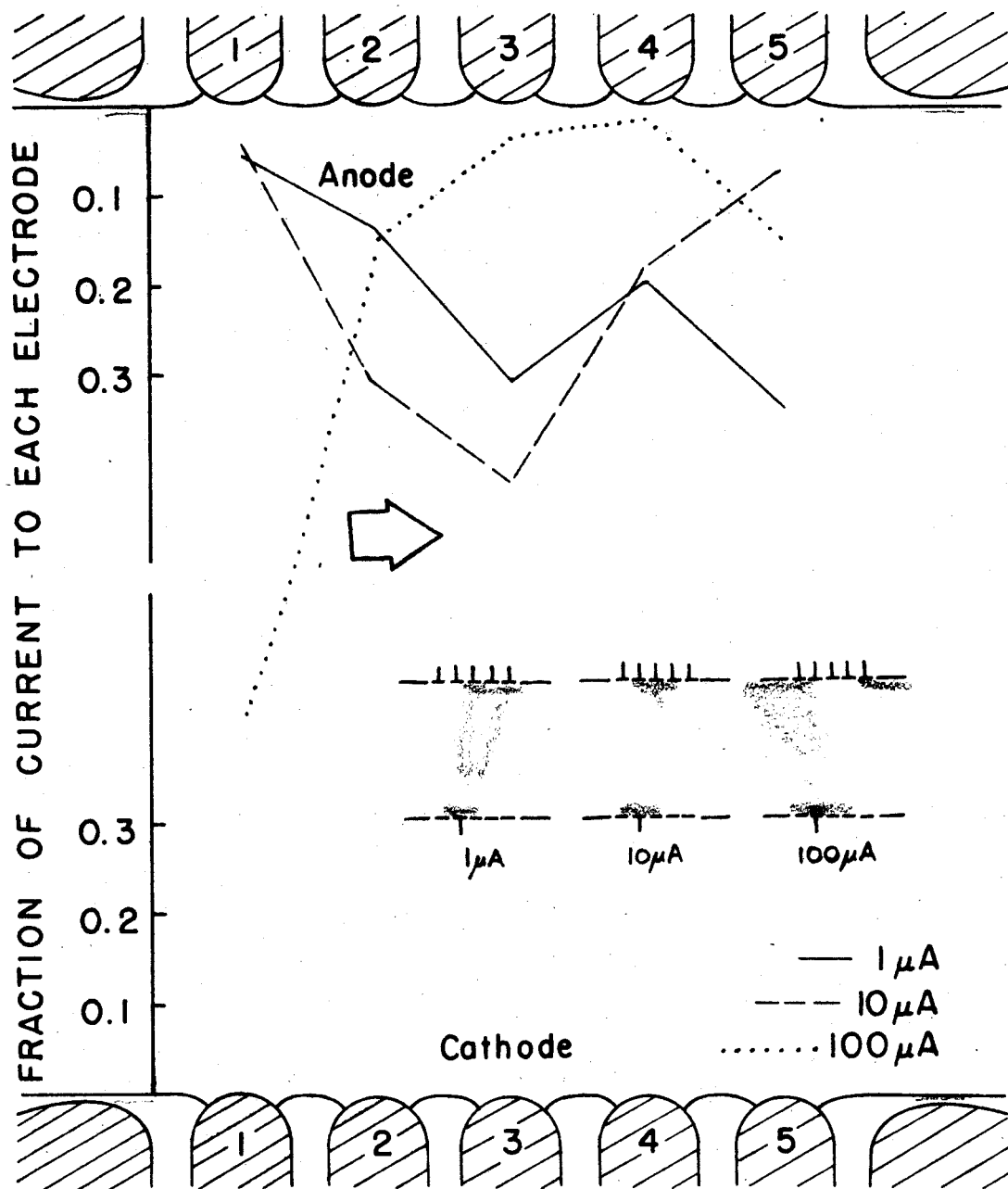


FIG. 37B - CURRENT DISTRIBUTION AT THE ANODE WITH NO.2 CATHODE SEGMENT OPERATING. $P_b = 40$ PSIG.

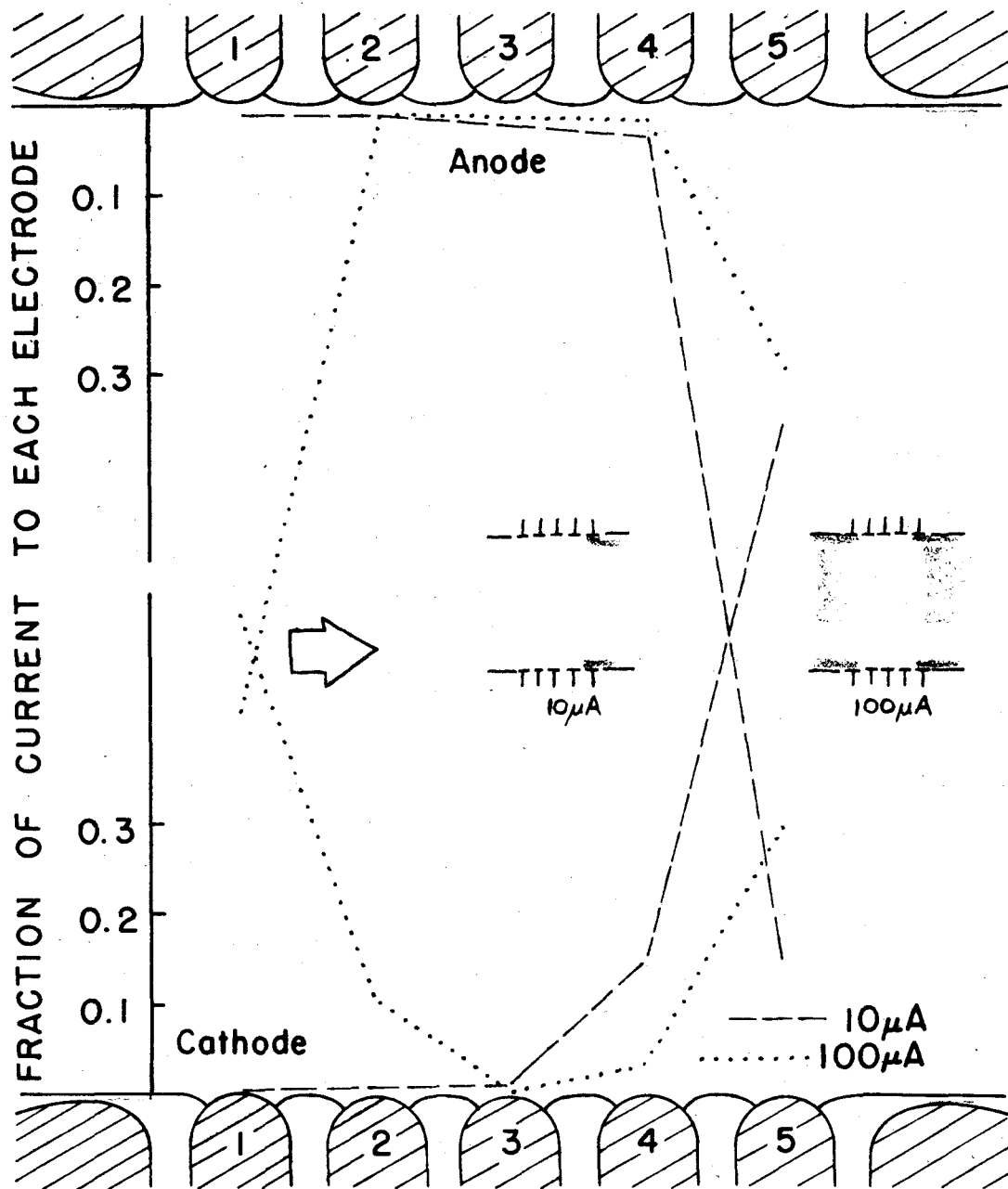


FIG. 38 - CURRENT DISTRIBUTIONS AT ANODE AND CATHODE. $P_0 = 60$ PSIG.

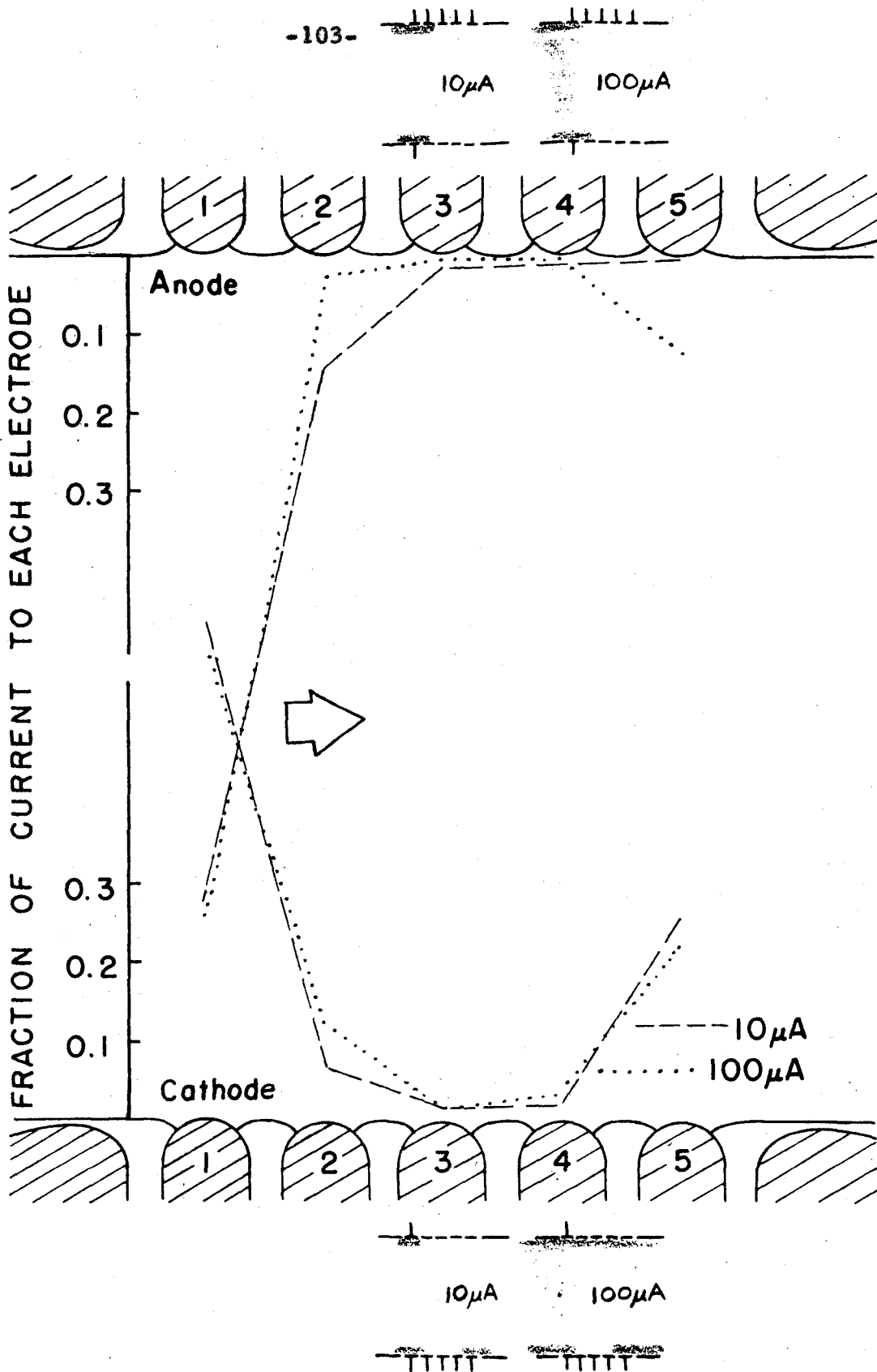


FIG. 39 - CURRENT DISTRIBUTION AT EACH ELECTRODE WITH NO.1 OPPOSITE ELECTRODE SEGMENT OPERATING. $P_0 = 60$ PSIG.

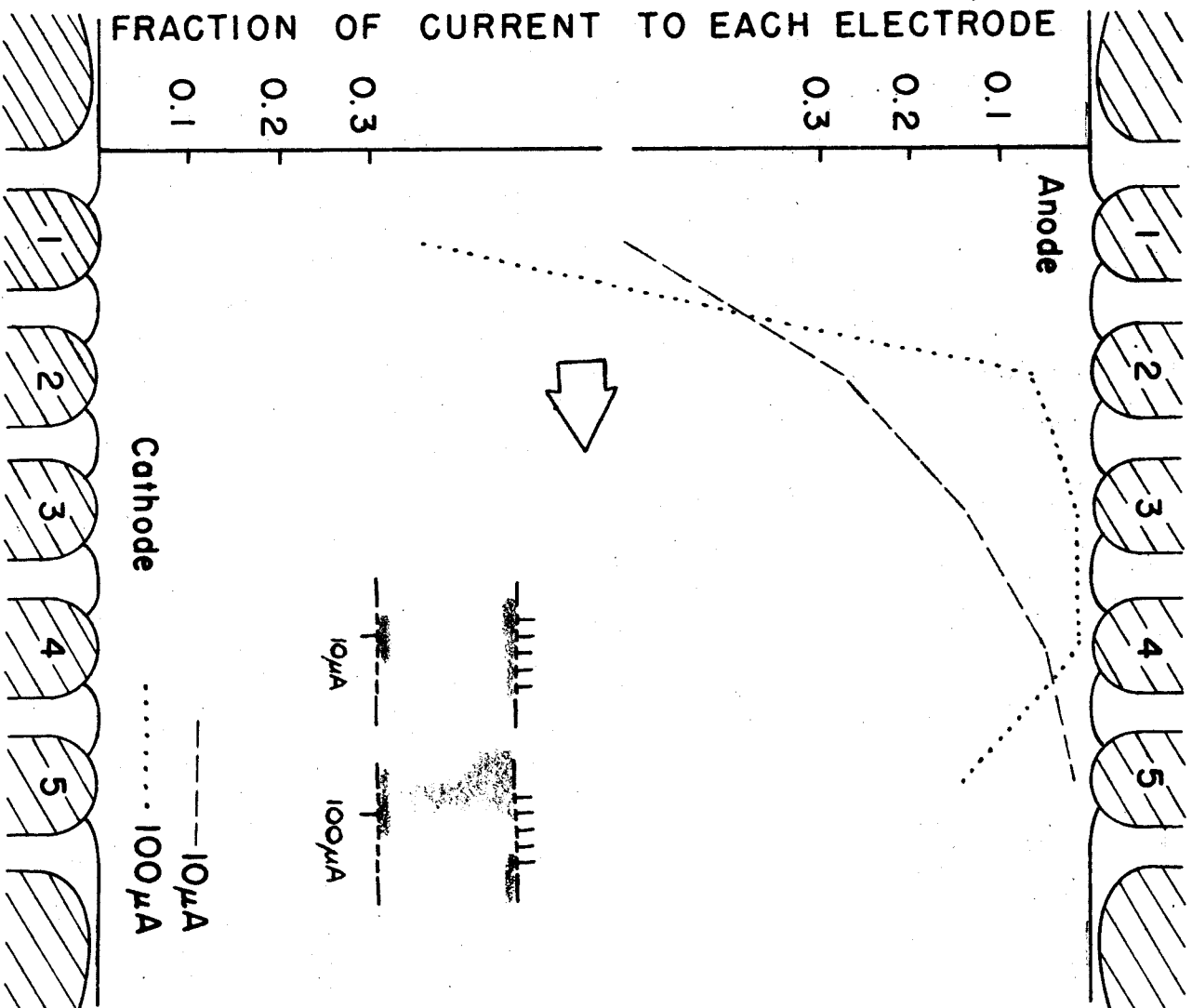
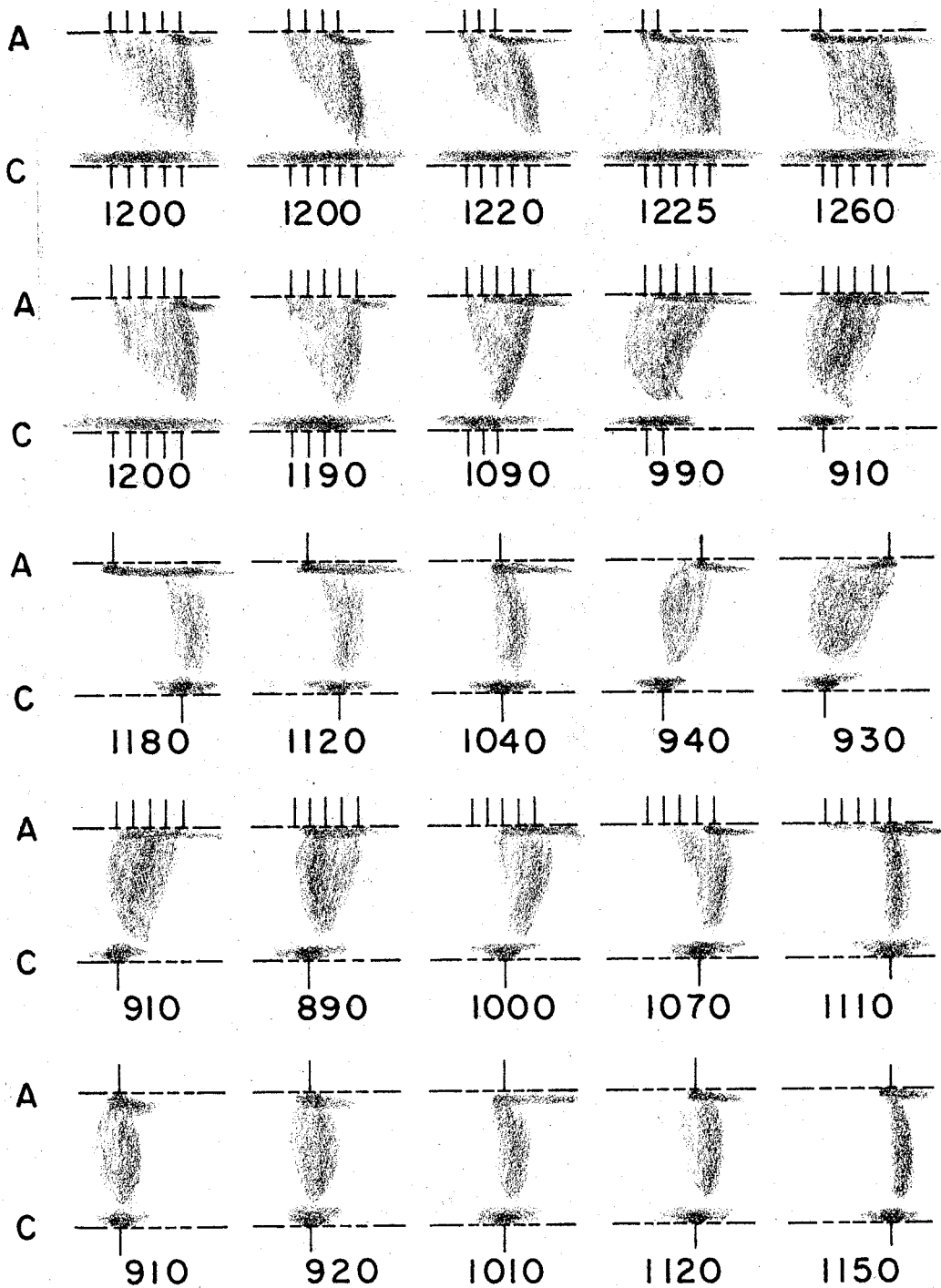


FIG.39B - CURRENT DISTRIBUTION AT THE ANODE
WITH NO.2 CATHODE SEGMENT OPERATING.
 $P_0 = 60$ PSIG.



Note: Discharge Voltage appears under cathode.

FIG. 40 - APPEARANCE OF DIFFERENT ELECTRODE SEGMENT COMBINATIONS. $P_0=0$ PSIG; $I=1\mu A$.